Universidade do Estado do Rio de Janeiro
Centro de Tecnologia e Ciências
Instituto Politécnico

Ranulfo Martins Carneiro Neto

Desenvolvimento de modelos de dano coesivo modificados para juntas coladas submetidas a fluência em modo II

Nova Friburgo
2022

Ranulfo Martins Carneiro Neto

Desenvolvimento de modelos de dano coesivo modificados para juntas coladas submetidas a fluência em modo II

Tese apresentada, como requisito parcial para obtenção do título de Doutor, ao Programa de Pós-Graduação em Modelagem Computacional, da Universidade do Estado do Rio de Janeiro.

Orientador: Prof. Dr. Joaquim Teixeira de Assis

Nova Friburgo

2022

CATALOGAÇÃO NA FONTE
UERJ / REDE SIRIUS / BIBLIOTECA CTC/E

C289 Carneiro Neto, Ranulfo Martins.
Desenvolvimento de modelos de dano coesivo modificados para juntas coladas submetidas a fluência em modo II / Ranulfo Martins Carneiro Neto. - 2022.
103 f. : il.

Orientadores: Joaquim Teixeira de Assis.
Tese (doutorado) – Universidade do Estado do Rio de Janeiro, Instituto Politécnico.

1.Métodos e Simulação– Teses. 2. Jutas (Engenharia) – Teses. 3. Adesivos – Teses. I Assis, Joaquim Teixeira de. II.. Universidade do Estado do Rio de Janeiro. Instituto Politécnico. III. Título.

CDU 004.9

Bibliotecária Pâmela Lisboa CRB7/ 5965

_____ _____

Assinatura Data

Ranulfo Martins Carneiro Neto

Desenvolvimento de Modelos de Dano Coesivo Modificados para Juntas Coladas Submetidas à Fluência em Modo II

Tese apresentada como requisito parcial para obtenção do título de Doutor ao Programa de Pós-Graduação em Modelagem Computacional do Instituto Politécnico, da Universidade do Estado do Rio de Janeiro.

Aprovada em 18 de maio de 2022.

Banca examinadora:

Prof. Joaquim Teixeira de Assis, D.Sc. (Orientador)
Instituto Politécnico – UERJ

Prof. Eduardo Martins Sampaio, D.Sc.
Instituto Politécnico – UERJ

Prof. Diego Campos Knupp, D.Sc.
Instituto Politécnico – UERJ

Prof. Silvio Romero de Barros, Ph.D.
Centro Federal de Educação Tecnológica Celso Suckow da Fonseca

Prof. Doina Mariana Banea, D.Sc.
Centro Federal de Educação Tecnológica Celso Suckow da Fonseca

Nova Friburgo
2022

DEDICATÓRIA

À minha esposa Andréa e a minha filha Vitória, pela força, amor e companheirismo.

AGRADECIMENTOS

Agradeço ao Grande Mestre pela oportunidade da vida.

A minha companheira Andréa, minha filha Vitória, aos meus pais e a todos os parentes, pela confiança, consideração e pelo apoio constante.

Ao meu orientador, Prof. Joaquim Assis, pelo apoio, disposição e confiança.

Ao Prof. Eduardo Sampaio pelo empenho e motivação dedicados nesse trabalho, a sua paciência agilidade e amizade, e também por disponibilizar toda a estrutura do Laboratório de Adesão e Aderência (LAA) para dar o suporte tão essencial a esse trabalho.

Ao Prof. Lucas da Silva e ao Pesquisador Alireza Safar, ambos vinculados a Faculdade de Engenharia da Universidade do Porto (FEUP), pela considerável contribuição ao trabalho.

Um agradecimento especial à Ricardo Hudson, que executou e acompanhou todos os experimentos dessa tese, a maioria deles com longas durações, superando assim os desafios encontrados por conta da pandemia. Considerável contribuição também tem o Marcelo Correia por todo trabalho de fabricação dos corpos de prova. Essas contribuições não teriam sido possíveis sem o apoio de toda equipe do LAA, cujas pessoas que são parte dele tornaram possível a concretização desse trabalho.

Agradeço também ao Prof. Felipe Sales, do Instituto Politécnico da UFRJ Macaé, pela contribuição com as funções de duas variáveis utilizadas no cálculo da energia crítica de fratura.

Aos meus amigos da vida, da União, e a todos que direta ou indiretamente contribuíram para a realização desse trabalho, minha gratidão.

RESUMO

CARNEIRO NETO, Ranulfo Martins. *Desenvolvimento de modelos de dano coesivo modificados para juntas coladas submetidas a fluência em modo II*. 2022. 103 f. Tese (Doutorado em Modelagem Computacional) – Instituto Politécnico, Universidade do Estado do Rio de Janeiro, Nova Friburgo, 2022.

Adesivos poliméricos apresentam comportamento viscoso quando submetidos a carregamentos constantes, resultando em deformações permanentes desses materiais. A fluência tem significativa influência nas propriedades mecânicas e coesivas das juntas adesivas, porém esta influência não é considerada nos modelos disponíveis na literatura que visam simular o comportamento mecânico das juntas coladas. Os modelos de dano coesivo (MDC) são vastamente utilizados na modelagem de juntas coladas em condições estáticas, porém, não há literatura MDC aplicados ao fenômeno da fluência. Os parâmetros coesivos são considerados constantes nos MDC, o que não é válido para a fluência. O objetivo principal dessa tese é desenvolver um modelo de dano coesivo que simule adequadamente a fluência nas juntas do ensaio *end notched flexure* (ENF), considerando assim a variação dos parâmetros coesivos no modelo. Os fatores tempo e carga de fluência foram avaliados em amostras do ensaio ENF, o qual é vastamente utilizado para calcular a energia crítica de fratura em modo II (cisalhamento). Além dos ensaios ENF usuais, que visaram calcular os valores de referência da força máxima e da energia crítica de fratura em modo II, foram realizados ensaios de fluência e ensaios pós fluência. Os ensaios de fluência foram realizados em duas etapas: i) tempos e cargas de fluência pré-definidos, ii) carga de fluência definida e aplicada até ocorrência da falha. Os ensaios pós fluência tiveram como objetivo mensurar a mudança nos parâmetros coesivos quando comparadas com os valores de referência. Os resultados dos ensaios pós fluência demonstraram que, em comparação com as condições estáticas, a força máxima e a energia de fratura em modo II do ensaio ENF são modificadas devido ao efeito de fluência. Assim, um aumento dessas propriedades de maneira significativa foi observado em alguns casos, havendo a oportunidade, portanto, de aumento da resistência das juntas adesivas quando pré-carregadas em fluência para condições controladas. Para que as evidências experimentais fossem consideradas nos modelos numéricos, duas funções de duas variáveis (tempo e carga) foram propostas, a fim de calcular o valor da energia de fratura residual para cada incremento de tempo na simulação numérica. Regressões lineares e não lineares foram realizadas para que os parâmetros das funções (modelos) fossem calculados. Após a validação desses modelos, os mesmos foram implementados em linguagem Fortran, descrevendo assim o comportamento constitutivo do material. Dessa forma, através de uma sub-rotina *user material* (UMAT), associada ao programa de elementos finitos Abaqus, a modelagem numérica das juntas ENF foi realizada, sendo então desenvolvido um modelo de dano coesivo modificado para a modelagem da fluência em juntas adesivas, sendo essa a principal contribuição dessa tese. O modelo proposto considerou tanto a mudança da energia crítica, como também a degradação da tensão de cisalhamento do adesivo. Os resultados numéricos e experimentais tiveram boa concordância, demonstrando o potencial do modelo de dano coesivo desenvolvido para simular a fluência de juntas coladas.

Palavras-chave: Junta Coladas. Modelagem numérica. Fluência. Modelos de dano coesivo.

ABSTRACT

CARNEIRO NETO, Ranulfo Martins. *Development of modified cohesive zone models for bonded joints submitted to creep in mode II*. 2022. 103 f. (Doutorado em Modelagem Computacional) – Instituto Politécnico, Universidade do Estado do Rio de Janeiro, Nova Friburgo, 2022.

Polymeric adhesives present viscous behavior when submitted to constant loads, resulting in permanent deformation of these materials. The creep has significantly influence on the cohesive and mechanical properties of bonded joints, however these changes are not taken into account on the numerical models available in literature that aim to simulate the mechanical behavior of bonded joints. The cohesive zone models (CZM) are widely applied in the modelling of bonded joints in static conditions, but there is no CZM applied to the creep phenomena. The cohesive properties are considered constants in CZM, what is not valid for creep. The main goal of this thesis is to develop a cohesive zone model that simulate the creep in end notched flexure (ENF) joints properly, taking the variation of the cohesive properties into account. Both creep time and creep load were evaluated in samples from the ENF test, which is extensively used to obtain the critical fracture energy in mode II (shear). In addition to the usual tests that aim to calculate the reference values of maximum load and critical fracture energy, creep and post creep tests were performed. The creep tests were carried out in two steps: i) with pre-defined creep times and creep loads, ii) creep load applied until the failure occurs. The post creep test aimed to measure the change in cohesive properties in relation to the reference values. The results showed that both maximum load and fracture energy are changed due to creep effect when compared to the values obtained in static conditions. A considerably increase was observed in some cases, therefore, there is the opportunity to increase the strength of adhesive joints when they are pre-creep loaded in controlled conditions. In order to consider the experimental evidences in the numerical models, two functions of two variables (time and load) were proposed aiming to calculate the residual fracture energy values for each time increment in the numerical simulation. Linear and non-linear regressions were carried out aiming to obtain the functions parameters. After the validation of the functions, they were implemented in Fortran language, describing this way the material constitutive behavior. Thus, the numerical modelling of creep in ENF joints was performed using a user material (UMAT) subroutine associated to the finite element program Abaqus, and so the cohesive zone models to simulate creep in bonded joints were developed, which was the main contribution of this thesis. The modified model proposed took both fracture energy change and shear strength degradation into account. A good agreement between numerical and experimental results was obtained, demonstrating the potential of the cohesive zone models developed to simulate creep in bonded joints.

Keywords: Bonded joints. Numerical modelling. Creep. Cohesive zone models.

LISTA DE FIGURAS

LISTA DE ABREVIATURAS E SIGLAS

CBBM	Compliance based beam method (método da viga baseado na flexibilidade)
DCB	Double cantilever beam (viga com duplo engastamento)
ENF	End notched flexure (flexão entalhada na extremidade)
LAA	Laboratório de adesão e aderência
MDC	Modelos de danos coesivos
MEF	Métodos dos elementos finitos
MLM	Método de Levenberg-Marquardt
MMQ	Método dos mínimos quadrados
UMAT	User material (material do usuário)
ZPF	Zona de processo de fratura

SUMÁRIO

INTRODUÇÃO

Contextualização

A união de materiais através de adesivos estruturais vem crescendo consideravelmente em diversos setores da engenharia, tais como óleo e gás, civil e aviação. A resistência das juntas coladas depende de diversos fatores, incluindo a espessura adesiva, o tratamento superficial, fatores ambientais como umidade e temperatura, além do tempo de aplicação das cargas. A fluência é caracterizada pela aplicação de uma carga a um determinado material por um longo período, resultando, no caso dos adesivos estruturais, em um comportamento viscoelástico, onde a deformação é dependente do tempo [1].

A utilização de modelos numéricos na previsão do comportamento das juntas coladas tem grande relevância científica e prática. Esses modelos devem prever fenômenos interdisciplinares, incluindo-se desde fenômenos químicos, como os tratamentos superficiais, até o comportamento mecânico, descrito através de relações constitutivas que englobam as propriedades do adesivo e do aderente, além das propriedades da interface. Dessa forma, a modelagem computacional vem sendo utilizada para, através da linguagem de programação e modelos matemáticos, auxiliar os projetistas e pesquisadores a descrever de maneira confiável o comportamento mecânico das juntas coladas.

Nesse sentido, diversos trabalhos experimentais e numéricos relacionados as juntas coladas têm sido desenvolvidos nos anos recentes no Laboratório de Adesão e Aderência (LAA), incluindo-se o estudo da fluência em juntas de cisalhamento simples (Albani, 2013; Siqueira, 2019), estudo do fator de forma de área em reparo de tubulações com chapa colada (da Silva, 2015), desenvolvimento de critério de falha para juntas coladas submetidas a carregamentos mistos (da Silva, 2010), análise numérica e experimental de juntas coladas em condições estáticas (Carneiro Neto, 2017), dentre outros. Dentre os adesivos utilizados nesses trabalhos, destaca-se o adesivo estrutural epóxi NVT 201E, o qual tem grande potencial na aplicação de reparos de tubulações com compósitos (Zugliani et. al., 2019) ou chapas coladas (da Silva et. al., 2020).

Os modelos de dano coesivo (MDC) associado com o método dos elementos finitos (MEF) vêm sendo amplamente utilizados na modelagem das juntas adesivas, pois permite a simulação do crescimento do dano através de princípios energéticos dependentes tanto do adesivo tanto do aderente (Campilho et al., 2013). Para a modelagem da fluência em juntas adesivas, os MDC são raramente utilizados, pois nesse caso poderá ocorrer variação nos

parâmetros coesivos das juntas, o que não ocorre na condição estática ou quase estática. Assim, como essa variação das propriedades não é considerada nos MDC, esse fator limita a aplicação dos mesmos na fluência das juntas coladas, havendo então a necessidade de maior investigação através de experimentos e modelagens nesse tema. Os modelos viscoelásticos clássicos simulam o comportamento de corpos de prova somente com adesivos, e em alguns casos com juntas adesivas específicas, porém na literatura não se encontra aplicação desses modelos nos corpos de prova do ensaio *end notched flexure* (ENF), o qual é vastamente utilizado para a determinação da energia crítica de fratura em modo de cisalhamento, também denominado modo II. Assim, não há na literatura modelos numéricos adequados e calibrados para simular a fluência no ensaio ENF, assim como não há trabalhos onde a fluência dessas juntas são avaliadas.

Objetivos

O presente trabalho tem como principal objetivo desenvolver um modelo numérico de dano coesivo modificado que considere as variações da energia crítica de fratura em modo II e da tensão máxima de cisalhamento devido a fluência, possibilitando a simulação numérica das juntas adesivas referentes ao ensaio (*end notched flexure*) ENF. Foi utilizado o programa de elementos finitos Abaqus, sendo desenvolvidas e implementadas sub-rotinas *user materials* (UMAT) para modelar o comportamento dos adesivos, que são os elementos coesivos.

Para avaliar a mudança nas energias críticas de fratura, diversos ensaios ENF foram realizados, tanto na condição estática (ou quase estática), quanto na condição de fluência, além dos ensaios pós fluência, os quais medem as propriedades modificadas das juntas. Assim, são objetivos específicos dessa tese:

- Determinar a energia de fratura em modo II nas condições estática e após a fluência, comparando-se os valores modificados da energia com o valor de referência;
- Obter o limite de resistência a fluência das juntas ENF;
- Propor funções de duas variáveis que possam calcular a energia de fratura em modo II de acordo com a carga e tempo de fluência, obtendo-se os parâmetros das mesmas através de regressões;
- Realizar a modelagem da fluência das juntas ENF no Abaqus, inserindo o modelo de dano coesivo nas sub-rotinas escritas em linguagem FORTRAN, levando em consideração tanto a degradação da tensão de cisalhamento com o tempo quanto a variação da energia de fratura em modo II;

- Validar o MDC através de experimentos adicionais.

Estrutura da tese

A estrutura dessa tese é composta, além dessa parte introdutória, por 3 capítulos, além das conclusões e sugestões de trabalhos futuros. Uma coletânea de 4 artigos também faz parte desse trabalho, todos publicados em revistas científicas. Todos os artigos são apresentados na íntegra nos Anexos A, B, C e D.

Na introdução os principais temas abordados no trabalho são apresentados, além dos objetivos da tese.

No primeiro capítulo a revisão bibliográfica é feita, sendo apresentados os principais conceitos de fluência, especialmente aqueles relacionados a modelagem. Os trabalhos relevantes ao tema da tese são descritos e discutidos, a fim de que as principais lacunas do tema de estudo sejam evidenciadas e a inovação desse trabalho fique demonstrada.

O segundo capítulo descreve a metodologia e os resultados do trabalho, referenciando-se a coletânea de artigos que compõem essa tese, sendo apresentados os principais legados de cada trabalho. Os detalhes da metodologia e dos resultados estão demonstrados nos artigos, todos anexos a essa tese.

No terceiro capítulo os resultados de todos os artigos são discutidos de maneira integrada.

Por fim, as conclusões são apresentadas, assim como as sugestões para trabalhos futuros.

1. REVISÃO BIBLIOGRÁFICA

1.1. Fluência

A aplicação de esforços constantes em materiais por um longo período de tempo conduz a uma deformação lenta e permanente, sendo esse fenômeno denominado fluência (*creep*). A norma ASTM D2293 define fluência como "*mudança dimensional com o tempo de um material sob carregamento, acompanhado de uma deformação instantânea elástica*". Em materiais metálicos a fluência ocorre majoritariamente a temperaturas maiores que a ambiente. Já em materiais poliméricos, como alguns adesivos estruturais, ocorrem mesmo a temperatura ambiente (Miravalles, 2007). A fluência pode resultar em perda da rigidez do adesivo, além de poder também reduzir sua resistência (Santos, 2008). Trata-se, portanto, de uma propriedade não trivial dentro da engenharia, devendo ser considerada pelos projetistas na previsão do comportamento e da durabilidade das juntas adesivas.

O processo de fluência em juntas adesivas pode ser descrito basicamente em 3 etapas, conforme representado na Figura 1, onde a tensão aplicada ao material polimérico, a umidade e a temperatura são mantidas constantes. Em $t = 0$, há uma deformação elástica instantânea (ε_0), dependente da tensão aplicada. As fases são então descritas como: i) primária ou transiente, ii) secundária ou estado estacionário e iii) terciária ou final (Dillard, 2010). No primeiro trecho a fluência ocorre de maneira relativamente rápida (alta taxa de deformação), diminuindo de intensidade ao final dessa etapa. Na fluência secundária ocorre uma estabilização da fluência, onde se verifica uma velocidade constante de deformação, sendo normalmente o trecho mais longo. Na fluência terciária ocorre considerável acréscimo da taxa de deformação, até que o material se rompe (Majda, 2009).

A recuperação das deformações depende de diversos fatores, incluindo-se a carga aplicada e as propriedades do adesivo. Se a carga for removida na fase primária, a recuperação tende a ser total. Já na fase secundária essa recuperação normalmente não é total, e na terciária nunca é total (Cavalcante, 2012). Conforme apresentado na Figura 1, caso a deformação continue a ser monitorada após a remoção da carga durante a fluência secundária, um decréscimo na deformação é observado, sendo este equivalente a deformação elástica instantânea (ε_0). Esse processo é denominado recuperação (*recovery*), sendo mais acentuado quanto maior o grau de reticulação do adesivo polimérico (Dillard, 2010).

Figura 1 – Curva típica de fluência para um material polimérico viscoelástico.

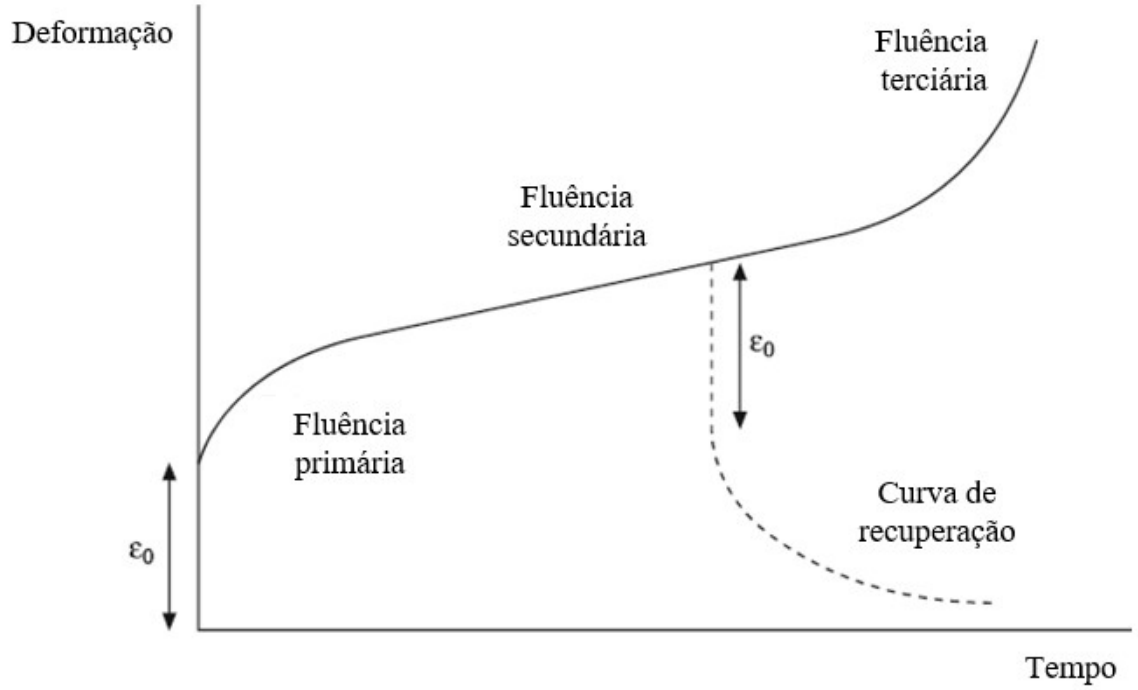

Fonte: Dillard, 2010.

De maneira geral, para um mesmo material, a deformação de fluência (ε) depende essencialmente de 3 fatores: i) tensão (σ), ii) tempo (t) e iii) temperatura. No presente trabalho o fator temperatura não será considerado como variável, portanto essa influência não será detalhada. A Equação (1.1) pode ser utilizada para prever a deformação total de fluência, descrevendo o comportamento apresentado na Figura 1 (Dillard, 2010).

$$\varepsilon = \varepsilon_o + B\sigma^m t + D\sigma^\alpha (1 - e^{-\beta}) \tag{1.1}$$

onde as constantes *B, m, D,* α *e* β são empíricas, determinadas através do ajuste da curva aos dados experimentais.

O segundo termo da Equação (1.1) representa a fluência secundária e o terceiro termo a fluência primária, a qual pode ser desprezada em algumas situações (Dillard, 2010). Nesses casos, a diferenciação da Equação (1.1) resulta em:

$$\dot{\varepsilon} = B\sigma^m \tag{1.2}$$

Existem outros modelos frequentemente utilizados na modelagem da fluência, conforme será apresentado nos tópicos seguintes.

Alguns trabalhos experimentais realizados em juntas de cisalhamento simples mostraram que os adesivos epóxis têm grande potencial para resistir a fluência, o que foi demonstrado nos testes de longa duração realizados por mais de 1000-h (Queiroz et. al., 2014; Carneiro Neto et. al. 2021). A literatura demonstra também que há um esforço a fim de melhorar a resistência da fluência em juntas adesivas. Khabazaghdam et. al (2020) investigou a influência do reforço de um adesivo epóxi com grafeno, obtendo uma redução de 12.4% no deslocamento de fluência quando comparado com os corpos de prova sem reforços. O trabalho experimental de Khalili et. al. (2009) demonstrou que o reforço do adesivo nas juntas de cisalhamento simples com substratos de alumínio conduz a um efeito considerável na deformação inicial e no tempo de falha. Os autores utilizaram três tipos de fibras ao longo da camada adesiva com diferentes orientações. Os experimentos, realizados a temperatura de 100º C, demonstraram que a orientação das fibras não teve efeito considerável na deformação inicial. As juntas reforçadas com fibras de carbono com $\pm 45^{\circ}$ tiveram maiores tempos de falha do que aquelas sem reforços. Em outro trabalho, Khalili (2014) demonstrou que quando os adesivos são reforçados com ligas de memória de forma, a vida útil das juntas aumenta. Esses experimentos foram realizados em três temperaturas distintas, todas acima da temperatura de transição vítrea. Foram também observadas melhorias na deformação inicial e na taxa de deformação de fluência. O tempo de vida útil da junta reforçada com seis tiras aumentou 55 % em relação aquelas sem reforços.

O comportamento do material viscoelástico está também relacionado ao rearranjo molecular, o qual pode ser reversível ou irreversível (Campo, 2008). Conforme relatado por Wu, et. al (2019), a aplicação da carga de fluência em materiais poliméricos pode inclusive resultar em um alinhamento das cadeias poliméricas, modificando dessa forma as propriedades dos materiais.

1.2. Modelos viscoelásticos

Nessa seção alguns modelos clássicos viscoelásticos são brevemente apresentados. Apesar desses modelos não terem sido utilizados no presente trabalho, a apresentação é válida para que os modelos disponíveis na literatura para modelar a fluência em juntas coladas sejam apresentados, e assim a inovação dessa tese fique ainda mais visível. Além disso, alguns autores utilizam uma abordagem híbrida, onde os modelos viscoelásticos são implementados nos programas de elementos finitos (Choi et. al., 2013; Sadigh et. al., 2020; Chen et. al., 2021).

Os modelos viscoelásticos são assim denominados por serem compostos tanto por elementos elásticos quanto por elementos viscosos. Dessa forma, pode-se representar um material intermediário entre os sólidos perfeitamente elásticos e o fluido newtoniano, já que a viscoelasticidade se caracteriza exatamente pela combinação dos efeitos elásticos e viscosos (da Silva et. al., 2018). Tal comportamento cabe perfeitamente aos adesivos poliméricos, especialmente quando submetidos a fluência. A mola linear é o elemento elástico utilizado em tais modelos, modelando as características de um sólido, tais como a elasticidade (E_o) e resistência (σ), de acordo com a Lei de Hooke ($\sigma = E_o \times \varepsilon$). Já o amortecedor é o elemento viscoso utilizado, o qual modela as características do fluido, tais como a dependência do fluxo com o tempo, temperatura e tensão aplicada, de acordo com a Lei de Newton da viscosidade ($\sigma = \eta_o \times \dot{\varepsilon}$) (Santos, 2008), onde η_o é a viscosidade e $\dot{\varepsilon}$ a taxa de deformação.

A Figura 2 mostra os modelos viscoelásticos clássicos. O modelo viscoelástico simplificado foi proposto por Maxwell em 1867, onde uma mola é associada em série com um amortecedor. Dessa forma, aplicada uma tensão nas extremidades do sistema, a deformação total pode ser obtida pela soma das parcelas elástica e viscosa. Já o modelo de Kelvin-Voigt propõe a associação da mola e do amortecedor em paralelo. Assim, tanto a mola quanto o amortecedor são submetidos a mesma deformação, sendo a tensão total aplicada na extremidade dividida entre as porções elásticas e viscosas. Já o modelo de Burger consiste em uma associação em série dos modelos de Kelvin-Voigt e Maxwell (da Silva et. al., 2018).

Figura 2 - Modelos viscoelásticos clássicos com suas respectivas equações diferenciais governantes.

HOOKE-elemento de mola (elasticidade linear) $\sigma = E_o \times \varepsilon$	
NEWTON-fluido (viscosidade linear) $\sigma = \eta_o \times \dot{\varepsilon}$	
KELVIN-VOIGT-sólido $\sigma = E_o \times \varepsilon + \eta_o \times \dot{\varepsilon}$	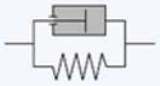
MAXWELL-fluido $\sigma + (\frac{\eta_o}{E_o}) \times \dot{\sigma} = \eta_o \times \dot{\varepsilon}$	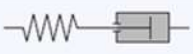
BURGERS $\sigma + \left(\frac{\eta_1}{E_1} + \frac{\eta_1}{E_2} + \frac{\eta_2}{E_2}\right) \cdot \dot{\sigma} + \left(\frac{\eta_1 \eta_2}{E_1 E_2}\right) \cdot \ddot{\sigma} = \eta_1 \cdot \dot{\varepsilon} + \left(\frac{\eta_1 \eta_2}{E_2}\right) \ddot{\varepsilon}$	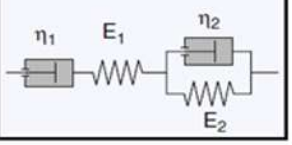

Fonte: da Silva et. al., 2018.

Os modelos viscoelásticos citados têm sido frequentemente utilizados para descrever o fenômeno reológico dos materiais viscoelásticos. Majda et. al. (2009) utilizou o modelo de Burger para modelar os ensaios de um adesivo epóxi considerando quatro cargas de fluência a temperatura ambiente. Os autores constataram que os parâmetros de Burgers são fortemente afetados pelo nível de tensão de fluência, sendo então proposto um modelo de Burger modificado, considerando uma viscosidade não Newtoniana para os amortecedores e uma mola não linear no elemento de Kelvin-Voigt. Esse novo modelo apresentou excelente ajuste com os dados experimentais da fluência primária e secundária. Zehsaz et. al (2015) apresentou resultados experimentais de testes uniaxiais de fluência em um adesivo epóxi com viscoelasticidade não linear. Um modelo constitutivo de fluência composto por um modelo de Maxwell e dois modelos de Zener (mola em paralelo com o modelo de Maxwell) foi proposto, o qual obteve melhor ajuste com os dados experimentais quando comparado com outros modelos numéricos existentes até então. Costa et. al (2015) também investigou a fluência de adesivos epóxis, sendo avaliado o efeito da fluência no módulo de Young após um carregamento de 1000-h. De maneira geral, o módulo de Young não foi consideravelmente alterado. Um modelo de Burger ajustado proposto por Feng et. al. (2005) foi utilizado naquele trabalho, exibindo uma boa concordância com os resultados experimentais.

A modelagem da viscoelasticidade não linear torna os modelos reológicos mais complexo e difíceis de implementar, além de necessitar muitos dados experimentais para a determinação dos parâmetros (Dillard, 2010). Uma alternativa para representar essas não linearidades é a adoção de abordagens empíricas, usadas frequentemente em modelos implementados nos programas de elementos finitos.

1.3. Modelos de fluência disponíveis no Abaqus

O Abaqus é um software de elementos finitos bastante difundido no meio científico, sendo um dos programas mais utilizados na modelagem de juntas adesivas, especialmente devido a sua vasta biblioteca de modelos coesivos. Alguns modelos de fluência também são disponibilizados na biblioteca do programa, embora não estejam diretamente relacionados aos modelos de dano coesivo. Outra alternativa para modelar a fluência no Abaqus é através das sub-rotinas, onde pode-se ter como entrada os dados experimentais da curva deformação x tempo, ou ainda, uma equação constitutiva que não faça parte da biblioteca do programa (Cavalcante, 2012). De maneira geral, o comportamento da fluência no Abaqus é especificado

por um comportamento uniaxial equivalente, sendo modelado especialmente a fluência secundária (Abaqus, 2014).

1.3.1 Lei Potencial

A Lei Potencial (*power law model*) disponível no Abaqus (ver Equação (1.3)) possui duas versões: i) *time-hardening* – adequada quando a tensão aplicada ao material é constante, ii) *strain-hardening* – quando ó material é submetido a uma deformação constante, variando-se então a tensão (relaxação). Os modelos disponíveis no Abaqus podem ser acessados na árvore dos Materiais (*Materials*), acessando o caminho Mechanical >> Plasticity >> Creep (Figura 3).

No modelo *power law* a taxa de deformação de fluência ($\dot{\varepsilon}$) é dada pela Equação (1.3) (Abaqus, 2014).

$$\dot{\varepsilon} = A\sigma^n t^m \tag{1.3}$$

onde σ é a tensão desviadora; t é o tempo total; A, m e n são parâmetros dependentes da temperatura definidos pelos usuários. Esses parâmetros podem ser obtidos através do ajuste dos dados experimentais ao modelo, caracterizando um problema inverso.

Figura 3 - Modelos de fluência disponíveis no Abaqus.

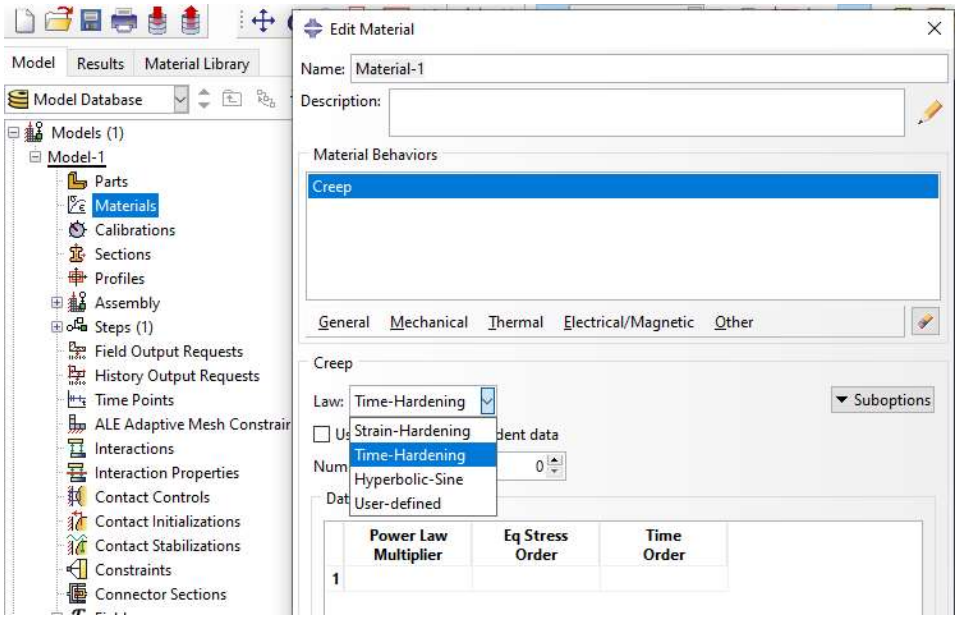

Fonte: O autor, 2022.

1.3.1.1 Teoria do endurecimento por tempo transcorrido (*time hardening theory*)

Essa teoria tem aplicabilidade quando o estado de tensões no material não varia consideravelmente, e assim a deformação é calculada ao longo do tempo para uma temperatura constante (Cavalcanti, 2012). Dessa forma, para uma tensão constante $\sigma = \sigma_o$, a resolução da equação diferencial (1.3) resulta em:

$$\varepsilon = \frac{t^{m+1} A \sigma_o^n}{m+1} \tag{1.4}$$

onde os valores de *n* e *A* devem ser positivos, e o valor de *m* deve situar-se entre -1 e 0, para que a taxa de deformação tenha sentido físico.

Utilizando o modelo apresentado, análises numéricas utilizando o método dos elementos finitos em juntas de cisalhamento simples demonstraram que a deformação de fluência se acumula nos locais dos corpos de prova onde há mudanças geométricas (cantos vivos) (Zehsaz, et. al. 2014). Os autores desse trabalho calcularam os parâmetros do modelo de potência através do ajuste dos dados experimentais obtidos nos ensaios uniaxiais do adesivo epóxi ao modelo (Equação (1.3)), sendo utilizado o método de Levenberg-Marquardt (a ser detalhado na Seção 1.4). Posteriormente, esses mesmos parâmetros foram aplicados na modelagem das juntas adesivas, que incluem o substrato e adesivo. Essa mesma metodologia foi utilizada em outros trabalhos, sendo avaliada numericamente a fluência em juntas de cisalhamento simples (Zehsaz, et. al., 2014; Khabazaghdam et. al., 2020) e juntas de cisalhamento duplo (Sadigh, 2016; Sadigh, et. al., 2019; Zehsaz, et. al., 2014a). Boa concordância numérica e experimental foram observadas nesses trabalhos. Quando a fluência é avaliada em juntas submetidas a diferentes temperaturas o procedimento descrito para o cálculo dos parâmetros deve ser feito separadamente para cada uma delas. Um estudo paramétrico da falha por fluência em juntas de cisalhamento duplo concluiu que a espessura adesiva não tem grande influência na vida útil da junta e as juntas com filetes apresentaram menor deflexão com maiores tempos de vida de fluência do que aquelas sem filetes (Zehsaz, et. al., 2014a). Não foram encontrados na literatura trabalhos similares nos corpos de prova do ensaio ENF.

1.3.1.2 Teoria do endurecimento por deformação (*strain hardening*)

A aplicação dessa teoria é adequada quando o estado de tensão é modificado ao longo da análise. Nesse caso a taxa de deformação de fluência é dada pela seguinte equação (Cavalcante, 2012):

$$\dot{\varepsilon} = (A\sigma^n[(m+1)\varepsilon]^m)^{\frac{1}{m+1}} \tag{1.5}$$

Quando não há dependência da temperatura as teorias "*time hardening*" e "*strain hardening*" são equivalentes (Abaqus, 2014).

1.3.2 Lei do Seno-Hiperbólica (*hyperbolic-sine law model*)

Essa Lei tem como diferencial a consideração do gradiente de temperatura, se adequando as aplicações onde há uma relação entre a temperatura e a taxa de deformação. A equação a seguir descreve matematicamente esse modelo (Cavalcante, 2012).

$$\dot{\varepsilon} = A(sinh\, B\, \sigma)^n\, exp(-\frac{Q}{R'(T-T_o)}) \tag{1.6}$$

onde T é a temperatura, T_o a temperatura inicial, Q é a energia de ativação, R' a constante universal dos gases, A, B e n são constantes do material.

Os parâmetros A, B, n, Q e R' não devem ser definidos em função da temperatura, pois a dependência da temperatura já está inclusa no modelo, diferentemente dos modelos apresentados anteriormente (Cavalcanti, 2012).

1.4. Estimação dos parâmetros de modelos

Cientistas de diversas áreas se deparam com situações onde precisam relacionar parâmetros físicos de um determinado modelo a um conjunto de resultados experimentais obtidos. Partindo-se do pressuposto de que o modelo é conhecido, pode-se então usar regressões lineares e/ou não lineares para obtenção dos parâmetros. Os modelos que descrevem a taxa de deformação de fluência descritos nas Seções 1.2 e 1.3 são exemplos de aplicações das

regressões. Nesta tese as regressões foram utilizadas para calcular os parâmetros de modelos que descrevem a energia de fratura em modo II (G_{IIC}) em função das variáveis tempo (t) e carga de fluência (F), sendo, portanto, essas variáveis utilizadas na apresentação das equações desta Seção.

1.4.1 Regressões lineares

Quando o modelo é linear no ajuste dos parâmetros, então um problema de regressão linear é definido (Aster, 2013). O modelo geral descrito na Equação (1.7) será considerado na apresentação do método dos mínimos quadrados, utilizado na obtenção dos parâmetros $(z_1, \ldots, z_m)$ da função (G_{IIC}) de duas variáveis (tempo e força de fluência, *t e F*, respectivamente).

$$G_{IIC}(t,F) = z_1 g_1(t,F) + \ldots + z_m g_m(t,F) \tag{1.7}$$

onde m é número total de parâmetros a serem determinados e $g_1(t,F),\ldots, g_m(t,F)$ são as funções geradoras, escolhidas de forma a representarem adequadamente o fenômeno em estudo.

Considerando que os valores experimentais da energia de fratura para cada condição experimental (t_i, F_i) são representados por I_i, pode-se então calcular o erro quadrático (E_r) pela Equação (1.8), representando a soma das diferenças quadráticas entre a energia crítica experimental e a calculada pelo modelo.

$$E_r(z_1, \cdots, z_m) = \sum_{i=1}^{n} [z_1 g_1(t_i, F_i) + \cdots + z_m g_m(t_i, F_i) - I_i]^2 \tag{1.8}$$

onde n é o número total de dados experimentais.

O mínimo dessa função, caso exista, satisfaz $\nabla E_r = 0$. Assim,

$$\frac{\partial E_r}{\partial z_k} = 2 \sum_{i=1}^{n} [z_1 g_1(t_i, F_i) + \cdots + z_m g_m(t_i, F_i) - I_i]\, g_k(t_i, F_i) = 0$$
$$\forall\, k = 1, \ldots, m \tag{1.9}$$

ou seja,

$$\sum_{i=1}^{n}[z_1 g_1(t_i,F_i)+\cdots+z_m g_m(t_i,F_i)]\; g_k(t_i,F_i)=\sum_{i=1}^{n} I_i\; g_k(t_i,F_i),\;\forall\; k=1,\ldots,m \tag{1.10}$$

Escrevendo-se na forma matricial, tem-se:

$$\begin{bmatrix} \sum_{i=1}^{n} g_1(t_i,F_i)g_1(t_i,F_i) & \cdots & \sum_{i=1}^{n} g_m(t_i,F_i)g_1(t_i,F_i) \\ \vdots & \ddots & \vdots \\ \sum_{i=1}^{n} g_1(t_i,F_i)g_m(t_i,F_i) & \cdots & \sum_{i=1}^{n} g_m(t_i,F_i)g_m(t_i,F_i) \end{bmatrix} \begin{bmatrix} z_1 \\ \vdots \\ z_m \end{bmatrix} = \begin{bmatrix} \sum_{i=1}^{n} I_i g_1(t_i,F_i) \\ \vdots \\ \sum_{i=1}^{n} I_i g_m(t_i,F_i) \end{bmatrix} \tag{1.11}$$

ou ainda:

$$\sum_{i=1}^{n} \begin{bmatrix} g_1(t_i,F_i)g_1(t_i,F_i) & \cdots & g_m(t_i,F_i)g_1(t_i,F_i) \\ \vdots & \ddots & \vdots \\ g_1(t_i,F_i)g_m(t_i,F_i) & \cdots & g_m(t_i,F_i)g_m(t_i,F_i) \end{bmatrix} \begin{bmatrix} z_1 \\ \vdots \\ z_m \end{bmatrix} = \sum_{i=1}^{n} \begin{bmatrix} I_i g_1(t_i,F_i) \\ \vdots \\ I_i g_m(t_i,F_i) \end{bmatrix} \tag{1.12}$$

Considerando que $g(t_i,F_i)$ seja dada por:

$$g(t_i,F_i)=\begin{bmatrix} g_1(t_i,F_i) \\ \vdots \\ g_m(t_i,F_i) \end{bmatrix} \tag{1.13}$$

a parte interior do somatório do lado esquerdo da Equação (1.12) pode ser reescrita da seguinte forma:

$$\begin{bmatrix} g_1(t_i,F_i)g_1(t_i,F_i) & \cdots & g_m(t_i,F_i)g_1(t_i,F_i) \\ \vdots & \ddots & \vdots \\ g_1(t_i,F_i)g_m(t_i,F_i) & \cdots & g_m(t_i,F_i)g_m(t_i,F_i) \end{bmatrix} = g(t_i,F_i)g(t_i,F_i)^T \tag{1.14}$$

Dessa forma, os coeficientes $(z_1, \ldots, z_m)$ que melhor se ajustam a função (modelo) dado pela Equação (1.7), de acordo com o método dos mínimos quadrados, são aqueles que satisfazem o sistema dado pela Equação (1.15).

$$[A]\begin{bmatrix} z_1 \\ \vdots \\ z_m \end{bmatrix} = [B] \tag{1.15}$$

onde

$$[A] = \sum_{i=1}^{n} g(t_i, F_i) g(t_i, F_i)^T \tag{1.16}$$

e

$$[B] = \sum_{i=1}^{n} I_i g(t_i, F_i)^T \tag{1.17}$$

Após a obtenção dos parâmetros do modelo, a validação dos mesmos deve ser realizada utilizando-se dados que não foram usados no processo de regressão.

1.4.2 Regressões não lineares

Quando os parâmetros do modelo utilizado têm uma relação inerentemente não linear com os experimentos, regressões não lineares devem ser utilizadas (Aster, 2013). Nesta Seção o método de Levenberg-Marquardt (Marquardt, 1963) é apresentado, o qual é amplamente utilizado na solução de problemas inversos que são formulados implicitamente, especialmente os problemas de otimização (Silva Neto, 2016). O método de Levenberg-Marquardt (LM) possui algumas vantagens em relação ao método de Newton, já que este último não pode ser diretamente aplicado a diversos problemas inversos (Aster, 2013).

Para apresentação do método de LM, vamos considerar que os valores da energia crítica de fratura obtidos pelos experimentos e pelo modelo sejam representados por I_i e $G_{IIC}(t, F)$, respectivamente. O vetor de resíduos (r_i) e a função de erro quadrático (E_r) devem ser calculados pelas Equações (1.18) e (1.19), respectivamente.

$$r_i = G_{IIC}(t_i, F_i) - I_i, \qquad para\ i = 1, \ldots, n. \tag{1.18}$$

$$E_r(z_1, \cdots, z_m) = \sum_{i=1}^{n} [G_{IIC}(t_i, F_i) - I_i]^2 \tag{1.19}$$

onde $(z_1, \cdots, z_m)$ são os parâmetros a serem determinados e *n* é quantidade de dados experimentais. Da mesma forma que apresentado na Seção 1.4.1, *t* é o tempo de fluência e *F* é a carga de fluência.

A Equação (1.19) pode ser reescrita em função do vetor de resíduos, conforme Equação (1.20).

$$E_r(z_1, \cdots, z_m) = r_i{}^T r_i \qquad para\ i = 1, \dots, n. \tag{1.20}$$

Para que a função de erro quadrático (E_r) seja otimizada, exige-se que ${\partial E_r}/{z_j} = 0$. Logo,

$$r_i J_{ij}^T = 0 \qquad para\ i = 1, \dots, n\ e\ j = 1, \dots, m. \tag{1.21}$$

onde J_{ij} é a matriz Jacobiana, dada pela Equação (1.22).

$$J_{ij} = \frac{\partial G_{IIC}(t_i, F_i)}{\partial z_j} \qquad para\ i = 1, \dots, n\ e\ j = 1, \dots, m. \tag{1.22}$$

Se a expansão de Taylor for escrita somente com os termos até a primeira ordem para o vetor de resíduos (Silva Neto, 2016), resulta em:

$$r_i^{k+1} = r_i^k + J_{ij} \Delta z_j^k, \qquad para\ i = 1, \dots, n\ e\ j = 1, \dots, m. \tag{1.23}$$

onde

$$z_j^{k+1} = z_j^k + \Delta z_j^k, \qquad para\ i = 1, \dots, n\ e\ j = 1, \dots, m. \tag{1.24}$$

sendo *k* o contador de iterações.

Combinando-se as Equações (1.21) a (1.23), obtêm-se:

$$(J_{ij}^k)^T J_{ij}^k \Delta z_j^k = -(J_{ij}^k)^T r_i^k, \qquad para\ i = 1, \dots, n\ e\ j = 1, \dots, m. \tag{1.25}$$

Marquardt (1963) propôs a adição de um termo a diagonal da matriz $(J_{ij}^n)^T J_{ij}^n$, visando melhorar o desempenho do algoritmo. Quando seu artigo foi avaliado, os revisores descreveram que Levenberg (1944) havia feito uma proposta semelhante. Assim, o método passou a ser denominado método de Levenberg-Marquardt. Dessa forma, a Equação (1.25) é reescrita como:

$$[(J_{ij}^k)^T J_{ij}^k \Delta z_j^k + \lambda^k I_d] = -(J_{ij}^k)^T r_i^k, \quad para\ i = 1, \dots, n\ e\ j = 1, \dots, m. \tag{1.26}$$

onde I_d é a matriz identidade e λ é o fator de amortecimento, o qual é alterado ao longo do processo iterativo, ficando normalmente próximo de 0 ao final do procedimento (Silva Neto, 2016).

É importante observar que o método de Levenberg-Marquardt necessita de uma estimativa inicial dos parâmetros. A partir dessa estimativa, a matriz Jacobiana é calculada pela Equação (1.22). Em seguida, o valor do modelo é obtido utilizando-se a estimativa inicial, sendo então calculados o vetor de resíduos (Equação (1.18)) e a soma dos erros quadráticos inicial - E_{ro} - (Equação (1.19)). Calcula-se agora Δz_j^k e z_j^{k+1} usando-se as Equações (1.26) e (1.24), respectivamente.

A próxima iteração é chamada desde que a nova soma dos erros quadráticos (E_r) seja menor do que a soma inicial E_{ro}. Nessa condição, um menor valor do fator de amortecimento é considerado. Caso contrário, o valor de λ aumenta, sendo novamente calculados os vetores Δz_j^k e z_j^{k+1}.

Enquanto o critério de parada pré-estabelecido não é alcançado, a matriz Jacobiana deve ser novamente calculada com os valores atualizados de z_j^{k+1}, acompanhado dos mesmos passos já descritos. Finalmente, o programa deve parar de funcionar quando o critério de parada pré-estabelecido for alcançado.

1.5. Modelos de dano coesivo

Os modelos de dano coesivo (MDC) são constantemente aplicados na modelagem das juntas coladas, tendo como característica a introdução de regiões de fratura na estrutura, o que é realizado através das leis de tração e separação (da Silva et. al., 2018). Assim, os elementos coesivos representam o comportamento das fraturas, enquanto os elementos volumétricos

representam as deformações dos meios contínuos (Espinha, 2011). A Figura 4 mostra uma representação esquemática dos elementos volumétricos e coesivos.

Figura 4 - Representação esquemática dos elementos volumétricos e coesivos.

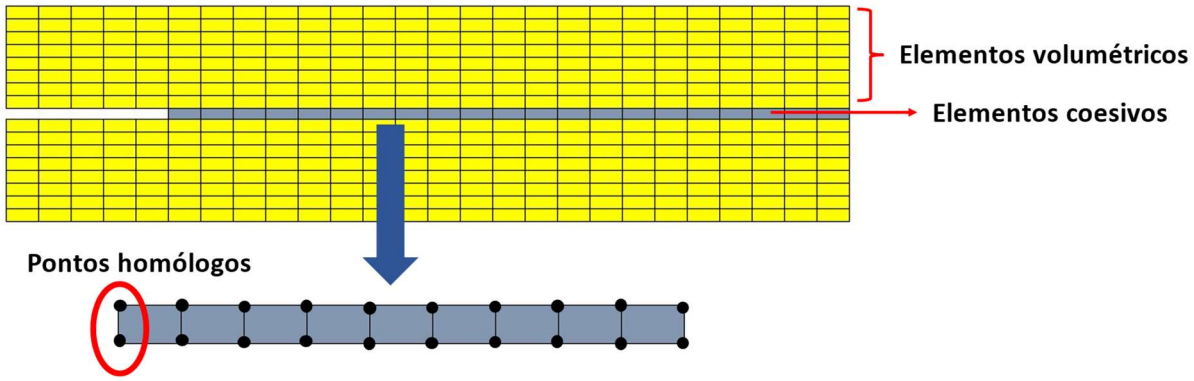

Fonte: O autor, 2022.

Nos modelos de dano coesivo a fratura é tratada como um fenômeno gradual, sendo que a propagação da trinca ocorre nas chamadas zonas coesivas, onde os elementos possuem resistência as trações coesivas. Tais conceitos foram apresentados inicialmente por Berenblatt (1959 e 1962) e Dugdale (1960) (Azevedo, 2014). O comportamento dos MDC é determinado através das leis coesivas, também denominadas leis de tração separação em alguns softwares. Essas leis consideram um comportamento elástico linear na primeira parte do carregamento, ocorrendo posteriormente o início e a propagação da trinca dentro do material coesivo (da Silva et. al., 2012). A depender do comportamento do material e da interface a ser simulada, diferentes formas da lei coesiva podem ser aplicadas, sendo as mais utilizadas as leis triangular, exponencial e trapezoidal (Figura 5). Por exemplo, quando são utilizados adesivos frágeis, como é o caso do adesivo NVT 201E (utilizado nessa tese), a lei triangular tende a fornecer resultados numéricos mais próximos dos experimentais, sendo que para os adesivos dúcteis a lei trapezoidal tende a retornar resultados mais precisos (Campilho, 2013).

Considerando a lei triangular (Figura 6), o comportamento elástico linear é representado pela reta crescente, sendo as tensões máximas nos modos puros representadas por t_n^o e t_s^o (normal e cisalhamento, respectivamente). O pico do gráfico representa o início do dano, e a partir desse deslocamento em tração ou cisalhamento (δ_n^o e δ_s^o, respectivamente) a trinca inicia a sua propagação e as propriedades do material coesivo começam a se modificar. Esse comportamento é descrito pela reta decrescente, ocorrendo a fratura completa nos respectivos deslocamentos finais em modo normal ou de cisalhamento (δ_n^f ou δ_s^f). A área sobre a curva nos carregamentos puros de tração e cisalhamento são representadas por G_I *e* G_{II}, que são as

energias de fratura em modo I e II, respectivamente. Para que os deslocamentos máximos sejam definidos (δ_n^f ou δ_s^f), considera-se que as energias de fratura assumem os valores críticos em modo I e II (G_{IC} e G_{IIC}, respectivamente), logo $G_I = G_{IC}$ e $G_{II} = G_{IIC}$ .Quando um carregamento misto é aplicado (esforços de tração e cisalhamento), a identificação dos deslocamentos e das tensões na curva é feita pelo índice *m*.

Figura 5 - Formas diferentes em modo puro das leis coesivas: triangular e exponencial (a) e trapezoidal (b).

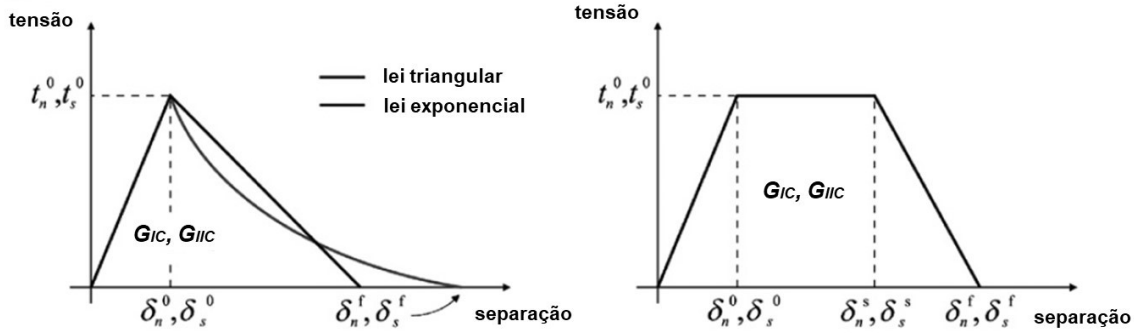

Fonte: Campilho et al., 2012.

Figura 6 - Modelo de dano coesivo com forma triangular.

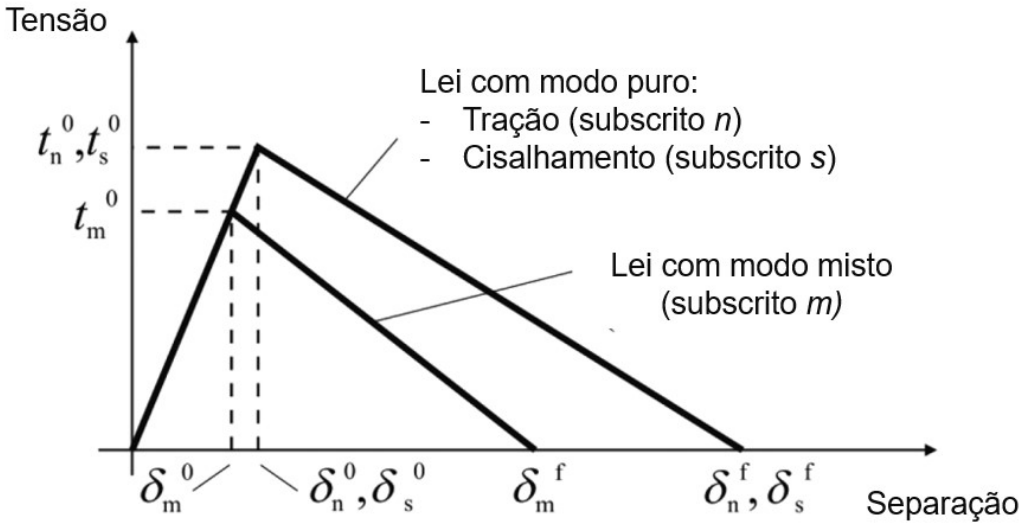

Fonte: Campilho et al., 2012.

As energias críticas de fratura devem ser calculadas através dos ensaios de fratura. Os ensaios *double cantilever beam* (DCB) e *end notched flexure* (ENF) são os mais utilizados para calcular G_{IC} e G_{IIC}, respectivamente (de Moura, 2008; Ajdani et. al., 2020). A vasta utilização desses ensaios se deve a praticidade e a fácil configuração dos mesmos (da Silva et. al., 2012). Umas das principais dificuldades dos ensaios de fratura, especialmente do ENF, é a medição do comprimento da trinca durante o ensaio (de Moura, 2006). Além da visualização não ser

trivial, a dimensão da zona de processo de fratura (ZPF) não pode ser desprezada, correspondendo a uma região do material deteriorada por conta de processos inelásticos (de Moura, 2008). Dessa forma, o método *compliance based beam method* (CBBM) vem sendo amplamente aplicado no tratamento de dados do ensaio ENF, sendo baseado unicamente na flexibilidade (*compliance*) do material (de Moura, 2006). Ou seja, as medições da força e do deslocamento ao longo do ensaio são suficientes para obtenção da energia crítica de fratura. O método considera o conceito de trinca equivalente, considerando inclusive a adição da dimensão da ZPF. Outros métodos para calcular as energias de fratura também estão disponíveis na literatura, porém a grande maioria destes exige a medição do comprimento da trinca, a exemplo dos métodos CCM (*compliance calibration method*) e DBT (*direct beam theory*) (Carneiro Neto, 2017).

A Equação (1.27) apresenta a relação entre as tensões na interface dos elementos finitos (σ) e o vetor de deslocamentos relativos entre os pontos homólogos (δ_r) antes do início do dano (ver Figura 4).

$$[\sigma] = [K][\delta_r] \tag{1.27}$$

onde *[K]* é a matriz diagonal que contém a rigidez dos elementos coesivos.

Em um carregamento puro a matriz de rigidez *[K]* pode ser aproximada por $K_{11} = E$ (módulo de Young), $K_{22} = K_{33} = G$ (módulos de elasticidade ao cisalhamento).

Para modelar o início do dano, diversos critérios podem ser adotados. Se o carregamento for com modo puro (I ou II), o início do dano é assumido quando a razão entre a tensão corrente (ou atual) e a tensão máxima em modo puro possui valor um (Abaqus, 2014). Se um carregamento misto é aplicado, o critério da tensão nominal quadrática pode ser utilizado, o qual é dado pela Equação (1.28).

$$\left\{\frac{\langle t_n \rangle}{t_n^o}\right\}^2 + \left\{\frac{t_s}{t_s^o}\right\}^2 = 1 \tag{1.28}$$

onde t_n *e* t_s são as tensões correntes normal e de cisalhamento, respectivamente, e o símbolo $\langle\ \rangle$ representa o a função de Macaulay, cujo objetivo é garantir que somente tensões compressivas não são suficientes para iniciar o dano.

A evolução do dano pode ser quantificada através do cálculo da variável de dano (*D*), representando o dano geral no material considerando todos os esforços combinados.

$$D = {\delta_f(\delta_c - \delta_o)}\Big/{\delta_c(\delta_f - \delta_o)} \tag{1.29}$$

onde δ_c representa o valor máximo do deslocamento efetivo alcançado em todo o histórico do carregamento (ABAQUS, 2014). Por simplicidade, adota-se os símbolos δ_o e δ_f para descrever o deslocamento no início e no final do dano, respectivamente.

A variável de dano (*D*) varia entre 0 (sem degradação) e 1 (degradação total). Dessa forma, quando o critério de início do dano é alcançado, o vetor de tensão nominal (σ) passará a ser regido pelo Equação (1.30), representando a reta decrescente da lei triangular.

$$[\sigma] = ([I_d] - [D])[K][\delta_r] \tag{1.30}$$

onde $[I_d]$ representa a matriz identidade.

Assim, quando a variável de dano tem valor 1, a tensão é nula no elemento, pois ocorreu a total ruptura do mesmo.

Os critérios energéticos devem ser utilizados para os carregamentos em modo misto. A Equação (1.31) apresenta o critério de fratura da lei de potência (*power law fracture criterion*), onde a fratura é regida pela energia necessária que cause a fratura nos modos individuais (normal ou cisalhamento).

$$\left\{\frac{G_I}{G_{IC}}\right\}^{\alpha} + \left\{\frac{G_{II}}{G_{IIC}}\right\}^{\alpha} = 1 \tag{1.31}$$

onde o critério linear (α = 1) e o quadrático (α = 2) são os mais utilizados (Araújo, 2016).

Quando um carregamento com modo puro é aplicado ao corpo de prova, por exemplo, modo de cisalhamento, a área sob a curva tensão-separação com formato triangular equivale a energia crítica de fratura em modo II (G_{IIC}). Assim, o deslocamento final (δ_f) pode então ser calculado através da Equação (1.32).

$$\delta_f = {2G_{IIC}}\Big/{t_s^o} \tag{1.32}$$

Se alguma propriedade coesiva variar, como é a proposta desta tese, então a biblioteca de modelos do Abaqus não pode mais ser utilizada, devendo-se então desenvolver uma sub-rotina para descrever o comportamento constitutivo do material.

1.6. Implementação de novos modelos de fluência no Abaqus

Os atuais modelos de fluência disponíveis na literatura não consideram a mudança da energia crítica de fratura devido aos esforços de fluência. Essa deve ser a principal razão que não foi encontrada na literatura a modelagem da fluência em juntas adesivas considerando esse aspecto. Os modelos de dano coesivo são vastamente utilizados na modelagem das juntas adesivas estruturais, devido as diversas vantagens já apresentadas ao longo desse trabalho, além de prever com excelente precisão diversos resultados experimentais. Assim, a principal lacuna que essa tese visa preencher é a adaptação do modelo de dano coesivo para que este contabilize as mudanças nas energias críticas de fratura em modo II de acordo com os diferentes tempos e cargas de fluência, prevendo também a degradação da tensão de cisalhamento máxima, já considerada anteriormente por Costa et. al (2018), porém para fadiga. Para que esse modelo seja desenvolvido, é necessário utilizar as sub-rotinas do Abaqus, já que a biblioteca de modelos possui apenas os modelos de dano coesivo tradicionais, ou seja, com tensão máxima de cisalhamento e a energia crítica de fratura constantes.

Existem diversas sub-rotinas disponíveis para implementação no Abaqus. Nesse trabalho é apresentada a sub-rotina *user material* (UMAT), que pode ser usada na definição do comportamento constitutivo do material (Abaqus, 2014). A sub-rotina UMAT é chamada em todos os pontos onde a mesma é definida, sendo no caso desse trabalho chamada em toda a camada adesiva. Um código em linguagem FORTRAN deve então ser desenvolvido para implementação da sub-rotina. Para que o Abaqus possa ler esse código, há a necessidade da instalação e integração de outros dois programas: *Visual Studio Community* e *oneAPI* (antigo *Intel Parallel Studio*). Esses programas devem estar corretamente integrados para que a sub-rotina funcione. O passo a passo para que esse link entre os programas ocorra devidamente pode ser consultado no relatório técnico elaborado por Cuevas (2021).

Para que o modelo constitutivo seja implementado, a matriz Jacobiana (J) deve ser fornecida pelo usuário, sendo dada pela Equação (1.33) (Abaqus, 2014).

$$J = \frac{\partial \Delta\sigma}{\partial \Delta\varepsilon} \tag{1.33}$$

onde $\Delta\sigma$é o incremento de tensão e $\Delta\varepsilon$ o incremento de deformação.

No Abaqus a matriz Jacobiana recebe o nome DDSDDE(I,J), a qual define a mudança no I-ésimo componente de tensão ao final do incremento de tempo causado por uma perturbação do J-ésimo componente da matriz de incremento de deformação (Abaqus, 2014). Quando um modo puro é aplicado, a matriz Jacobiana é diagonal, conforme Equação (1.34).

$$J = \begin{bmatrix} E & 0 & 0 \\ 0 & G & 0 \\ 0 & 0 & G \end{bmatrix} \tag{1.34}$$

onde E é o módulo de Young e G é o módulo de cisalhamento.

Definida a matriz Jacobiana, a matriz de tensões (*STRESS* na sub-rotina UMAT) pode ser calculada. A matriz *STRESS* é então passada como o tensor de tensão no início de cada incremento, sendo atualizada na sub-rotina UMAT para ser o tensor de tensão no final do incremento, de acordo com a matriz Jacobiana e com o incremento de deformação (*DSTRAN*).

Quando uma carga de fluência é aplicada, tanto a máxima tensão quanto a energia crítica de fratura podem ser alteradas, de acordo com os tempos e cargas de fluência aos quais as juntas foram submetidas. Dessa forma, a sub-rotina UMAT deverá prever a variação desses parâmetros coesivos, de acordo com os diferentes tempos e cargas de fluência. Consequentemente, o deslocamento final calculado pela Equação (1.32) não será mais constante, assim como a área do gráfico tração-separação. Portanto, para que a fluência seja modelada, devem ser previstas equações que modelem: i) a mudança da tensão de cisalhamento máxima de acordo com os parâmetros de fluência (tempo e carga), ii) a mudança da energia de fratura em modo II, também de acordo com o tempo e a carga de fluência. Como consequência, tanto os deslocamentos no início do dano quanto ao final do dano (δ_s^0 e δ_s^f, respectivamente) são atualizados a cada incremento da simulação. Assim, uma lei triangular com parâmetros variáveis deverá ser obtida, conforme apresentado na Figura 7.

Figura 7 - Lei de tração-separação modificada para modelagem da zona coesiva nas juntas ENF submetidas a fluência.

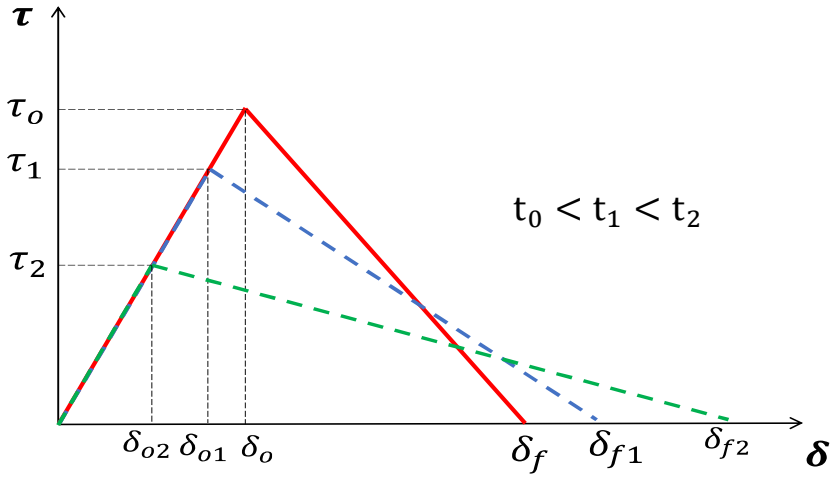

Fonte: O autor, 2022.

2. METODOLOGIA E RESULTADOS

A descrição completa da metodologia e dos resultados desse trabalho estão apresentadas detalhadamente em cada um dos artigos da coletânea que compõe a presente tese, os quais estão nos Anexos A, B, C e D, na ordem que são apresentados a seguir. Destaca-se aqui a intensa campanha experimental realizada, sendo submetidos ao teste de fluência mais de 60 corpos de prova do ensaio ENF. No presente capítulo, a metodologia e os resultados de cada um dos artigos são apresentados de maneira resumida.

2.1. Artigo 1 – Efeito da fluência na energia de fratura residual de adesivos em modo II (*Effect of creep on the mode II residual fracture energy of adhesives) – Journal of Applied Polymer Science*

Nesse artigo a variação da força máxima e da energia crítica de fratura em modo II foi investigada experimentalmente no ensaio ENF. Os experimentos foram divididos em três etapas:

1. **Ensaios quase estáticos**: Nessa etapa os ensaios ENF foram realizados da maneira tradicional, sem nenhuma carga de fluência. Os valores de referência da força máxima (P_{max}) do ensaio (quando se inicia a propagação da trinca) e da energia crítica de fratura em modo II (G_{IIC}) foram obtidos, para posterior comparação;
2. **Ensaio de fluência nos corpos de prova do ensaio ENF**: Os ensaios de fluência ocorreram com diferentes cargas constantes de fluência (40%, 50%, 60% de P_{max}) aplicadas por tempos pré-determinados (12-h, 24-h, 48-h, 60-h). As curvas de deslocamento versus tempo foram comparadas para diferentes cargas e tempos de fluência;
3. **Ensaios pós fluência nos corpos de prova do ensaio ENF**: Os mesmos corpos de prova testados na etapa 2 foram submetidos ao ensaio ENF tradicional, a fim de medir a mudança em P_{max} e G_{IIC}.

Os resultados demonstraram que tanto as cargas quanto os tempos de fluência têm considerável influência tanto na força máxima quanto na energia crítica de fratura. Um aumento na força máxima (P_{max}) foi observado na comparação entre valores das etapas 1 e 3, chegando a ocorrer um aumento de 26% (ver Figura 8a). O aumento na energia crítica foi ainda mais considerável, chegando a um crescimento de 47% (ver Figura 8b), novamente comparando-se o valor da etapa 3 com o valor de referência (etapa 1). De maneira geral, maiores cargas

conduzem a maiores valores de P_{max} e G_{IIC}, e também maiores tempos de fluência conduzem a maiores P_{max} e G_{IIC}. Porém, esse aumento das propriedades tem um limite, o qual foi investigado para a carga de fluência de 60%, sendo obtido um "ponto ótimo", ou seja, é a melhor condição para que os ganhos nas propriedades da junta ocorra. O tempo de fluência para o "ponto ótimo" foi 48-h, o que significa que tempos maiores de fluência levarão a diminuição dos valores das propriedades mecânicas e coesivas do adesivo.

O principal legado desse trabalho foi mostrar que o pré-carregamento de fluência em juntas ENF pode melhorar de maneira significativa a energia de fratura em modo II e a resistência estáticas dessas juntas.

Figura 8 - Aumento percentual devido a fluência: a) força máxima (P_{max}), b) energia crítica de fratura em modo II (G_{IIC}).

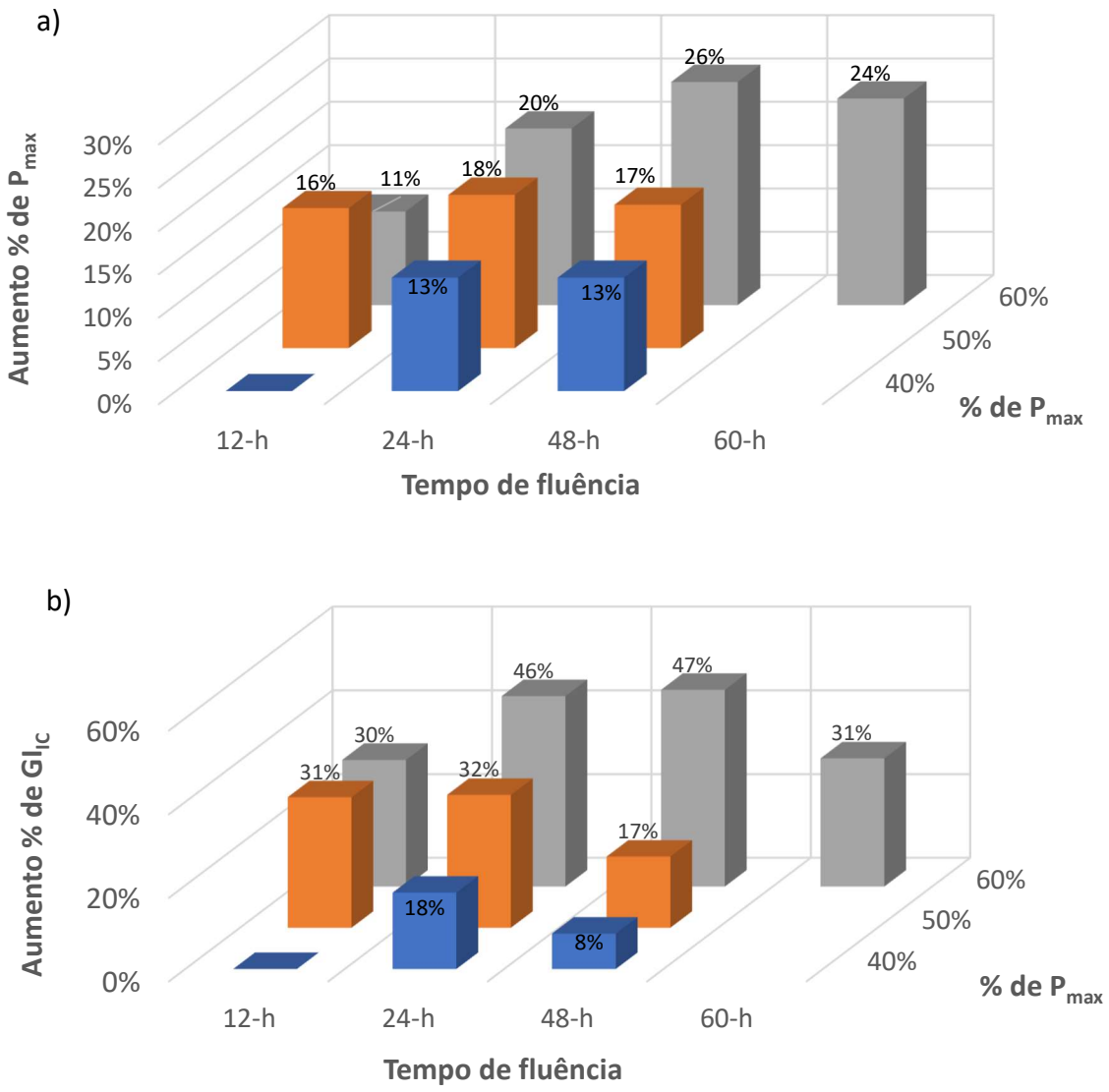

Fonte: O autor, 2022.

2.2. Artigo 2 – Avaliação da vida útil de fluência em juntas adesivas usando amostras do ensaio ENF (*Assessment of the creep life of adhesively bonded joints using the end notched flexure samples*) – *Engineering Failure Analysis*

Nesse artigo os ensaios de fluência foram realizados com cargas distintas até a ocorrência da falha, portanto, nessa etapa, os tempos não são pré-definidos conforme ocorreu nos experimentos do Artigo 1. As cargas de fluência consideradas foram: 70%, 75% e 80% de P_{max}. O tempo máximo considerado no ensaio foi de 720-h (30 dias), assim, quando a trinca não se propagou após esse tempo o ensaio foi interrompido e, em seguida, um ensaio usual ENF quase estático foi realizado, a fim de se medir a energia residual de fratura em modo II (da mesma forma que a etapa 3 do Artigo 1).

Os principais resultados obtidos nesse artigo foram os seguintes:

- Curvas típicas de fluência apresentadas para as diferentes cargas de fluência consideradas. Houve uma grande mudança no tempo de falha para juntas submetidas a cargas relativamente próximas. O tempo até a falha para as juntas testadas a 75% de P_{max} foi de cerca de 12-h, já para a carga de 70% de P_{max} não houve ruptura após os 30 dias (720-h). Dessa forma, a fluência terciária ocorreu somente para os corpos de prova testados a 80% e 75% de P_{max}. O limite de resistência de carga para as juntas ENF foi então obtido como sendo 70% da força máxima (P_{max}). Para a fluência, o limite de resistência de carga é definido como a máxima carga que uma junta pode resistir sem propagação da trinca após um determinado tempo (no caso, 30 dias);
- As curvas de fluência foram plotadas em um mesmo gráfico, obtendo-se assim o diagrama de resistência de fluência em relação ao tempo. Conectando-se os pontos do início da fluência terciária, o envelope de falha foi então obtido, conforme mostrado na Figura 9. Esse envelope apresenta uma referência do tempo e da carga que uma junta submetida a fluência deve falhar. Assim, para diferentes cargas de fluência, os tempos até a ruptura podem ser estimados por esse envelope;
- A energia de fratura de fluência em modo II (G_{IICr}) foi obtida utilizando-se o método CBBM. Para maiores cargas de fluência maiores valores de G_{IICr} são obtidos. Quando a carga de fluência diminuiu de 80% para 75% de P_{max}, G_{IICr} diminuiu 30%. Já quando a força de fluência diminuiu de 75% para 70% de P_{max}, G_{IICr} diminuiu 14%. Essa menor redução se deve a menor taxa de deslocamento que ocorreu nas

juntas testadas a 70% da força máxima. Assim, a energia de fratura de fluência obtida para a carga de 70% de P_{max} é a máxima quantidade de energia que a junta pode absorver quando submetida a esse esforço por 30 dias. Assim como a energia crítica de fratura em modo II (G_{IIC}) é uma propriedade essencial na modelagem de juntas submetidas a carregamentos estáticos, a energia de fratura de fluência em modo II (G_{IICr}) se apresenta como uma propriedade útil na modelagem de juntas submetidas a carregamentos de fluência;

- A curva de carga versus vida de fluência foi apresentada, demonstrando o limite de resistência de carga para as condições testadas;
- A curva G_{IICr} versus vida de fluência também foi apresentada, sendo proposta uma função exponencial para descrever o comportamento observado. Assim, de acordo com o tempo até a falha, o valor de G_{IICr} pode ser obtido;
- As falhas adesivas e coesivas das juntas foram analisadas, concluindo-se que maiores cargas de fluência conduzem a um maior espalhamento da rugosidade ao longo da camada adesiva, resultando em maiores valores de G_{IICr}.

Figura 9 – Curvas típicas de fluência e envelope de falha.

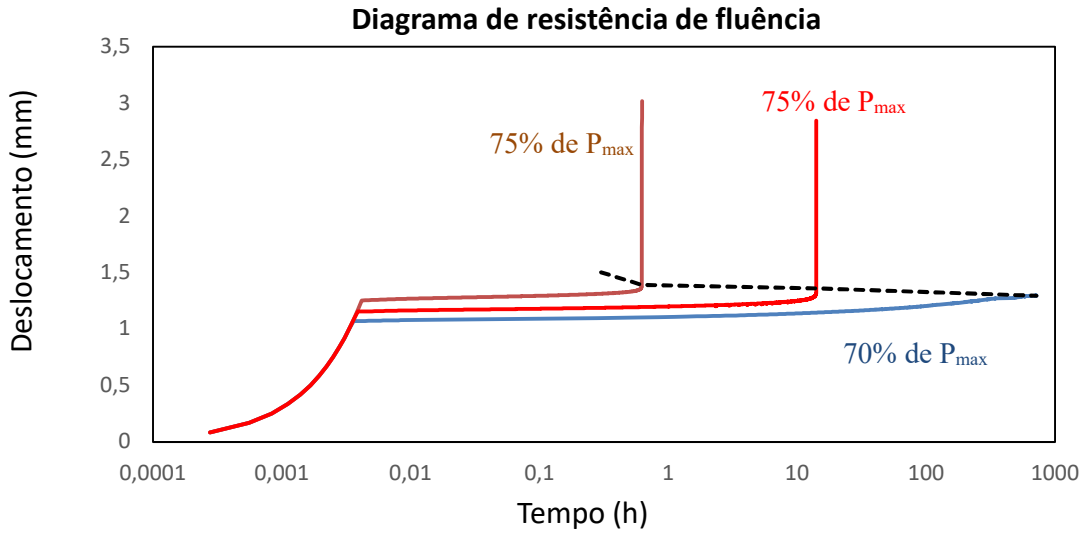

Fonte: O autor, 2022.

O principal legado desse trabalho foi apresentar o conceito de energia de fratura de fluência e demonstrar sua utilidade para fins de projeto. Além disso, foi investigada a fluência nos ensaios ENF, o que não tinha sido feito até então. Resultados impactantes confirmaram a relevância desse estudo, especialmente a grande diferença na vida de fluência para cargas relativamente próximas.

2.3. Artigo 3 – Modelos de dano coesivo para a avaliação da vida de fluência de cisalhamento em juntas coladas (*Cohesive zone models for the shear creep life assessment of bonded joints*) – *Mechanics of Time-Dependent Materials*

O objetivo desse artigo foi propor duas funções que pudessem calcular a energia de fratura em modo II para diferentes cargas e tempos de fluência, devendo os resultados estar em acordo com os dados experimentais obtidos no Artigo 1. Com esse propósito, regressões lineares e não lineares foram realizadas para que os valores dos parâmetros dos dois modelos (funções) fossem obtidos. Dois métodos foram utilizados nas regressões: i) método dos mínimos quadrados (MMQ), e ii) método de Levenberg-Maquardt (MLM). Alguns resultados experimentais adicionais (não utilizados nas regressões) foram usados para avaliar e validar os modelos propostos. Por fim, as funções propostas foram implementadas em uma sub-rotina UMAT para que a curva de fluência numérica fosse comparada com a curva experimental, verificando-se assim a adequabilidade das funções propostas.

As funções de duas variáveis (tempo (t) e carga (F)) propostas para calcular a energia de fratura residual (G_{IIR}) estão apresentadas nas Equações (2.1) (modelo 1) e (2.2) (modelo 2).

$$G_{IIR}(t,F) = \left[\left(\frac{1}{z_1}\right)(1.93z_1 + t)\left(1 - \frac{t}{720}\right)^{z_2}\right][z_3F + z_4] \tag{2.1}$$

$$G_{IIR}(t,F) = a_1 + a_2t + a_3F + a_4t^2 + a_5F^2 + a_6tF \tag{2.2}$$

onde z_1, z_2, z_3, e z_4 (Equação (2.1)) e $(a_1, \dots, a_6)$ (Equação (2.2)) são os coeficientes que devem ser obtidos através das regressões, sendo ajustados para que os resultados obtidos pelos modelos estejam condizentes com os experimentos.

Para o modelo 1 foi utilizado apenas o MLM na regressão. Para o modelo 2, foram utilizados tanto o MLM quanto o MMQ. Comparando-se os valores de G_{IIR} obtidos experimentalmente com aqueles obtidos pelos modelos propostos, baixos erros percentuais foram obtidos, sendo o valor máximo de 13.5% (para o modelo 2 – MMQ), conforme mostrado na Tabela 1. Os resultados experimentais adicionais foram utilizados para validar os modelos, já que esses dados não foram utilizados na obtenção dos parâmetros dos modelos (células em cinza na Tabela 1). Apesar de um erro percentual mais alto do que o esperado (28.1 %) ter sido obtido no modelo 1 – MLM, os demais erros foram menores que 11%, demonstrando a adequabilidade dos modelos. Os valores dos resíduos foram também apresentados,

demonstrando a baixa diferença das energias críticas experimentais e as obtidas nos modelos propostos.

A soma quadrática dos resíduos foi utilizada para que o modelo e método com maior precisão fosse identificado, sendo este o modelo 2 com o método de Levenberg-Marquardt.

Os modelos calibrados foram utilizados na sub-rotina UMAT, sendo obtidas três curvas de fluência para a carga constante de 60% da P_{max}: i) modelo 1 – MLM, ii) modelo 2 – MLM e iii) modelo 2 – MMQ. As curvas numéricas foram comparadas com as curvas experimentais obtidas com a mesma carga de fluência (60% da P_{max}) e tempos de 12-h e 48-h. Boa concordância numérica e experimental foi observada em todos os casos, demonstrando a adequabilidade dos modelos propostos.

Finalmente, em cada carga de fluência avaliada, a variação de G_{IIR} ao longo do teste de fluência para cada modelo foi apresentada.

Tabela 1 – Valores da energia de fratura experimentais e numéricos com os respectivos erros.

Tempo (h)	F (% da força máxima)	I – Resultados experimentais (N/mm)	Modelo 1 MLM - (N/mm)	Modelo 1 MLM – Erro percentual (%)	Modelo 2 MMQ - (N/mm)	Modelo 2 MMQ - Erro percentual (%)	Model 2 MLM - (N/mm)	Model 2 MLM - Erro percentual (%)
12	0.4	1.877	2.01	6.9%	2.130	13.5%	2.007	6.9%
24	0.4	2.283	2.21	3.3%	2.266	0.7%	2.221	2.7%
48	0.4	2.094	2.09	0.3%	1.979	5.5%	2.026	3.2%
12	0.5	2.533	2.31	8.8%	2.344	7.5%	2.337	7.7%
24	0.5	2.544	2.54	0.2%	2.556	0.5%	2.574	1.2%
48	0.5	2.259	2.40	6.3%	2.420	7.1%	2.425	7.4%
12	0.6	2.515	2.61	3.9%	2.493	0.8%	2.581	2.6%
24	0.6	2.808	2.87	2.2%	2.781	1.0%	2.841	1.2%
48	0.6	2.837	2.72	4.3%	2.796	1.5%	2.738	3.5%
60	0.6	2.522	1.81	28.1%	2.524	0.1%	2.376	5.8%
24	0.7	3.300	3.20	2.9%	2.941	10.9%	3.022	8.4%

Fonte: O autor, 2022.

O principal legado do trabalho foi apresentar duas funções de duas variáveis que calculassem adequadamente as energias críticas de fratura, levando em consideração o efeito da fluência. Essas funções são essenciais para a modelagem numérica, já que nas simulações realizadas os parâmetros coesivos variam em cada incremento de tempo. Assim, deve-se conhecer tais propriedades não somente nos tempos de fluência utilizados nos experimentos (12-h, 24-h, 48-h), mas também ao longo de toda simulação, incluindo-se os tempos entre 0 e 12-h, 12-h e 24-h e 24-h e 48-h.

2.4. Artigo 4 – Lei de tração-separação de cisalhamento customizada para modelagem de zonas coesivas de juntas ENF submetidas a fluência (*A customized shear traction separation law for cohesive zone modelling of creep loaded ENF adhesive joints*) – *Theoretical and Applied Fracture Mechanics*

Esse trabalho trata da simulação numérica dos ensaios de fluência nas juntas do tipo ENF descritos no Artigo 1. Os modelos de danos coesivos, apesar de amplamente utilizados na modelagem de juntas coladas, não haviam sido utilizados até então no estudo da fluência. Assim, o principal objetivo desse artigo foi simular o comportamento de fluência de juntas adesivas submetidas a cargas de cisalhamento utilizando um modelo de dano coesivo (MDC) customizado (modificado). Esse modelo é a principal contribuição científica dessa tese. A sub-rotina UMAT foi utilizada nas simulações efetuadas no software Abaqus.

A evolução do dano do MDC customizado é simulado pela lei triangular. Porém, essa lei triangular não é mais estática, e sim dinâmica. Isso significa que a máxima tração suportada pelos pares de nós homólogos (τ) dos elementos coesivos é modificada ao longo do ensaio de fluência (ver Figura 7), assim como o deslocamento final (δ_f). Em outras palavras, as dimensões do triângulo são ajustadas ao longo da simulação, variando-se assim a energia de fratura em modo II, o que precisa ser feito em acordo com os valores experimentais apresentados no Artigo 1.

As equações (2.3) e (2.4) foram apresentadas nesse artigo, representando as variações da energia de fratura em modo II (G_{IIR}) e da tensão de cisalhamento máxima (τ_m), respectivamente.

$$G_{IIR}(t,F) = z_1 + z_2 t + z_3 F + z_4 t^2 + z_5 F^2 + z_6 tF \tag{2.3}$$

onde *t* é o tempo de fluência ao longo da simulação, *F* é a carga de fluência, e $(z_1, \dots, z_n)$ são os parâmetros do modelo proposto, obtidos através do método dos mínimos quadrados (ver Seção 1.4.1).

$$\tau_m = (\tau_o - b)(1 - \frac{t}{t_t})^k \tag{2.4}$$

onde τ_o é a tensão de cisalhamento máxima inicial, t_f é o tempo total até a falha, *t* é o tempo corrente da simulação, *b* e *k* são parâmetros de ajuste do modelo.

O MDC modificado foi então implementado através da sub-rotina UMAT, sendo obtidas as curvas numéricas de fluência para os diferentes conjuntos de valores de *b* e *k*, os quais foram ajustados para que ocorresse uma aproximação dos resultados numéricos e experimentais. Dessa forma, para cada carga de fluência considerada, diversas curvas numéricas foram geradas, cada uma referente a um conjunto de valores de *b* e *k* (ver Equação (2.4)), conforme exemplificado na Figura 10 (carga de fluência de 50% de P_{max}). A faixa de valores *b* e *k* foram, respectivamente, de 0.5 a 3.5 e de 1 e 4. O parâmetro *b* influencia majoritariamente a fluência primária, sendo observado que maiores valores de *b* conduzem a maiores taxas de deslocamento. Já a fluência secundária é afetada principalmente pelo parâmetro *k*, já que maiores valores de *k* conduzem a maiores deslocamentos de fluência.

Figura 10 – Curvas experimental e numéricas para a carga de fluência equivalente a 50% de P_{max}.

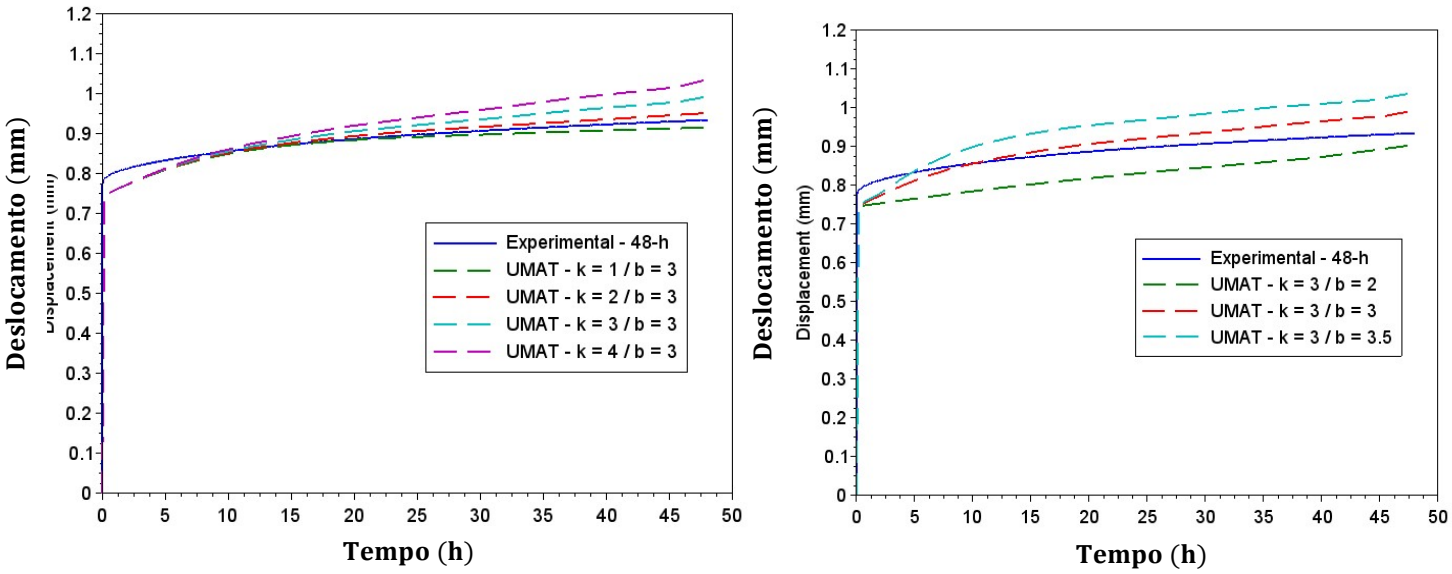

Fonte: O autor, 2022.

Em geral, as curvas de fluência (deslocamento x tempo) numéricas e experimentais apresentaram boa concordância. A fim de se obter a melhor curva numérica para cada carga de fluência simulada, uma análise estatística foi realizada. As diferenças entre os deslocamentos obtidos numericamente e experimentalmente foram registradas em diversos instantes (2-h, 4-h, 8-h, etc.), sendo calculada a soma quadrática dessas diferenças para cada conjunto de parâmetros *b* e *k*. Assim, o conjunto de valores *b* e *k* com menor valor caracterizou a melhor curva numérica para cada carga de fluência. Para tais curvas, a menor diferença percentual entre as simulações e os experimentos foi de 11%, considerando os diversos instantes avaliados ao longo da simulação. De qualquer forma, é importante destacar que as outras curvas numéricas

também apresentaram resultados aceitáveis, já que o erro percentual máximo para todos os casos foi de 20%.

Para validar o modelo de dano coesivo customizado um teste de fluência adicional em uma junta ENF foi realizado, onde a carga de fluência foi equivalente a 45% de P_{max} e o tempo total de ensaio foi 18-h. Os resultados desse ensaio não foram utilizados na calibração dos parâmetros *b* e *k*. A curva de fluência experimental foi então comparada com a curva numérica obtida nas mesmas condições, sendo novamente obtida uma boa proximidade entre as curvas experimental e numérica, confirmando a adequabilidade do modelo proposto.

Por fim, a lei de tração separação customizada para a carga de fluência de 50% de P_{max} foi apresentada, assim como os gráficos que mostram as variações de alguns parâmetros coesivos: deslocamento final (δ_f) e energia de fratura residual em modo II (G_{IIR}).

O principal legado desse trabalho foi apresentar detalhadamente um modelo de dano coesivo customizado capaz de modelar a fluência das juntas ENF, desenvolvido especialmente para considerar a mudança dos parâmetros coesivos por conta da fluência ao longo da simulação.

3. DISCUSSÃO

O desenvolvimento de um modelo de dano coesivo para investigar a fluência de juntas coladas submetidas a esforços de cisalhamento necessita de uma análise experimental prévia. Assim, pode-se mensurar como a energia de fratura em modo II está variando de acordo com o tempo e com a carga de fluência. Durante a intensa investigação experimental realizada (especialmente nos Artigos 1 e 2), resultados não intuitivos foram constatados, com destaque para o aumento de G_{IIC} e P_{max} para maiores tempos e maiores cargas de fluência. Dessa forma, para condições controladas de tempo e carga, a fluência nas juntas ENF não degrada as propriedades da junta, mas sim aumenta a resistência das mesmas, chegando a um crescimento de 26% na força máxima e 47% na energia de fratura. A principal razão para esse aumento das propriedades são as tensões residuais, as quais são induzidas pela deformação viscosa que ocorre frequentemente em materiais poliméricos quando submetidos a fluência. Outra possível razão para este crescimento é o alinhamento das cadeias poliméricas, que ocorre devido ao fluxo viscoso causado pela aplicação de cargas constantes por longos períodos (Wu, 2019). Assim, como a resistência é maior na direção paralela as cadeias, o aumento da força máxima é observado. Esses efeitos devem ser considerados no modelo numérico desenvolvido, para que a simulação traduza adequadamente o que ocorre nos experimentos.

As energias de fratura residuais foram então obtidas (Artigo 1) para condições específicas de tempos (12-h, 24-h, 48-h) e cargas de fluência (40%, 50% e 60% de P_{max}). Na análise numérica realizada com elementos coesivos, essa propriedade deve ser informada a cada incremento de tempo da simulação, ou seja, é necessário informar G_{IIR} para tempos entre 0 e 12-h, 12-h e 24-h e entre 24-h e 48-h, pois G_{IIR} não foi obtido experimentalmente nesses intervalos. Essa é a principal razão da proposição das funções apresentadas nas Equações (2.1) e (2.2) (Artigo 3), possibilitando assim a obtenção de G_{IIR} para quaisquer tempo e carga dentro das faixas avaliadas experimentalmente. Porém, essa função deve traduzir a tendência observada nos experimentos: i) para um mesmo tempo, maiores cargas de fluência levam a maiores valores de G_{IIR}, ii) fixando-se a carga de fluência, G_{IIR} aumenta até um tempo específico (ponto ótimo) e depois começa a diminuir. As regressões lineares e não lineares foram realizadas para que as constantes das funções propostas fossem calculadas de maneira consistente, ou seja, fazendo com que as funções estimassem a energia de fratura de acordo com a tendência experimental. Para tal intuito, foram aplicados os métodos de Levenberg-Marquardt e o método dos mínimos quadrados. Os resultados foram validados com experimentos adicionais, os quais não foram previamente utilizados na obtenção das constantes

de cada função proposta. O principal objetivo do Artigo 3 foi obter essas constantes, além de avaliar qual das duas funções produz curvas numéricas de fluência mais próximas das experimentais.

O modelo de dano coesivo modificado apresentado detalhadamente no Artigo 4 considerou, além da mudança da energia crítica residual, a degradação da tensão de cisalhamento ao longo do tempo, de acordo com a Equação (2.4). Equação similar foi apresentada no trabalho de Costa et. al. (2018) na modelagem de adesivos degradados por conta da umidade e fadiga. A degradação da tensão é parte essencial do modelo de dano coesivo proposto, pois como a simulação realizada é estática, forças constantes iriam gerar deslocamentos constantes. Já com a diminuição da tensão ao longo do tempo, os deslocamentos aumentam durante a simulação, assim como ocorre nos experimentos. As constantes b e k da Equação (2.4) foram calibradas de acordo com os resultados experimentais obtidos para cada condição de carga e tempo, podendo posteriormente serem implementadas na sub-rotina UMAT.

De maneira geral, as curvas de fluência numéricas tiveram boa proximidade com as curvas experimentais (Artigos 3 e 4). Um teste de fluência adicional foi realizado a 45% de P_{max} por 18-h (Artigo 4), para que o modelo coesivo modificado fosse então validado. Novamente, uma boa concordância numérica e experimental foi verificada.

O Artigo 2 complementou a investigação experimental, onde foi apresentado o conceito de energia de fratura de fluência em modo II (G_{IICr}), sendo realizados ensaios de fluência até a ocorrência da falha, o que não havia sido feito para os ensaios ENF. Esse trabalho constatou uma grande diferença no tempo de falha de fluência das juntas ENF para cargas relativamente próximas. Obteve-se também a carga de endurecimento por fluência, sendo considerado o tempo de 30 dias. Assim, a carga máxima na junta ENF (nas mesmas condições apresentadas) que pode ser aplicada por 30 dias sem que ocorra propagação da trinca por conta da fluência é equivalente a 70% da força máxima (P_{max}) obtida no ensaio ENF estático.

CONCLUSÕES

O principal objetivo da presente tese foi desenvolver um modelo de dano coesivo modificado para juntas do tipo ENF. Para tal intuito, foi investigado experimentalmente os efeitos da fluência na energia crítica de fratura em modo II (G_{IIC}), assim como na força máxima do ensaio ENF (P_{max}). Foram considerados dois fatores de influência: tempo e carga. Os experimentos foram divididos em duas partes: i) fluência com tempo pré-definido e ii) fluência até a propagação da trinca.

Na primeira parte dos experimentos as juntas foram testadas com cargas e tempos pré-definidos (Artigo 1). Os resultados experimentais mostraram que, de maneira geral, G_{IIC} e P_{max} aumentam para maiores tempos e maiores cargas de fluência. Porém, o aumento das propriedades tem um limite, a partir do qual as propriedades das juntas começam a se degradar até a ruptura. Dessa forma, um "ponto ótimo" pode ser investigado para cada carga de fluência. No caso que a carga de fluência foi igual a 60% da força máxima, o tempo de fluência do "ponto ótimo" foi 48-h.

Na segunda parte dos experimentos os testes de fluência foram realizados até a ocorrência da falha (Artigo 2), sendo pré-determinado um tempo máximo de 720-h (30 dias). O limite de endurecimento a fluência foi obtido, sendo equivalente a 70% de P_{max}. Ou seja, essa é a máxima carga que a uma junta colada pode absorver sem que ocorra propagação da trinca após os 30 dias do teste de fluência. Quando a carga de fluência aumentou para 75% de P_{max} o tempo de falha foi inferior a um dia, demonstrando a sensibilidade das juntas a fluência mesmo com pequenas diferenças de cargas. Maiores valores da energia de fratura de fluência em modo II foram obtidos para maiores cargas. Um comparativo com as energias de fratura crítica e residual foi realizado.

Duas funções para descrever a energia residual (G_{IIR}) em função das pré-cargas de fluência e dos tempos foram propostas e validadas no Artigo 3. De posse dessas funções, o modelo de dano coesivo modificado foi testado, apresentando boa concordância numérica e experimental. O Artigo 4 apresentou de forma detalhada o modelo de dano coesivo modificado, demonstrando a variação nas dimensões da lei de tração-separação triangular de acordo com a evolução do tempo na simulação. Uma equação para descrever a degradação da tensão de cisalhamento máxima do adesivo foi proposta (Equação (2.4)), sendo também utilizada a Equação (2.2) (a mesma do Artigo 3) para descrever a mudança da energia de fratura residual ao longo das simulações. Os efeitos dos parâmetros b e k da Equação (2.4) foi investigado, os quais influenciam predominantemente a fluência primária e secundária, respectivamente. Os

erros do modelo de dano coesivo proposto foram quantificados, sendo a maior diferença percentual entre os dados numéricos e experimentais de 20%. Um experimento adicional foi realizado para que o MDC modificado fosse validado. Por fim, os parâmetros coesivos foram avaliados através da variação da lei triangular, deslocamento final e energia de fratura residual.

SUGESTÕES PARA TRABALHOS FUTUROS

Investigações experimentais em modo I poderão ser realizadas posteriormente, para que seja avaliada se a mudança das propriedades das juntas submetidas a carregamentos em modo I ocorrem de maneira similar aquelas carregadas em modo II. Após os resultados experimentais, um modelo de dano coesivo modificado também poderá ser implementado para descrever a fluência do ensaio *double cantilever beam* (DCB).

Para que o modelo desenvolvido seja mais abrangente, estudos relacionados ao modo misto também devem ser realizados, o que tornaria o modelo mais robusto e completo, sendo em contrapartida consideravelmente mais complexo.

Por fim, o modelo numérico apresentado nesse trabalho foi aplicado somente na modelagem da fluência primária e secundária. Assim, esforço adicional poderá ser realizado para simular também a fluência terciária, podendo os resultados experimentais do Artigo 2 serem usados para validar tal modelo.

REFERÊNCIAS

AJDANI, A. et. al. Mixed mode fracture characterization of brittle and semi-brittle adhesives using the SCB specimen, International Journal of Adhesion and Adhesives, 101, 102629, 2020. https://doi.org/10.1016/j.ijadhadh.2020.102629

ARAÚJO, Rui Valdemar Correia, Validação numérica de leis coesivas triangulares para previsão de resistência de juntas adesivas em tração e corte puros, Dissertação (Mestrado em Engenharia Mecânica), Instituto Superior de Engenharia do Porto, Porto, 2016.

ASTER, R. C.; BORCHERS, B.; THURBER, C.H. Parameter Estimation and Inverse Problems, 2th ed, Elsevier, Waltham, USA, 2013.

ASTM D2293 - Standard Test Method for Creep Properties of Adhesives in Shear by Compression Loading (Metal-to-Metal), 1996.

AZEVEDO, João Carlos Silva. Determinação da tenacidade a fratura em corte (GIIc) de adesivos estruturais pelo ensaio End-Notched Flexure (ENF), Dissertação (Mestrado em Engenharia Mecânica), Faculdade de Engenharia da Universidade do Porto, Porto, 2014.

BOTELHO, Fabrício Vieira Cunha. Análise Numérica do Comportamento Mecânico do Sal em Poços de Petróleo, Dissertação (Mestrado em Engenharia Civil), PUC-RJ, Rio de Janeiro, 2008.

CAMPILHO, R. D. S. G. et al. Modelling adhesive joints with cohesive zone models: effect of the cohesive law shape of the adhesive layer, International Journal of Adhesion & Adhesive, p. 48-56, 2013.

CAMPILHO, R. D. S. G. et al. Modelling of Single-Lap Joints Using Cohesive Zone Models: Effect of the Cohesive Parameters on the Output of the Simulations, The Journal of Adhesion, p. 513-533, 2012.

CAMPO, E. A. Selection of Polymeric Materials, William Andrew Publishing, 2008.

CARNEIRO NETO, R. M. et. al. Study of the Life Span of Adhesively Bonded Single Lap Joint Due to Creep, Revista Matéria, vol. 26, nº 4, 2021.

CARNEIRO NETO, Ranulfo Martins. Análise numérica e experimental de juntas coladas em duas configurações: junta de cisalhamento simples e junta de carregamento combinado, Dissertação (Mestrado em Modelagem Computacional), Universidade Estadual do Rio de Janeiro, Nova Friburgo, 2017.

CAVALCANTE, Alberto Douglas Silva. Modelagem Numérica de Escavações de Túneis em Maciços Evaporíticos, Dissertação (Mestrado em Geotecnia), Escola de Engenharia de São Carlos da Universidade de São Paulo, São Carlos, 2012.

CHEN, Y.; SMITH, L. V. A nonlinear viscoelastic–viscoplastic constitutive model for adhesives under creep, Mechanics of Time-Dependent Materials, 2021.

CHOI K. K.; TAHA M. M. R. Rheological modeling and finite element simulation of epoxy adhesive creep in FRP-strengthened RC beams, Journal of Adhesion Science and Technology, 27:5-6, 523-535, 2013.

COSTA, I.; BARROS, J. Tensile creep of a structural epoxy adhesive: Experimental and analytical characterization, International Journal of Adhesion & Adhesives, 59, 115–124, 2015. http://dx.doi.org/10.1016/j.ijadhadh.2015.02.006

COSTA, M.; VIANA, G.; CRÉAC'HCADEC, R., DA SILVA, L. F. M.; CAMPILHO, R. D. S. G. A cohesive zone element for mode I modelling of adhesives degraded by humidity and fatigue, International Journal of Fatigue, 112, 173-182, 2018.

CUEVAS, Victor Crespo. Linking ABAQUS 2019 and Intel oneAPI Base Toolkit (FORTRAN Compiler), Technical Report, University of Colorado Boulder, 2021.

DA SILVA, L. F. M.; CAMPILHO, R. D. S. G. Advances in Numerical Modelling of Adhesive Joints, Springer Briefs in Computational Mechanics, 2012.

DA SILVA, L. F. M.; OCHSNER, A.; ADAMS, R. D. (eds), Handbook of Adhesion Technology, Springer-Verlag Berlin Haidelberg, 2018.

DA SILVA, Ricardo Hudson. Estudo do fator de forma de área em reparo com chapa colada em tubulações com furo, Dissertação (Mestrado em Ciência e Tecnologia dos Materiais), Universidade Estadual do Rio de Janeiro, Nova Friburgo, 2015.

DA SILVA, R. H.; SAMPAIO E. M.; ROHEM, N.R.; CARNEIRO NETO, R. M. Development of pipe repairs using bonded metal plate – Part I: Shape factor, stiffness and surface treatment, 100, 102594, 2020. DOI https://doi.org/10.1016/j.ijadhadh.2020.102594

DE MOURA, M. F. S. F. Numerical simulation of the ENF test for the mode-II fracture characterization of bonded joints, Journal of Adhesion Science and Technology, 20:1, 37-52, 2006. https://doi.org/10.1163/156856106775212422

DE MOURA, M. F. S. F.; MORAIS, J. J. L.; DOURADO, N. A new data reduction scheme for mode I wood fracture characterization using the double cantilever beam test, Engineering Fracture Mechanics, 75, 3852-3865, 2008.

DILLARD, D. A. (eds), Advances in Structural Adhesive Bonding, Woodhead Publishing Limited, 2010.

ESPINHA, Rodrigo de Souza Lima, Suporte topológico em paralelo para malhas de elementos finitos em análises dinâmicas de fratura e fragmentação, 2011. 122 f. Tese (Doutorado em Informática), Pontífica Universidade Católica do Rio de Janeiro, Rio de Janeiro, 2011.

FENG C. W. et. al. Modeling of long-term creep behavior of structural epoxy adhesives. Int J Adhes Aches, 25(5):427–436, 2005.

KHABAZAGHDAM, A. et. al. Creep behaviour of a graphene-reinforced epoxy adhesively bonded joint: experimental and numerical investigation, The Journal of Adhesion, 97(13), 1189-1210, 2020. DOI: 10.1080/00218464.2020.1742114

KHALILI, S. M. R.; FATHOLLAHI, M. R. Creep analysis in smart single-strap adhesive joints reinforced by shape memory alloys—Experimental study, International Journal of Adhesion & Adhesives, 54, 21-29, 2014. https://doi.org/10.1016/j.ijadhadh.2014.03.008

KHALILI, S. M. R.; JAFARKARIMI, M. H.; ABDOLLAHI, M. A. Creep analysis of fibre reinforced adhesives in single lap joints—Experimental study, International Journal of Adhesion & Adhesives, 29, 656–661, 2009.

LEVENBERG, K. A Method for the Solution of Certain Non-Linear Problems in Least Squares. The Quarterly of Applied Mathematics, 2, pp. 164-168, 1944.

MAJDA, P.; SKRODZEWICZ, J. A modified creep model of epoxy adhesive at ambient temperature, International Journal of Adhesion & Adhesives, 29, 396–404, 2009.

MARQUARDT, D. W. An Algorithm for Least-Squares Estimation of Nonlinear Parameters. Journal of the Society for Industrial and Applied Mathematics, vol. 11, no. 2, Society for Industrial and Applied Mathematics, pp. 431–41, 1963.

MIRAVALLES, Miguel. The creep behaviour of adhesives: A numerical and experimental investigation, Dissertação (Mestrado em Engenharia Estrutural), Chalmers University of Technology, 2007.

QUEIROZ, R. A. et. al. Study on the creep behavior of bonded metallic joints, Applied Adhesion Science, 2:8, 2014. DOI 10.1186/2196-4351-2-8

QUEIROZ, Rodrigo Albani, Estudo do comportamento em fluência de juntas metálicas coladas, Dissertação (Mestrado em Ciência e Tecnologia dos Materiais) – Instituto Politécnico do Rio de Janeiro, Nova Friburgo, 2013.

SADIGH, M. A. S. Creep simulation of adhesively bonded joints using modified generalized time hardening model, Journal of Mechanical Science and Technology, 30, 1555-1561, 2016. DOI 10.1007/s12206-016-0310-7

SADIGH, M. A. S. et. al. Creep behaviour and tensile response of adhesively bonded polyethylene joints: Single-Lap and Double-Strap, International Journal of Adhesion and Adhesives, 102, 102666, 2020.

SADIGH, M. A. S. et. al. Creep deformation simulation of adhesively bonded joints at different temperature levels using a modified power-law model, Polymer Testing, 79 (2019). https://doi.org/10.1016/j.polymertesting.2019.106087

SANTOS, João Paulo Lima. Análise de modelos reológicos viscoelásticos através de formulações mistas em elementos finitos, Dissertação (Mestrado em Ciências e Engenharia Civil), Universidade Federal do Rio de Janeiro, Rio de Janeiro, 2008.

SILVA NETO, A. J.; BECCENERI, J. C.; CAMPOS VELHO, H. F. Inteligência computacional aplicada a problemas inversos em transferência radiativa, Rio de Janeiro, EdUERJ, 278 p. ISBN 978-85-7511-368-4, 2016.

SIQUEIRA, Mila. Análise do comportamento em fluência de juntas metálicas coladas, Dissertação (Mestrado em Ciência e Tecnologia dos Materiais), Universidade Estadual do Rio de Janeiro, Nova Friburgo, 2019.

WU, C, et. al. Understanding Creep Behavior of Semicrystalline Polymer via Coarse-Grained Modeling, Journal of Polymer Science, Part B: Polymer Physics, 2019. https://doi.org/10.1002/polb.24912

ZEHSAZ, M.; FARID, V. T.; SADIGH, M. A. S. Modified creep constitutive equation for an epoxy-based adhesive with nonlinear viscoelastic behavior, J Strain Analysis, Vol. 50(1) 4–14, 2015. DOI: 10.1177/0309324714554965

ZEHSAZ, M.; TAHAMI, F. V.; SADIGH, M. A. S. Creep analysis of adhesively bonded single lap joint using finite element method, Journal of Mechanical Science and Technology, 28, 2743-2748, 2014. DOI 10.1007/s12206-014-0508-5

ZEHSAZ, M.; VAKILI-TAHAMI, F.; SADIGH, M. A. S. Parametric study of the creep failure of double lap adhesively bonded joints, Materials and Design, 64, 520-526, 2014a.

ZUGLIANI, P. A. et al., Bonded composite repair of metallic pipeline using energy release rate method, Journal of Adhesion Science and Technology, 33:19, 2141-2156, 2019. DOI: 10.1080/01694243.2019.1632537.

ANEXO A – Efeito da fluência na energia de fratura residual de adesivos em modo II (*Effect of creep on the mode II residual fracture energy of adhesives) – Journal of Applied Polymer Science*

Received: 2 April 2021 | Revised: 24 June 2021 | Accepted: 28 June 2021

DOI: 10.1002/app.51387

ARTICLE

Applied Polymer SCIENCE WILEY

Effect of creep on the mode II residual fracture energy of adhesives

Ranulfo M. Carneiro Neto[1] | **Alireza Akhavan-Safar**[2] | **Eduardo M. Sampaio**[3] | **Joaquim T. Assis**[3] | **Lucas F. M. da Silva**[4]

[1]Center of Technology and Application of Composite Materials, Federal University of Rio de Janeiro, Macaé, Brazil

[2]Institute of Science and Innovation in Mechanical and Industrial Engineering (INEGI), Porto, Portugal

[3]Laboratory of Adhesion and Adherence, University of State of Rio de Janeiro, Polytechnic Institute, Nova Friburgo, Brazil

[4]Departamento de Engenharia Mecânica, Faculdade de Engenharia, Universidade do Porto, Rua Dr. Roberto Frias, Porto, Portugal

Correspondence
Alireza Akhavan-Safar, Institute of Science and Innovation in Mechanical and Industrial Engineering (INEGI), Rua Dr. Roberto Frias, Porto 4200-465, Portugal.
Email: aakhavan-safar@inegi.up.pt

Abstract

Viscous flow that often occurs in adhesive materials leads to a permanent deformation when adhesives are subjected to creep loading. Creep loading has a significant influence on the strength of bonded structures. Due to the viscous behavior, the fracture energy also may change with time for joints that experience creep loading in service. In this work the effects of two creep parameters (creep load and time) on the residual mode II fracture energy of an adhesive was investigated using end notched flexure (ENF) specimens. To achieve this, ENF samples were subjected to different creep loading levels at different creep times followed by quasi static tests to obtain the residual shear fracture energy of the adhesive. Experimental results showed that pre-creep loading of the bonded structures can significantly improve the fracture energy and the static strength of the joints.

KEYWORDS

adhesive, creep, ENF, fracture energy, mode II

1 | INTRODUCTION

The industrial use of structural adhesives has increased in recent years due to several advantages such as the capacity of bonding dissimilar materials, ability in bonding very thin specimens, improving the fatigue life, weight reduction, and good damping properties.[1–3] In some applications, the joints are subjected to a constant static load for a long time. In these cases, a pronounced time-dependent stress–strain behavior in the adhesive is observed.[1] Polymers are considered to be viscoelastic materials, therefore their material behavior is time and temperature dependent. This time dependent response must be considered in mechanical models aiming to increase the reliability of bonded structures, although this makes the design more difficult.[4] Dead loads (creep loading) may often occur due to gravity, resulting in many cases in plastic deformation of the adhesives, which can make their properties time dependent. Creep can be defined as a time dependent permanent deformation of materials when submitted to a constant load,[5] which is generally referred to as creep or retardation.[1] Under static strain conditions, creep is referred as relaxation and a decrease in stress is observed over time, which can occur in a joint with a confined construction.[1] In both cases the adhesives can exhibit viscoelastic and viscoplastic behavior when they are subjected to high temperature and high stress levels.[5] Above the glass transition temperature (T_g) the adhesives present a rubbery state, therefore the displacements at this state are greater than in glassy state,

which can contribute to the failure. Thus, in general the application of adhesives in temperatures close to the T_g is not recommended, as the strength of bonded joints decreases at higher temperatures.[6] Even at room temperature polymeric adhesives present time dependent deformation, although this effect is increased for higher temperatures.[7,8] The rate of deformation depends mainly on the temperature, load, and time.[1,5] One of the main properties of adhesives is the fracture energy, which is employed to simulate the response of bonded joints. For this purpose, cohesive zone model (CZM) approach has been extensively applied in the modeling of bonded joints.[9–11] This methodology combines a stress based analysis and fracture mechanics to model the onset damage and crack propagation, respectively. The critical fracture energy in mode I and II (G_{IC} and G_{IIC}, respectively) can be obtained using non-local parameters (force and displacement), beyond the crack length.[12] To calculate G_{IC}, the DCB (double cantilever beam) test is the most used,[12,13] while the end notched flexure (ENF) test is the most widespread test method to calculate G_{IIC} of adhesives due to its simplicity and easy test set up.[14] The values of critical fracture energy are considered constant in the numerical models, because they do not take into account changes in the residual fracture energy due to creep. In order to obtain mechanical models more consistent, the effects of creep on the critical fracture energies must be evaluated in tensile and shear modes. In saturated bulk adhesive samples at 50°C, creep tests revealed large viscoplastic deformations even at low loads.[15] In this same study, mixed mode flexure (MMF) specimens were tested at various levels of moisture in order to evaluate their dependence on the interfacial fracture strength. The parameters of CZM were moisture dependent and were determined by associating the predicted and experimental results of the MMF tests. The numerical and experimental results were in good agreement, although the model did not consider residual strains. In order to verify the numerical model efficiency, it was applied in thick adherend shear test (TAST) and single lap joint (SLJ) specimens, obtaining a good numerical and experimental correlation.[16] Both works[15,16] did not include adhesive plasticity in the numerical model, which was done by Liljedahl et al.[17]

The mode I and II fracture energies are affected by the temperature level, especially for temperatures above the glass transition temperature (T_g).[18,19] The work of Banea et al.[19] investigated the change in G_{IIC} due to temperature, concluding that G_{IIC} values increase for temperatures well below T_g and decrease as the temperature approaches T_g. The increase in G_{IIC} occurred because as the temperature increases the ductility increases, which results in an additional plastic deformation of the adhesive. In another work, Banea et al.[18] investigated the change in G_{IC} due to temperature. For temperatures below T_g the fracture energy in mode I did not vary considerably. A major change in G_{IC} was verified when the adhesive T_g was overpassed. Xu et. al[20] investigated the effect of environmental aging conditions in the fracture energy in mode I (G_{IC}). DCB tests were performed prior to and after aging at 177 and 204°C for 22 months. Comparing the joints without aging conditions and the joints with aging at 177°C for 22 months, the maximum fracture energy decreased by 34%. Considering the aged joints at 204°C (for 22 months), the maximum fracture energy decreased by 81%. Fernandes et. al[21] investigated the effect of temperature in the fracture behavior of composite joints for pure mode I and II. The specimens were exposed to three temperature levels (0, 25, and 50°C) during 3 months. The results showed that G_{IC} values are similar for 0 and 25°C. A reduction of 33% was observed comparing the specimens tested at 50°C with those tested at 25°C. It must be due to the proximity of T_g. The fracture energy in mode II (G_{IIC}) was similar for the joints aged in 0 and 25°C conditions, and a slight increasing was observed for the specimens aged at 50°C.

The investigation of the creep effect on the strength of adhesive joints are rare in the literature. There are some numerical and experimental studies that aim to predict creep behavior (displacement-time curve) for SLJs[22,23] and double lap joints,[24,25,26] however there is no evaluation in the change of fracture energy.

The degradation of fracture energies may occur due to load application for extended time (sustained load). This specific investigation was not found in literature. Thus, this work aims to study the variation in critical fracture energy in mode II due to creep loading. Mode II was considered in this work, as the whole bonded layer is loaded when a creep load is applied to the joint. But in double cantilever beam (DCB) tests the creep stresses are localized ahead of the crack tip and creep load is not supposed to influence the mode I fracture energy (G_{IC}) because this energy is obtained from the regions in the specimens where creep stresses are not applied to.

The main contribution is the analysis of how the variation in G_{IIC} occurs, according to different times and loads. The usual ENF tests were performed without creep load so that the reference value of G_{IIC} was obtained corresponding to a maximum load (P_{max}). Next, the ENF specimens were submitted to a constant load (creep), considering a fraction of P_{max}. After the creep tests in ENF specimens, the usual ENF test was performed, and the residual fracture energy was obtained.

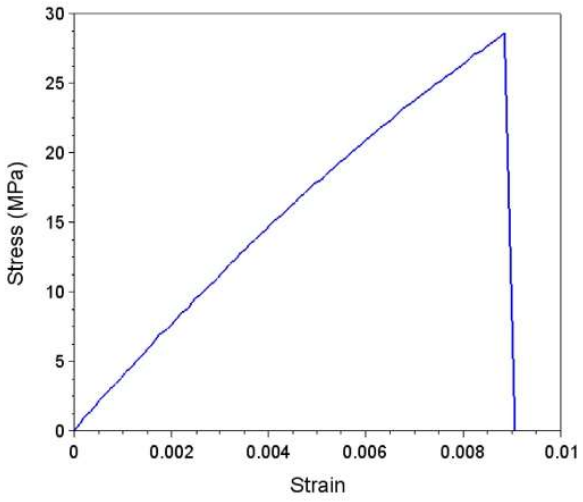

FIGURE 1 Typical stress–strain curve of a tensile test in a bulk specimen of NVT 201E adhesive [Color figure can be viewed at wileyonlinelibrary.com]

2 | EXPERIMENTAL PROCEDURE

In order to investigate the effect of creep on the shear fracture energy of adhesives, ENF specimens were manufactured and tested in the following conditions: (a) quasi-static testing condition, (b) creep test followed by a quasi-static test.

2.1 | Materials

The structural NVT 201E epoxy adhesive (Fine Composites - Brazil) was used to bond carbon steel A1020 substrates for all the tested specimens. This adhesive was used in previous works.[27,28] It is a two-component (with the weight ratio of 100 × 52, resin to hardener, respectively), with the glass transition temperature of 71°C and density of 1.24 g/cm^3. As recommended by the manufacturer, the curing time for this adhesive is 24 h at room temperature. Figure 1 shows a typical stress–strain curve of a bulk specimen obtained in a tensile test, in accordance with ASTM D638 recommendations. Considering five samples, the Young's modulus (E), Poisson' ratio (ν) and tensile failure strength were determined (see Table 1). The transverse and longitudinal deformations were measured by an optical extensometer, so, the Poisson' ratio was calculated. The shear modulus (G) was calculated by the Equation (1). The substrate properties are also presented in Table 1.

$$G = \frac{E}{2(1+\nu)} \quad (1)$$

TABLE 1 Substrate and adhesive properties

Description	Adhesive NVT 201E	Carbon steel A1020[29]
Young's modulus - E	3.13 ± 0.37 GPa	207 GPa
Shear modulus - G	1.21 GPa	75 GPa
Poisson's ratio - ν	0.29 ± 0.09	0.30
Tensile failure strength	28.70 ± 1.66 MPa	400 MPa

2.2 | Joint geometry and manufacturing

The details of the geometry and dimensions of the ENF specimens are shown in Figure 2. The thickness of the metal substrates and the epoxy adhesive were considered as $t_s = 12.7$ mm, and $t_a = 0.4$ mm, respectively. The total length was $2L = 298$ mm, the initial crack length was $a_o = 46$ mm and the width (not shown in Figure 1) was $B = 25.4$ mm. The joint geometry is similar to the one proposed by ASTM D-3433-99 standard. Although this standard treats the fracture energy in mode I (DCB specimens), it is usual to use a similar geometry for mode II, which facilitates the manufacturing process and the comparison of the obtained results.[30]

To manufacture the joints, the substrates were initially sandblasted and then were cleaned with acetone. To guarantee the adhesive thickness in the joint, a calibrated metal strip with the thickness of the adhesive layer was placed at one end, and a double-beveled plate with the same thickness was placed on the other end. The length of the plate with the double-bevel at the end was defined in accordance with the initial crack length (a_o), with an excess length to allow its removal after the curing process.

NVT 201E adhesive was applied on both parts of the substrates. The steel substrates were then bonded and the excess adhesive was removed. The pressure is manually applied by the operator at the mold top. The required adhesive thickness is obtained by adjusting the height between the bottom and top mold parts. The total height is the sum of both substrates' thicknesses and adhesive thickness. Right after the steel substrates are bonded, the excess of adhesive is carefully removed using a spatula. The mold has pins that prevent the substrate misalignment. The average cure time was 24 h, as recommended by the manufacturer. The ambient temperature and humidity were controlled around 22°C and 62%, respectively.

2.3 | Testing conditions

In the first step, usual ENF tests were carried out on some samples using a universal testing machine

(Shimadzu, Autography AG-X Plus, Japan). The tests were performed under displacement control conditions at a rate of 0.5 mm/min. For this step, four specimens were tested. The load and displacement were measured during the tests using the compliance-based beam method (CBBM)[31] for the determination of the critical fracture energy in mode II (G_{IIC}). The average value of the maximum load (P_{max}) was also calculated to be considered as a reference value for the creep loads. The boundary conditions are those shown in Figure 2.

In the second step, creep tests were performed on ENF specimens. During the creep tests, the displacement and the time were measured by the universal testing machine. Two main factors that influence creep are time and load. The creep times considered in this study are 12, 24, and 48 h. For each creep time, the joints were tested at three different load levels: 40%, 50%, and 60% of P_{max}. Three specimens were tested for each condition. Additional tests were performed to investigate the adhesive sensitivity to creep, including testing at higher load level (80% of P_{max}) and for a longer creep time (60 h). Table 2 shows the description of the experiments considered in this study. After the creep test, a visual inspection was done in order to verify if the crack has propagated and also to see if plastic deformation on adherend had occurred. As the creep effect in metals is usually associated with elevated temperatures, which are often greater than roughly half of the absolute melting temperature, the creep effect on the adherends tested at room temperature was considered negligible.[32,33]

The third step occurred about 10 min after the conclusion of the second step. The residual fracture energy in mode II (G_{IIR}) was obtained by performing quasi static tests on ENF samples that had already experienced creep loading based on the conditions explained in Table 2.

3 | DATA REDUCTION METHOD

The CBBM method is based on the concept of the equivalent crack length. It intends to solve the monitoring difficulties in ENF tests.[31] Indeed, this method does not need the direct crack length measurement and the effects of fracture process zone (FPZ) ahead of the crack tip are also taken into account. In the CBBM method, the experimental compliance (C) is obtained from the Castigliano theorem, as a function of the crack length (a)[31]:

$$C = \frac{(3a^3 + 2L^3)}{8EBt_s^3} + \frac{3L}{10GBt_s} \tag{2}$$

where E is the Young's modulus of the substrate and G is the shear modulus. The other parameters are described in Section 2.2.

The flexural modulus of the specimen (E_f) is obtained by rearranging Equation (2), considering the initial compliance (C_o) and the initial crack length (a_o). This procedure is very important because the changeability of the material properties between different samples are taken into account.[31]

$$E_f = \frac{3a_o^3 + 2L^3}{8Bt_s^3 C_{0corr}} \tag{3}$$

where C_{0corr} is calculated by Equation (4)[31]:

$$C_{0corr} = C_0 - \frac{3L}{10GBt_s} \tag{4}$$

Using the flexure modulus of the specimen (E_f) instead the flexure modulus of the substrate in Equation (2), the equivalent crack length is obtained as[31]:

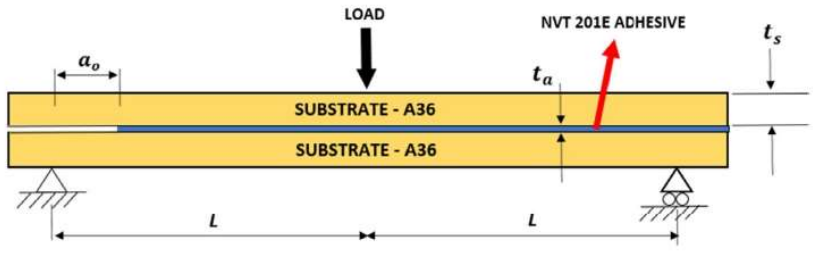

FIGURE 2 Schematic representation of ENF specimens [Color figure can be viewed at wileyonlinelibrary.com]

TABLE 2 Description of the creep experiments

Creep time	12-h	24-h	48-h	60-h
Load (% static strength)	40%, 50%, 60%, 80%[a]	40%, 50%, 60%	40%, 50%, 60%	60%

[a]The crack propagated for both specimens before the creep test completion.

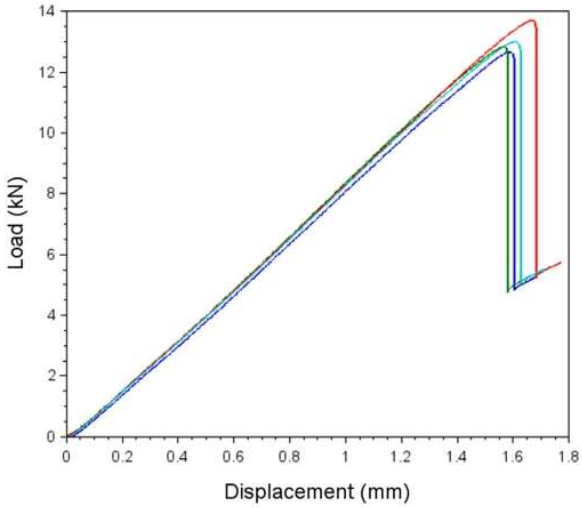

FIGURE 3 Load–displacement curves in ENF tests [Color figure can be viewed at wileyonlinelibrary.com]

$$a_e = a + \Delta a_{ZPF} = \left[\frac{C_{corr}}{C_{0corr}} a_o^3 + \frac{2}{3}\left(\frac{C_{corr}}{C_{0corr}} - 1\right) L^3\right]^{(1/3)} \quad (5)$$

Finally, the critical fracture energy in mode II (G_{IIc}) can be calculated by Equation (6)[31]:

$$G_{IIC} = \frac{9P^2 {a_e}^2}{16B^2 {t_p}^3 E_f} \quad (6)$$

Thus, using the load–displacement (P-δ) data and the equivalent crack length (Equation 5), the R-curve can be obtained. This procedure was done on the first step of experiments (static ENF tests) and in the third step, when ENF tests were performed shortly after the creep tests (second step).

4 | RESULTS AND DISCUSSIONS

4.1 | Quasi-static tests

The curves from of the initial four ENF specimens tested are shown in Figure 3. Good repeatability was observed for the stiffness of the specimens and also for the maximum load. Using the CBBM method, as described in Section 3, the equivalent crack length (a_{eq}) was calculated as well the fracture energy in mode II. Thus, the R-curves were generated (Figure 4) in order to find the critical fracture energy in mode II (G_{IIc}), which is obtained considering the plateau values in the R-curves. As the failure is brittle and the crack propagates in one step, a clear plateau in the R-curve cannot be defined. This way, an average of the energy values was calculated considering the extreme values of the stretch of the R-curve that approaches a straight line, which occurs when the crack (a_{eq}) propagates from 62 to 158 mm approximately.

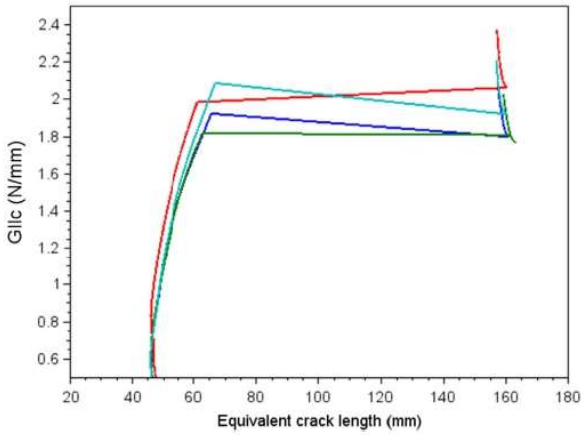

FIGURE 4 R-curves from the ENF tests obtained by the CBBM method [Color figure can be viewed at wileyonlinelibrary.com]

TABLE 3 Static results: Maximum load and critical fracture energy in mode II

Specimen	P_{max} (kN)	G_{IIC} (N/mm)
1	12.66	1.86
2	12.83	1.81
3	13.69	2.05
4	12.99	2.00
Average	13.04	1.93
SD	3%	5%

Table 3 shows the average values of the maximum load (P_{max}) and the shear fracture energy (G_{IIc}). The mean value of P_{max} is used as a reference in step 2, when a percentual value of P_{max} is considered. The mean value of G_{IIc} is used to check the change in the fracture energy of the creep tested ENF samples. This way, this reference value (G_{IIc}) can be compared with the fracture energy values obtained in ENF samples that already experienced creep (the third step).

After the tests, the specimens were opened in order to verify if the failure was cohesive or adhesive. The crack propagation occurred in only one step for all the specimens. Cohesive failures were observed, although the crack path is closer to one interface than the other. These fracture surfaces are presented in Section 4.3.3 and compared with the tested creep aged specimens.

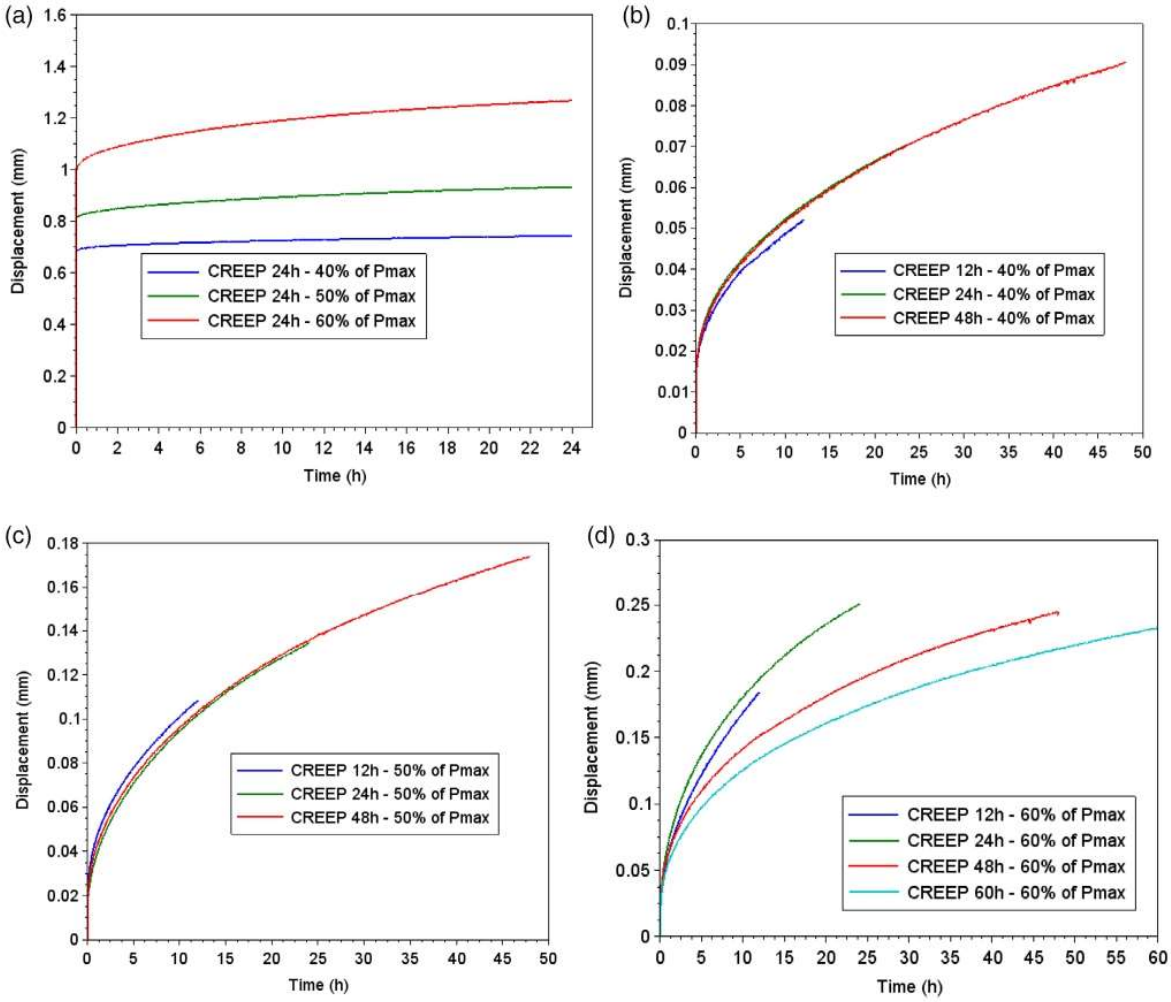

FIGURE 5 Displacement versus time for the creep tests performed: (a) specimens tested for 24-h with different creep loads, (b) specimens submitted to 40% of P_{max} (the primary and secondary creep), (c) specimens submitted to 50% of P_{max} (the primary and secondary creep), (d) specimens submitted to 60% of P_{max} (the primary and secondary creep) [Color figure can be viewed at wileyonlinelibrary.com]

4.2 | Creep tests

As the final goal is to calculate the change in G_{IIc}, the creep tests were monitored with one camera in order to be sure that the crack would not propagate. During creep testing, no plastic deformation of the adherends was observed.

Typical creep curves (displacement vs. time) are shown in Figure 5. In Figure 5(a) there are two regions well defined in the graph: primary and secondary creep - preceded by the instantaneous elastic strain. The instantaneous elastic strain occurs quickly and it is represented by the vertical lines just at the beginning of the creep tests. Then, the primary and secondary creep take place and a delayed elastic strain is observed. In adhesive materials a viscous flow often occurs and it may lead to viscous deformation (non-recoverable),[1] which can create residual stresses. The creep curves do not present tertiary creep because the tests were interrupted and not continued until crack propagation.

Figure 5(a) shows that higher creep loads lead to greater deformations for the same creep time. For the samples tested for 24-h, the final displacement varied from 0.76 mm (40% of P_{max}) to 1.27 mm (60% of P_{max}). Most of the final displacement (more than 75%) is due to the instantaneous elastic deformation. Additionally,

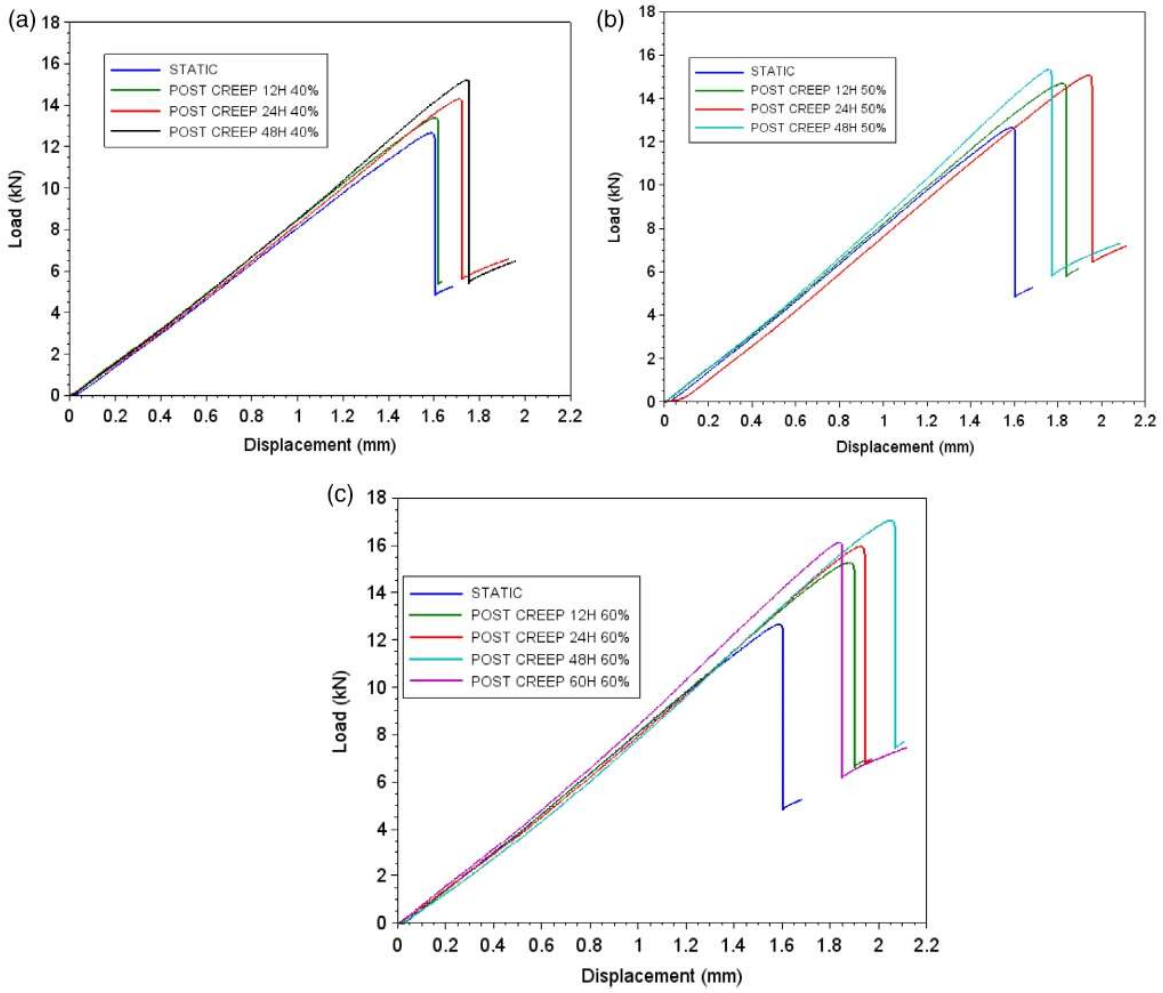

FIGURE 6 Typical load–displacement curves of ENF specimens tested post creep and initial static results without creep for different creep loads: (a) 40% of P_{max}, (b) 50% of P_{max}, and (c) 60% of P_{max} [Color figure can be viewed at wileyonlinelibrary.com]

generally at higher creep times creep displacements are higher. Figure 5(b–d) show the primary and secondary creep curves (the initial displacements were normalized and set to zero), for the samples tested at 40%, 50%, and 60% of P_{max}, respectively. Considering a constant load, the deformation rate for the conditions tested are similar as expected, which can be seen by the proximity of the curves obtained for different creep times, mostly in Figure 5(b,c). This juxtaposition of curves at different times was not observed for the creep load of 60% of P_{max} (Figure 5(d)). The differences observed occurred probably due to small variations in manufacture of the samples, as for example the pre-crack condition or the presence of voids within the adhesive layer. Despite the effort invested in the manufacture of joints to avoid voids or bubbles, these factors are difficult to control and can lead to some variations such as those observed. Furthermore, the applied load is 60% of the average value of P_{max}, this way, in practices the percentual of P_{max} can be higher than 60% for some samples and lower than 60% for the others. These differences are observed for all the tested joints but are more pronounced for the joints tested at higher load levels.

These data are important to verify the creep behavior in ENF specimens. Besides that, the verification of no plastic deformation of the adherends is essential, which did not occur as already described. The elastic deformation observed at the samples during the creep tests was quickly recovered.

The specimens tested with 80% of P_{max} did not complete the 12 h test. For this group, the crack propagation occurred during the first hour of creep testing.

4.3 | Quasi-static results after creep tests

4.3.1 | Load–displacement curve analysis

In order to analyze the creep effect on the fracture energy in mode II, the classical three-point bending load was performed on the ENF samples that had already experienced creep loading. As creep is a function of time and load, these factors were considered to investigate how the maximum load varies. Figure 6 compares the typical load–displacement curves for all the tested conditions along with the quasi-static results. There was no considerable change in the initial compliance (C_o), which suggests that for the tested conditions the creep load did not introduce any damage in the joints. It is very interesting to note that an increase in the maximum load compared to the original value (P_{max}) obtained in static conditions (without creep) occurs. This modified value of maximum load is hereafter called P_{mod}, which is the peak of the curves in Figure 6.

The modified maximum load values for all the times and creep loads investigated are shown in Figure 7. Considering the same time and different loads, the results show that in general higher creep loads lead to greater joint strength (P_{mod}). Considering the specimens creep tested at 40% of P_{max} for 12 h, no major change occurred in the modified maximum load (P_{mod}). For the other groups, an increase in maximum load occurred, varying from 11% to 28% when compared to the reference value (P_{max}), see Figure 8. The increase in maximum load after creep must have occurred due to the viscous deformation of the adhesive. The non-recoverable deformation leads to residual stresses, specially ahead of the crack tip where the stress is concentrated, which can result in joint strength improvement.[34,35] The plastic deformation of the adherends could also contribute for that, but it was not considered for two main reasons: (a) plastic deformation on steel was not observed visually, and (b) creep in metals usually occurs at higher temperatures for longer times, which was not the case.

4.3.2 | Residual fracture energy analysis

The ENF specimens that had been already creep loaded (see Table 2) were tested under quasi static loading conditions in order to investigate the effects of creep on mode II fracture energy. By performing these tests, the residual fracture energies in mode II (G_{IIR}) were obtained. Figure 9 shows the obtained R-curves for different test conditions. The points where the crack propagation onsets as well as the point where the crack propagation stops are marked by crosses on the curves shown in Figure 8. An increase in the level of the plateau of the R-curves is observed which means that the fracture energy increases for the joints subjected to creep loads. For the samples tested for 12 and 48 h, a similar behavior occurred, as shown in Figure 10. For a creep time of 12 h, no major changes occurred in G_{IIR} considering the loads

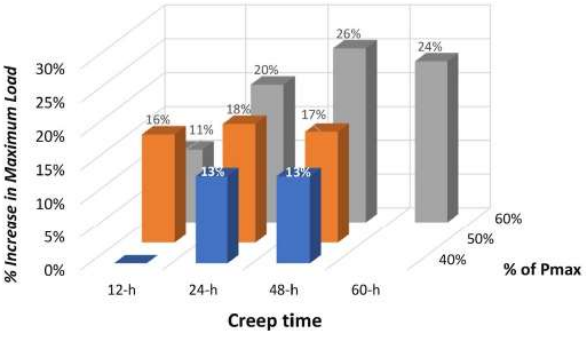

FIGURE 8 Average percentage increase in the ENF failure load after creep testing of the ENF samples [Color figure can be viewed at wileyonlinelibrary.com]

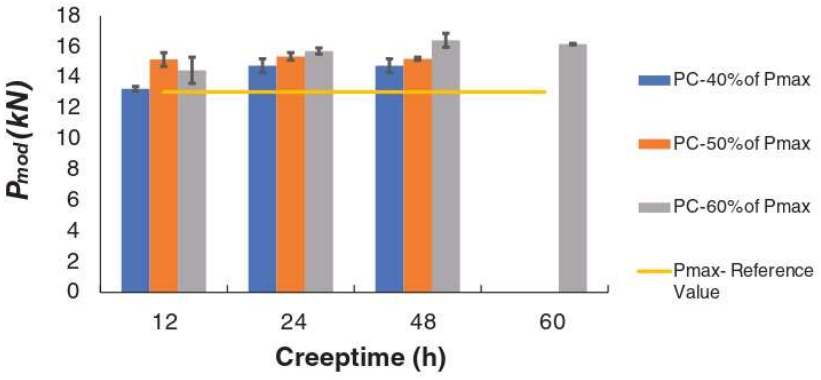

FIGURE 7 Comparison of the modified maximum loads (P_{mod}) post creep (PC) for different creep times and load levels [Color figure can be viewed at wileyonlinelibrary.com]

of 50% and 60% of P_{max}. This may be due to the short creep time which does not have a significant influence on the viscous deformation of the adhesive. It is important to note in Figure 10 that for all the tested conditions the fracture energy increased, which indicates that pre-creep loading of the bonded structure improves the joint strength. The only exception were the samples tested for 12 h with 40% of P_{max}, which did not present significant changes in fracture energy, as both the applied load and the creep time are too small to affect the fracture energy of the adhesive. However, these results are limited to the adhesive considered in this study and further investigations are needed to confirm the same response for other adhesive types.

If the creep load is kept constant, generally longer creep times lead to a higher improvement in G_{IIR}, but certainly it has a limit. This limit was investigated for a creep load of 60% of P_{max}. An optimum value of G_{IIR} was obtained for the samples tested for 48 h (2.84 N/mm). Times longer than 48 h lead to smaller fracture energies. It can be explained by the viscous deformation of the adhesive which generates residual stresses that increase the joint strength. After 48 h, the adhesive properties are degraded and the residual fracture energy decreases, as occurred for the samples tested for 60 h. The degradation process is caused by the creep damage that occurs at some material points. The load is constant, but the stress at some points is higher, so, at those points the adhesive will undergo some plastic deformation. On the other hand, by increasing the creep time, the points with higher stress levels will experience the third creep stage, which causes damage and degradation of material at those points. Figure 11 shows the percentage of improvement of shear fracture energy values compared with G_{IIC} (reference value). As already discussed, all groups achieved an increase in the shear fracture energy, reaching a 47% increase for the joints tested for 48-h and 60% of P_{max}, which is a significant improvement in shear fracture energy.

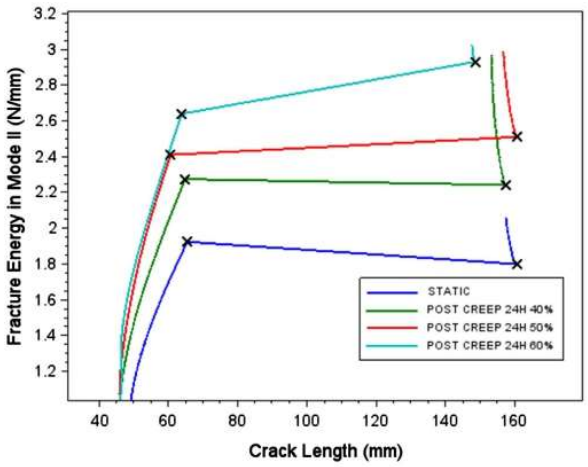

FIGURE 9 R-curves for ENF tests performed after creep tests for 24 h [Color figure can be viewed at wileyonlinelibrary.com]

The results suggest that viscous deformation occurs gradually on the adhesive as the load or time increase. This is the reason why both maximum load and residual fracture energy increase for longer times and higher loads. The permanent deformation causes residual stresses on the adhesive, which leads to an accumulation of energy that contributes to the increase in G_{IIC}. The residual stresses considerably influence the failure mechanisms in materials.[34] Besides, the plastic deformations can change the material properties and increase the strength of materials.[35] Thus, as the permanent deformation takes place due to viscous flow at the adhesive resulting in residual stresses, an additional load in relation to P_{max} is needed after creep tests to propagate the

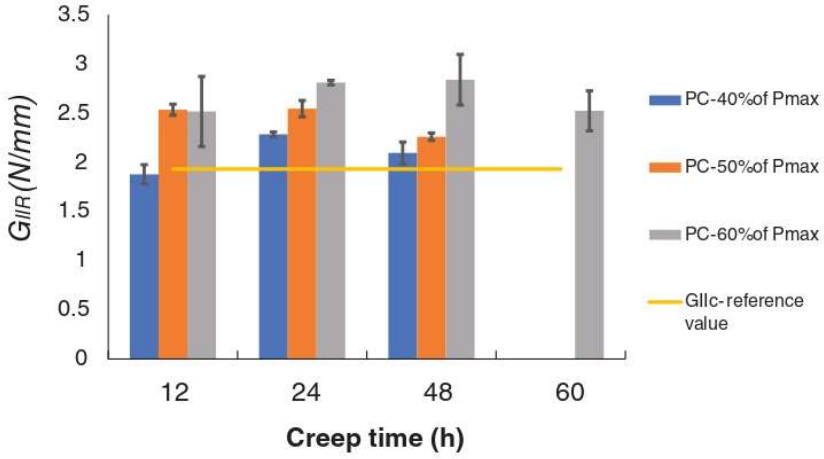

FIGURE 10 Residual fracture energy in mode II for all groups analyzed [Color figure can be viewed at wileyonlinelibrary.com]

crack in the adhesive layer. Another possible reason to the strength improvement is that, in general, tensile strength is greater in direction parallel to the polymer chains than in directions normal to them.[36,37] The alignment of the chains occurs due to viscous flow caused by creep[38] and consequently the joint strength increases, however further increases in creep time or in creep load will damage the chains and will degrade the adhesive properties, as was observed for the samples tested for 60 h at 60% of the P_{max}.

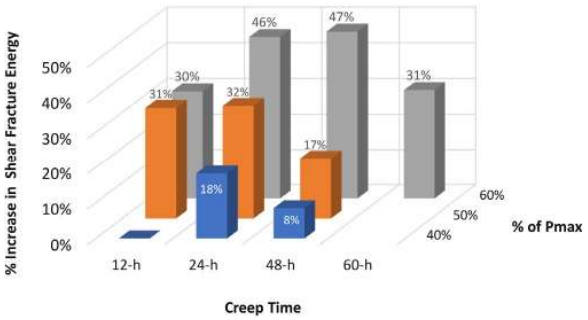

FIGURE 11 Percentage increase in shear fracture energy values obtained after creep tests performed on ENF samples [Color figure can be viewed at wileyonlinelibrary.com]

4.3.3 | Failure on ENF specimens

Cohesive failure was predominant in all the tested specimens, although the crack path was closer to one interface than the other. Figure 12 shows some fracture surfaces for both static loading (with no creep) and also for the ENF tests performed after creep loading with 50% of P_{max}. The specimens tested in static conditions (Figure 12(a)) present similar quantities of adhesive in both sides at the upper part, followed by an adhesive concentration on one side of the joint in the lower part. The specimen tested at 50% of P_{max} for 12 h (Figure 12(b)) had a similar behavior. The specimen tested for 24 and 48 h presented peaks and valleys (more roughness compared to Figure 11(a)) on the fracture surface. In ENF test the stress is distributed along the bondline. As expected for brittle adhesives, the crack propagates in only one step.[39] Right before the abrupt failure occurs, several regions along the bondline are micro/

FIGURE 12 Failure surfaces of ENF specimens: (a) after static tests (no creep). Static test after creep testing at 50% of P_{max} for (b) 12 h, (c) 24 h, and (d) 48 h [Color figure can be viewed at wileyonlinelibrary.com]

macro cracked.[40] By increasing the load, the crack coalescence takes place and the joint fails. As stated in Section 4.3.2, creep loading introduces residual stresses and viscous deformation in the adhesive layer which leads to a change in stress distribution. Based on the new gradients of the stresses, the crack does not propagate along a straight line as it occurs for the joints with no creep, as shown in Figure 12(a). Crack kinking and multisite cracking were observed in some specimens submitted to creep, which can be a possible reason to postpone the failure (increase the strength) and consequently allow a higher energy absorption, which leads to a higher shear fracture energy. Based on these results, it is not possible to relate the creep time with the type of failure, as there is no characteristic behavior of failure.

5 | CONCLUSIONS

The aim of this work was to investigate the effects of creep loading on mode II fracture energy of adhesives by considering two influencing factors: creep time and applied creep load. All specimens supported the expected time of creep test without crack propagation, with the exception of the specimens tested at 80% of P_{max}. After the creep tests, no plastic deformation of the adherends was observed.

The results show that, generally, for greater loads and longer creep times, P_{mod} and G_{IIR} increase. Additionally, it was found that creep loading for most of the tested conditions not only does not introduce any degradation on the fracture energy and the joints strength, but also improves the strength and consequently the shear fracture energy of the joints. A possible reason for the increase in P_{mod} and G_{IIR} is the viscous deformation of the adhesive and consequently the induced residual stresses. Obviously, the increase in these properties has a limit, which was investigated for the samples tested with 60% of P_{max}. It was also concluded that the optimum value of G_{IIR} occurs in the specimens previously creep tested for 48 h. For the samples creep tested for longer times (60 h), G_{IIR} decreases because the damage initiates and propagates through the adhesive layer, consequently both the strength and the shear fracture energy decrease. The failures were predominantly cohesive in all specimens. An important conclusion of this work is demonstrating that for specific loads and creep times, pre-creep loading of bonded structures can significantly improve the fracture energy and the static strength of the joints.

ORCID

Alireza Akhavan-Safar https://orcid.org/0000-0002-7168-7079

REFERENCES

[1] S. da LFM, A. Ochsner, R. D. Adams Eds., *Handbook of Adhesion Technology*, Springer-Verlag, Berlin Haidelberg **2018**.
[2] F. Kadioglu, R. D. Adams, *Int. J. Adhes. Adhes.* **2015**, *56*, 73.
[3] J. Zhou, Y. Wan, N. Liu, H. Yin, B. Li, D. Sun, Q. Ran, *J. Appl. Polym. Sci.* **2018**, *135*, 45688.
[4] K. Houjou, K. Shimamoto, H. Akiyama, C. Sato, *J. Adhes.*, **2021**, 1.
[5] R. A. Queiroz, E. M. Sampaio, V. J. Cortines, N. R. F. Rohem, *Appl. Adhes. Sci.* **2014**, *2*, 8.
[6] J. Na, W. Mu, G. Qin, W. Tan, L. Pu, *Int. J. Adhes. Adhes.* **2018**, *85*, 138.
[7] R. A. Mohammad, H. Soran, V. T. Farid, *Polym. Test.* **2019**, *75*, 107.
[8] S. S. R. Nomula, D. K. Rathore, B. C. Ray, R. K. Prusty, *J. Appl. Polym. Sci.* **2019**, *47674*, 47674.
[9] R. M. Carneiro Neto, E. M. Sampaio, J. T. Assis, *Int. J. Adhes. Adhes.* **2019**, *90*, 61.
[10] C. D. M. Liljedahl, A. D. Crocombe, M. A. Wahab, I. A. Ashcroft, *Int. J. Fract.* **2006**, *141*, 147.
[11] J. Monteiro, A. Akhavan-Safar, R. Carbas, E. Marques, R. Goyalc, M. El-zeind, L. F. M. da Silva, *Theor. Appl. Fract. Mechan.* **2019**, *103*, 102253.
[12] M. F. S. F. De Moura, J. J. L. Morais, N. Dourado, *Eng. Fract. Mechan.* **2008**, *75*, 3852.
[13] A. Ajdani, M. R. Ayatollahi, A. Akhavan-Safar, L. F. M. da Silva, *Int. J. Adhes. Adhes.* **2020**, *101*, 102629.
[14] L. F. M. da Silva, R. D. S. G. Campilho, *Advances in Numerical Modelling of Adhesive Joints*, Springer, Berlin, Heidelberg **2012**.
[15] C. D. M. Liljedahl, A. D. Crocombe, M. A. Wahab, I. A. Ashcroft, *J. Adhes. Sci. Technol.* **2005**, *19*, 525.
[16] A. D. Crocombe, Y. X. Hua, W. K. Loh, M. A. Wahab, I. A. Ashcroft, *Int. J. Adhes. Adhes.* **2005**, *26*, 325.
[17] C. D. M. Liljedahl, A. D. Crocombe, M. A. Wahab, I. A. Ashcroft, *J. Adhes.* **2006**, *82*, 1061.
[18] M. D. Banea, L. F. M. da Silva, R. D. S. G. Campilho, *Int. J. Adhes. Adhes.* **2011**, *31*, 273.
[19] M. D. Banea, L. F. M. da Silva, R. D. S. G. Campilho, *J. Adhes.* **2012**, *88*, 534.
[20] S. Xu, G. Shu, D. A. Dillard, *J. Adhes.* **2004**, *80*(12), 1153.
[21] R. L. Fernandes, D. M. MFSF, M. RDF, *Compos. Part B* **2016**, *96*, 35.
[22] M. Zehsaz, F. V. Tahami, M. A. S. Sadigh, *J. Mech. Sci. Technol.* **2014**, *28*, 2743.
[23] A. Khabazaghdam, B. Behjat, M. Yazdani, L. F. M. da Silva, E. A. S. Marques, X. Shang, *J. Adhes.* **2020**, 1. https://doi.org/10.1080/00218464.2020.1742114.
[24] M. A. S. Sadigh, *J. Mech. Sci. Technol.* **2016**, *30*, 1555.
[25] M. A. S. Sadigh, B. Paygozarb, d. S. LFM, F. V. Tahamid, *Polym. Test.* **2019**, *79*, 106087.
[26] M. Zehsaz, F. Vakili-Tahami, M. A. S. Sadigh, *Mater. Des.* **2014**, *64*, 520.
[27] da Silva RH, Sampaio EM, Rohem NR, Carneiro Neto RM, Development of pipe repairs using bonded metal plate – Part I: Shape factor, stiffness and surface treatment, **2020**, *100*, 102594
[28] P. A. Zugliani, M. D. Banea, S. Budhe, R. Carbas, L. F. M. da Silva, N. R. F. Rohem, et al., *J. Adhes. Sci. Technol.* **2019**, *33*, 2141.

[29] W. D. Calister Jr., D. G. Rethwisch, *Materials Science and Engineering: an Introduction*, Vol. 9, Wiley, New York, **1994**.
[30] Akhavan-Safar A, Monteiro J, Carbas R, Marques E, Goyal RK, da Silva LFM, A modified degradation technique for fatigue life assessment of adhesive materials subjected to cyclic shear loads, Proc. of the Institution of Mechanical Engineers, Part C: Journal of Mechanical Engineering Science, 1–10, **2020**., *235*.
[31] M. F. S. F. De Moura, A. B. De Morais, *Eng. Fract. Mechan.* **2008**, *75*, 2584.
[32] M. E. Kassner, *Fundamentals of Creep in Metals and Alloys*, 3rd ed. Butterworth-Heinemann, United Kingdom **2015**.
[33] P. N. Randall, *J. Basic Eng.* **1962**, *84*(2), 239.
[34] B. H. Rabin, R. L. Williamson, S. Suresh, *MRS Bull.* **1995**, *20*(1), 37.
[35] R. Z. Valiev, *Adv. Eng. Mater.* **2003**, *5*, 296.
[36] E. A. Campo, *Selection of Polymeric Materials*, William Andrew Publishing, New York, US **2008**.
[37] N. T. Tsui, A. J. Paraskos, L. Torun, T. M. Swager, E. L. Thomas, *Macromolecules* **2006**, *39*, 3350.
[38] C. Wu, R. Wu, W. Xia, L. Tam, *J. Polym. Sci. B Polym. Phys.* **2019**, *57*, 1779.
[39] L. F. M. Da Silva, F. A. C. R. G. de Magalhães, F. J. P. Chaves, M. F. S. F. de Moura, *J. Adhes.* **2010**, *86*, 891.
[40] M. F. S. F. De Oliveira, R. D. S. G. Campilho, F. J. G. Silva, R. J. B. Rocha, *J. Adhes.* **2018**, *94*, 910.

How to cite this article: R. M. Carneiro Neto, A. Akhavan-Safar, E. M. Sampaio, J. T. Assis, L. F. M. da Silva, *J. Appl. Polym. Sci.* **2021**, *138*(47), e51387. https://doi.org/10.1002/app.51387

ANEXO B – Avaliação da vida útil de fluência em juntas adesivas usando amostras do ensaio ENF (*Assessment of the creep life of adhesively bonded joints using the end notched flexure samples) – Engineering Failure Analysis*

Engineering Failure Analysis 133 (2022) 105969

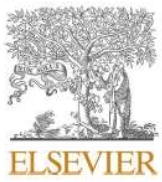

Contents lists available at ScienceDirect

Engineering Failure Analysis

journal homepage: www.elsevier.com/locate/engfailanal

Assessment of the creep life of adhesively bonded joints using the end notched flexure samples

R.M. Carneiro Neto [a], A. Akhavan-Safar [b,*], E.M. Sampaio [c], J.T. Assis [c], L.F. M. da Silva [d]

[a] Center of Technology and Application of Composite Materials, Federal University of Rio de Janeiro, Macaé, RJ, Brazil
[b] Institute of Science and Innovation in Mechanical and Industrial Engineering (INEGI), Rua Dr. Roberto Frias, 4200-465 Porto, Portugal
[c] Laboratory of Adhesion and Adherence, University of State of Rio de Janeiro, Polytechnic Institute, Nova Friburgo, RJ, Brazil
[d] Departamento de Engenharia Mecânica, Faculdade de Engenharia, Universidade do Porto, Rua Dr. Roberto Frias, 4200-465 Porto, Portugal

ARTICLE INFO

Keywords:
Creep
ENF test
Creep fracture energy
Mode II
Bonded joints
Durability

ABSTRACT

The behavior of polymeric adhesives is time and temperature dependent, as they are considered viscoelastic materials. These materials can undergo creep deformation even at low stress levels and room temperature. This way, a viscous flow can occur at the adhesive layer and it can lead to viscous deformation, causing a modification in the adhesive properties. The current work aims to investigate the shear creep fracture energy of an epoxy adhesive using end notched flexure (ENF) samples creep tested until failure. The endurance creep limit for cracked bonded joints subjected to pure shear loading conditions is also investigated using ENF samples, representing the maximum creep load which ENF bonded joints can sustain without creep fracture after a specified time. The G_{IICr}-life curve was obtained where the G_{IIcr} is the mode II creep fracture energy. Results showed that small changes in creep load can significantly change the creep endurance limit. Creep fracture energy can be employed for joint design against creep service loads.

1. Introduction

Structural adhesives are widely applied in the joining of structural components due to their advantages over other conventional mechanical joining methods. They provide design flexibility, service life extension, simple application, in addition to more uniform stress distribution [1,2]. Various sectors have applied bonded joints in their structures such as aeronautics, automotive, marine, oil, etc. When an adhesive joint is submitted to a constant load for an extended period of time the creep takes place and a pronounced time-dependent stress–strain behavior occurs on the adhesive [3]. As the adhesives have synthetic polymers as components, they are considered viscoelastic materials, thus their behavior are time and temperature dependent. Viscoelastic materials can undergo creep deformation even at low stress levels and room temperature, although this effect is amplified for higher temperatures [4,5]. This way, a viscous flow can occur at the adhesive layer and it can lead to viscous deformation, causing a modification in the adhesive properties [1,6]. Temperature, load and time are the factors that most influence the rate of creep deformation [3,7].

The change in material properties depends on the creep strain. When the dead load is applied to a material an instantaneous elastic strain occurs, followed by three regions of creep curve [8,9]: i) primary creep – also called as transient, where the creep strain increases non-linearly, ii) secondary creep, also known as steady state, characterized by linear increase of creep strain at a lower rate, and iii)

* Corresponding author.
E-mail address: aAkhavan-Safar@inegi.up.pt (A. Akhavan-Safar).

https://doi.org/10.1016/j.engfailanal.2021.105969
Received 18 October 2021; Received in revised form 10 December 2021; Accepted 10 December 2021
Available online 15 December 2021

Table 1
Substrate and adhesive properties [6].

Description	Adhesive NVT 201E	Carbon steel A1020
Young's modulus - E	3.13 ± 0.37 GPa	207 GPa
Shear modulus – G	1.21 GPa	75 GPa
Poisson's ratio - ν	0.29 ± 0.09	0.30
Tensile failure strength	28.70 ± 1.66 MPa	400 MPa

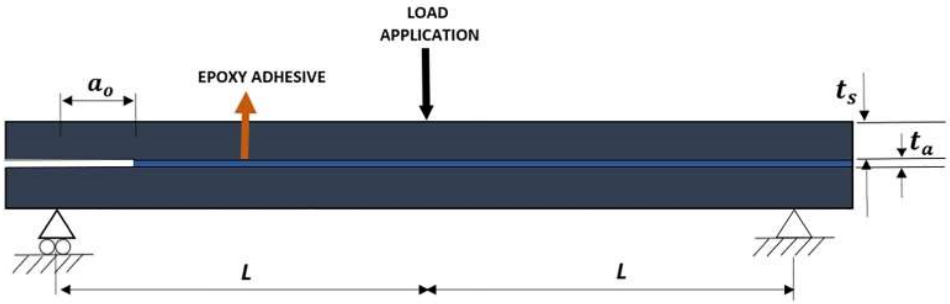

Fig. 1. Schematic representation of ENF specimens.

tertiary creep, the final stage where the creep strain increases considerably until failure occurs [10]. Both instantaneous elastic strain and creep strain can be reduced by adding multi-walled carbon nanotubes [11].

Cohesive zone models (CZMs) have been extensively applied to model bonded joints [3]. The critical fracture energy in mode II (G_{IIC}) is a key property used in the CZM, which is usually obtained by testing an ENF sample. When CZM associated with the finite element method (FEM) is applied, the fracture energy is used as input to the programs as a constant value, as this analysis is often performed for static conditions. However, when the creep takes place in bonded joints these properties must vary [6]. This investigation is rarely found in literature, although there are some works that evaluated the change in cohesive parameters due to hygrothermal ageing and fatigue loading conditions [12–15]. However, works related to the change in creep fracture energies due to a sustained load application have not been considered so far.

The creep data can be represented by different forms, including plotting the log of time to rupture against stress, which is similar to the S-N curve produced by fatigue testing. The endurance limit concept is very often used in fatigue, representing the stress level (S) below which an infinite number of loading cycles (N) can be applied to a material without failure. This concept can be extended to creep, as the designers must know how long the bonded joints will resist without crack propagation when a dead load is applied. Accordingly, the endurance load limit for creep is defined as the maximum load that the joint can withstand without any crack propagation after a specific time. When experiments are performed at different creep loads, the creep rupture envelope can be constructed by connecting the points of onset of the tertiary creep [3]. This envelope gives a reference related to the time and load that a joint must fail, contributing to the safety in structural designs. According to the requested creep load, the respective time until failure must be obtained by the envelope. This investigation is rarely carried out in bonded joints. Thus, this work aims to investigate the shear creep fracture energy of an epoxy based adhesive using ENF specimens. Furthermore, the endurance load limit for ENF samples submitted to creep load is also investigated and the creep rupture envelope is presented. The main goal is to obtain the shear creep fracture energy versus creep time that can be used for the joint design purposes.

2. Experimental procedure

2.1. Materials

Carbon steel substrates were bonded using the structural NVT 201E epoxy adhesive (Fine Composites - Brazil), which has been previously used on pipe repairs [16,17]. This adhesive has two-component (with the weight ratio of 100 × 52, resin to hardener, respectively), a glass transition temperature of 71 °C and a density of 1.24 g/cm^3. The curing time was 24-h at room temperature for all the samples. The steel and adhesive properties are shown in Table 1.

2.2. Joint geometry and manufacturing

Fig. 1 presents the geometry of the ENF specimens. It is similar to the joint proposed by ASTM D-3433–99. The dimensions used were $2L = 298$mm (total length), $a_o = 46$mm (initial crack length), $t_s = 12.7$ mm (substrate thickness), and $t_a = 0.4$ mm (adhesive thickness). The width is B = 25.4 mm (not shown in Fig. 1).

The manufacturing process included sandblasting on the substrates, followed by a cleaning with acetone. A metal shim with the

same thickness of the adhesive layer was placed at one end of the joint in order to guarantee the adhesive thickness required. At the other end a double-beveled plate was placed with the same thickness of the adhesive layer, also aiming to guarantee the adhesive thickness. It had an excess length (more than the length without adhesive) to allow its removal after the required time to cure.

The epoxy adhesive was applied to the substrates and the excess of adhesive was carefully removed using a spatula. In order to obtain the adhesive thickness required the height between the bottom and top model parts can be adjusted. The total height must take into account the thickness of both adhesive and substrates. The substrate misalignment is prevented by the mold pins. As recommended by the manufacturer, the joints were tested only after the cure time of 24-h. The ambient humidity and temperature were controlled around 62% and 22 °C, respectively.

2.3. Testing conditions

The tests in ENF samples were performed at different creep loads until crack propagation for most groups. The shear creep fracture energy (G_{IICr}) was then obtained using the data from the creep tests by the compliance-based beam method (CBBM) [18]. The run out condition in this study was considered as 30 days (720-h). It means that if the joint did not fail after this time, the creep test was concluded and a quasi-static test was conducted on the ENF sample to obtain the residual fracture energy in mode II. In this condition the obtained energy is called residual fracture energy (G_{IIR}).

The creep tests in ENF samples were performed using a universal testing machine (Shimadzu, Autography AG-X Plus, Japan). In case of post creep tests, a static test was performed under displacement control at a rate of 0.5 mm/min. In all the considered cases the load and displacement were recorded aiming to be used for obtaining the creep fracture energy (G_{IICr}) or the post creep (residual) fracture energy (G_{IIR}). For this purpose, the compliance-based beam method (CBBM) was used to treat the raw data. The creep loads were defined considering a percentage of maximum load (P_{max}) obtained on the quasi static ENF test, which were 70%, 75%, and 80% of P_{max}. At least 3 specimens were tested for each condition.

After completing the tests, a visual inspection in all samples was done in order to check if any plastic deformation occurred on adherend. If it happened the results obtained in that cases could not be validated. Besides that, the creep effect on the adherends was considered negligible, as the creep in metals usually occurs at temperatures greater than roughly half of the absolute melting [19,20].

The creep curves were evaluated for different conditions, as well as the R-curves. Furthermore, the endurance load limit was also obtained, which is an important parameter to the designers.

3. Data reduction method

The CBBM method was applied in order to calculate the fracture energy in mode II. This method overcomes the difficulty of measuring the crack length during its propagation as it is based on a crack equivalent concept [21]. Furthermore, this method takes into account the effects of the fracture process zone (FPZ), consequence of plastification and nucleation of multiple micro-cracks along the adhesive thickness [21]. The experimental compliance (C) has great importance in the CBBM method and should be calculated by Eq. (1) [18].

$$C = \frac{(3a^3 + 2L^3)}{8EBt_s^3} + \frac{3L}{10GBt_s} \tag{1}$$

where a is the crack length, E is the Young's modulus of the substrate and G is the shear modulus. The other parameters are described in Section 2.2 (see Fig. 1).

The material properties of different samples may vary, this way a flexural modulus becomes necessary to consider this aspect [21]. Furthermore, the flexural modulus takes into account the contact between the two arms at the region without adhesive and the stress concentration on the crack tip [21]. If Eq. (2) is rearranged, the flexural modulus (E_f) can be obtained considering the initial compliance (C_o) and the initial crack length (a_o) [18].

$$E_f = \frac{3a_o^3 + 2L^3}{8Bt_s^3 C_{0corr}} \tag{2}$$

where C_{0corr} is calculated by Eq. (3) [18]:

$$C_{0corr} = C_0 - \frac{3L}{10GBt_s} \tag{3}$$

If the flexural modulus of the specimen is used in Eq. (1) (not E) then the equivalent crack length can be then obtained by Eq. (4) [18].

$$a_e = a + \Delta a_{ZPF} = \left[\frac{C_{corr}}{C_{0corr}} a_o^3 + \frac{2}{3}\left(\frac{C_{corr}}{C_{0corr}} - 1\right)L^3\right]^{(1/3)} \tag{4}$$

Finally, the critical fracture energy in mode II (G_{IIc}) can be now obtained by Eq. (5) [18]:

$$G_{IIC} = \frac{9P^2 a_e^2}{16B^2 t_p^3 E_f} \tag{5}$$

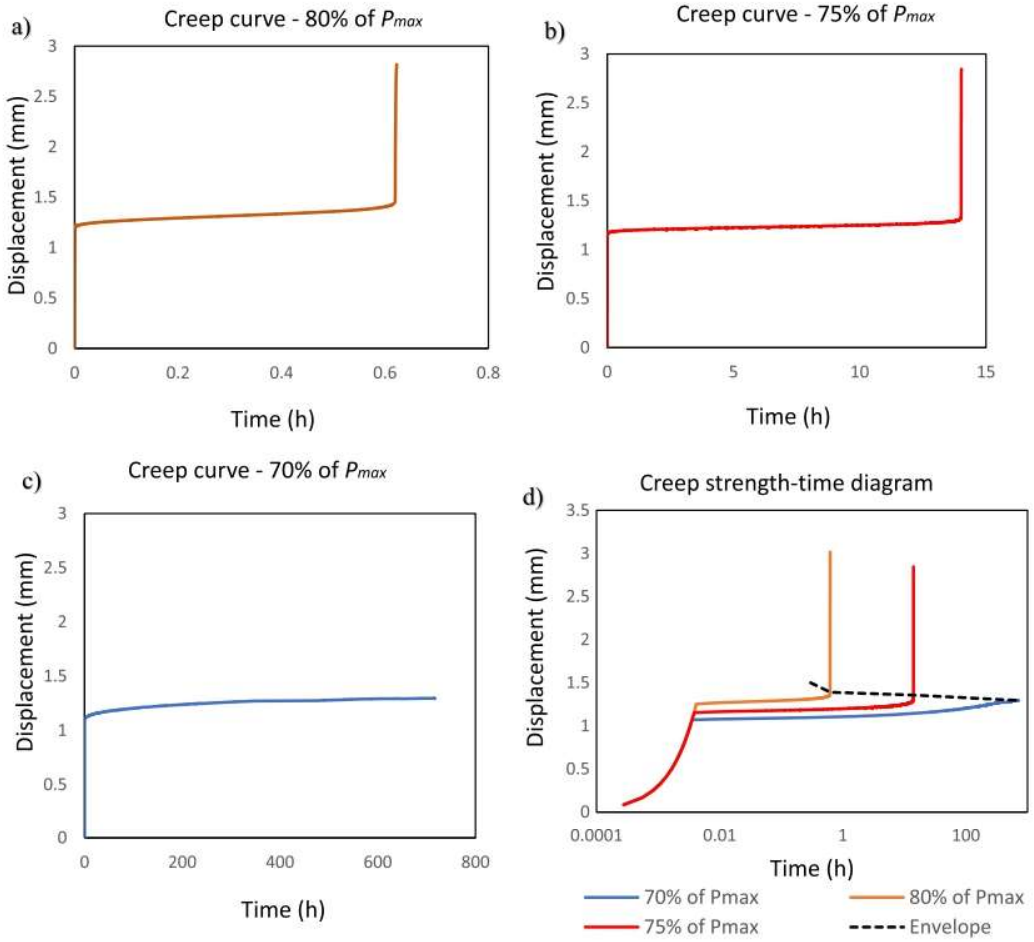

Fig. 2. Typical creep curves for different load levels: a) 80% of P_{max}, b) 75% of P_{max}, c) 70% of P_{max}, d) creep strength-time diagram.

Accordingly, the R-curves can be obtained using the load–displacement data and the equivalent crack length. For the joints where the crack did not propagate after 30 days, a post creep ENF test was performed, thus the load increases until a peak followed by a drop. For the joints tested until crack propagation the load was constant along almost all the test time, but as soon as the crack propagates the load decreases and the displacement increases considerably. The data from these points are essential to obtain the shear creep fracture energy.

4. Results and discussions

4.1. Creep tests

After the creep tests no plastic deformation on the adherends was observed. The joints tested at 70% of P_{max} did not fail after 30 days. As discussed in Section 2, 30 days is considered as run out and the joints subjected to creep for 30 days were tested in quasi static conditions to measure the residual fracture energy in mode II. For the joints tested at creep loads of 75% and 80% of P_{max}, creep life was shorter than 30 days and the creep tests were continued until failure.

Typical creep curves (displacement vs. time) are presented in Fig. 2(a–c) for all the creep loads applied, besides the creep strength-time diagram (Fig. 2d), where all the three typical curves are plotted in the same graph and then the envelope can be drawn by connecting the points of onset of the tertiary creep (black line). For this last graph a logarithm scale was used in × axis (time). For the creep loads of 80% and 75% of P_{max} the creep curves have the three regions (primary, secondary, and tertiary). For 70% of P_{max} the tertiary region was not presented as the crack did not propagate. As higher the creep load as higher the instantaneous elastic displacement (see Fig. 2d), demonstrating the consistency of the results obtained.

The displacement at the onset of the tertiary creep region for the creep loads of 80% and 75% of P_{max} was 1.39 mm and 1.36 mm, respectively. The final displacement for the joint tested at 70% of P_{max} was only 1.29 mm after 30 days, and smaller than the displacement of the other load levels. It was also observed that the displacement rate significantly decreases by a small reduction in the

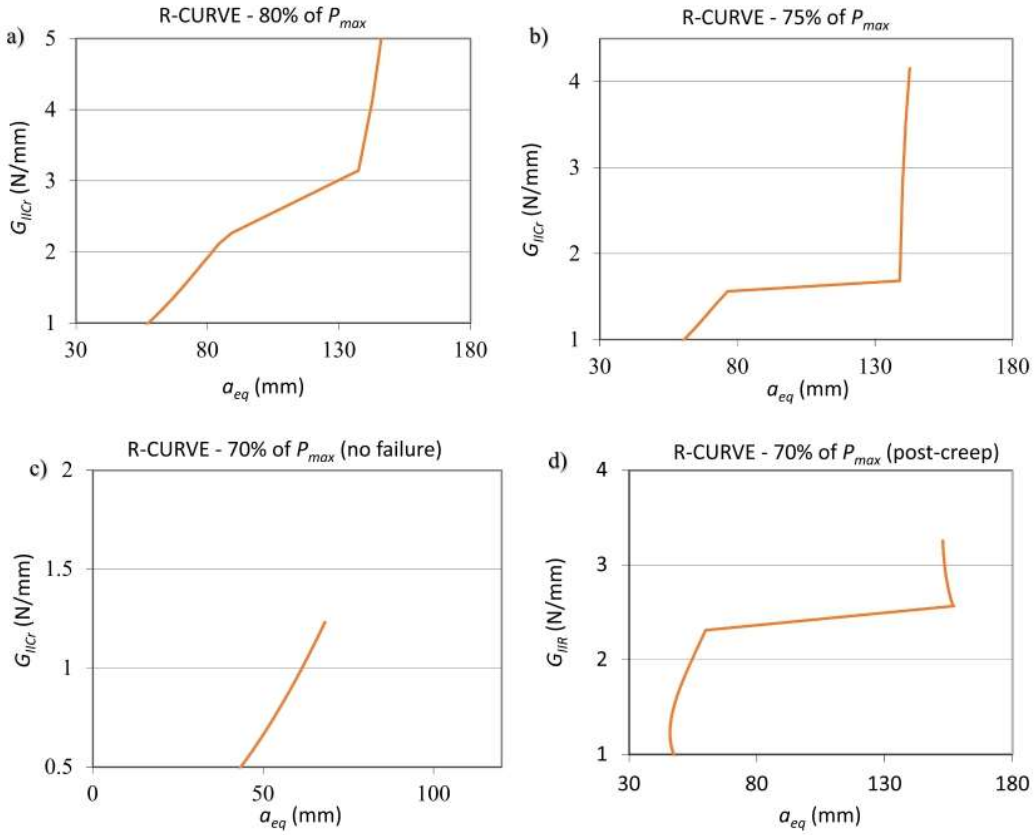

Fig. 3. Typical R-curves for the different creep loads.

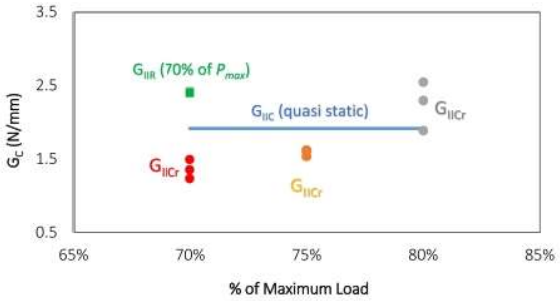

Fig. 4. Mode II creep fracture energies as a function of the applied creep load.

creep load. For example, from 300-h to 720-h the displacement increased by only 2.4% (from 1.26 mm to 1.29 mm) for the joints subjected to the 70% creep load. Thus, the creep endurance limit for the tested ENF samples is between 70% and 75% of the static strength if the 30 days creep life is considered as run out.

4.2. Shear creep fracture energy

The shear creep fracture energies (G_{IICr}) for different creep load levels were analyzed. Fig. 3 shows typical resistance curves (R-curves) for each one of the creep loads applied to the ENF samples. CBBM method was used for all the groups. When a plateau is not well defined in R-curves, as occurred for 80% of P_{max}, the fracture energy was considered as the slope inflection region of the R-curve [22].

For higher creep loads, higher values of G_{IICr} were obtained as shown in Fig. 4. As shown by Eq. (5), the higher the creep load the higher the shear creep fracture energy (G_{IICr}), although other variables also influence it, as e.g., the compliance (C). The average value of G_{IICr} decreased by 30% when the creep load varied from 80% to 75% of the P_{max}. By reducing the creep load from 75% to 70% of P_{max}

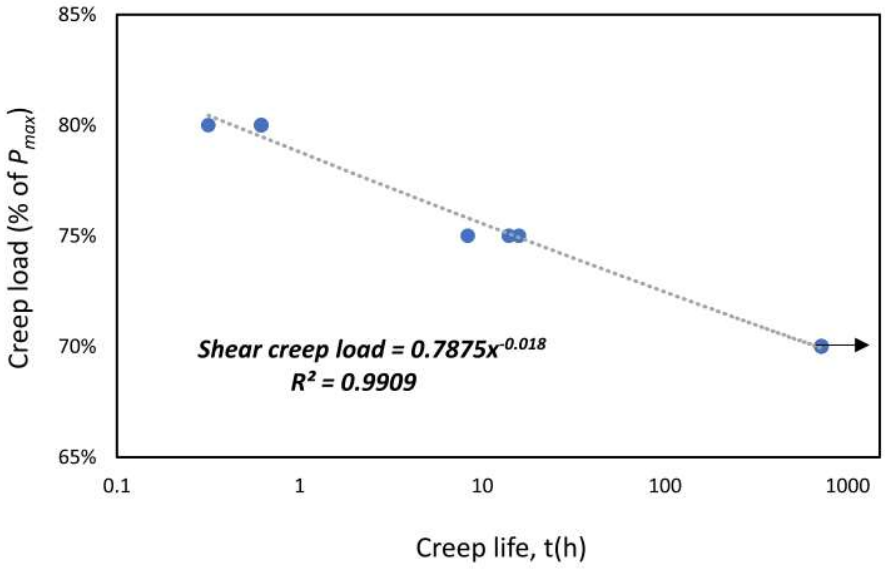

Fig. 5. Creep load versus creep life.

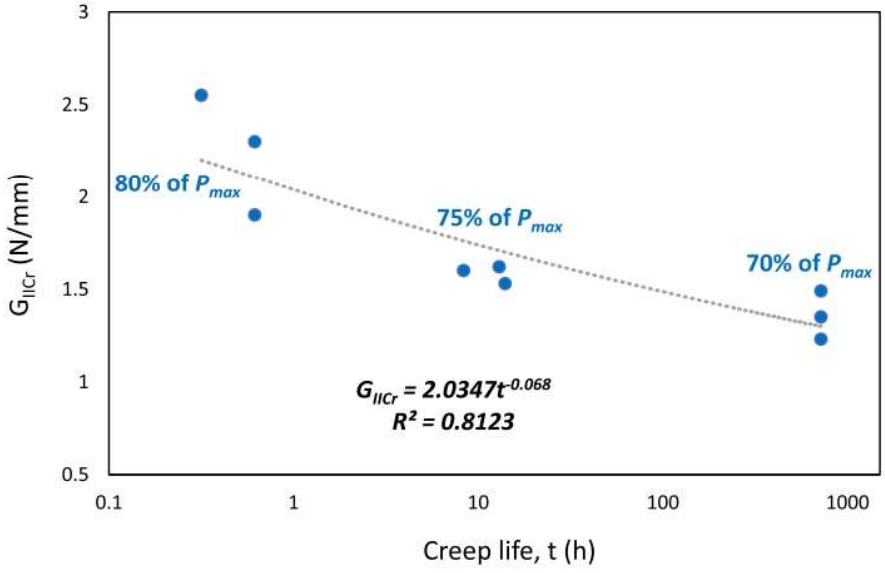

Fig. 6. G_{IICr}-life curve.

a reduction of 14% in G_{IICr} occurred. This small reduction is because of the displacement rate observed for the joints tested at 70% of the P_{max} which is lower for longer times (above 300-h). It suggests that the shear creep fracture energy obtained for the creep load of 70% of the P_{max} is the maximum amount of the energy that the cracked joint can absorb without rupture. In other words, G_{IICr} for 70% of the P_{max} indicates the maximum strain energy release rate that the joint can experience due to the creep loading for 30 days. The shear critical fracture energy (G_{IIC}) is a key property for the design and mechanical behaviour simulation of bonded joints in static conditions. Similarly, the creep fracture energy (G_{IICr}) is a useful parameter for the joint design purposes subjected to creep loading.

For a creep load of 70% of P_{max}, the joint didn't fail after 30 days and consequently the post creep quasi static test was conducted where the residual fracture energy (G_{IIR}) was obtained as 2.42 ± 0.02 N/mm. The result is in accordance with the work of Carneiro Neto [6], where an increase in the critical fracture energy obtained in static condition (1.93 N/mm [6]) is expected due to creep effect. According to the results, 25% of improvement in fracture energy occurred, confirming that creep loading of ENF samples can lead to an increase in their cohesive properties. Fig. 4 shows the different energies evaluated in this work, including the residual, critical and shear creep fracture energies in mode II (G_{IIR}, G_{IIC} and G_{IICr}, respectively) for all the samples tested. The highest value is the residual fracture energy. Considering the average values, the creep fracture energy is higher than the critical fracture energy only for a creep

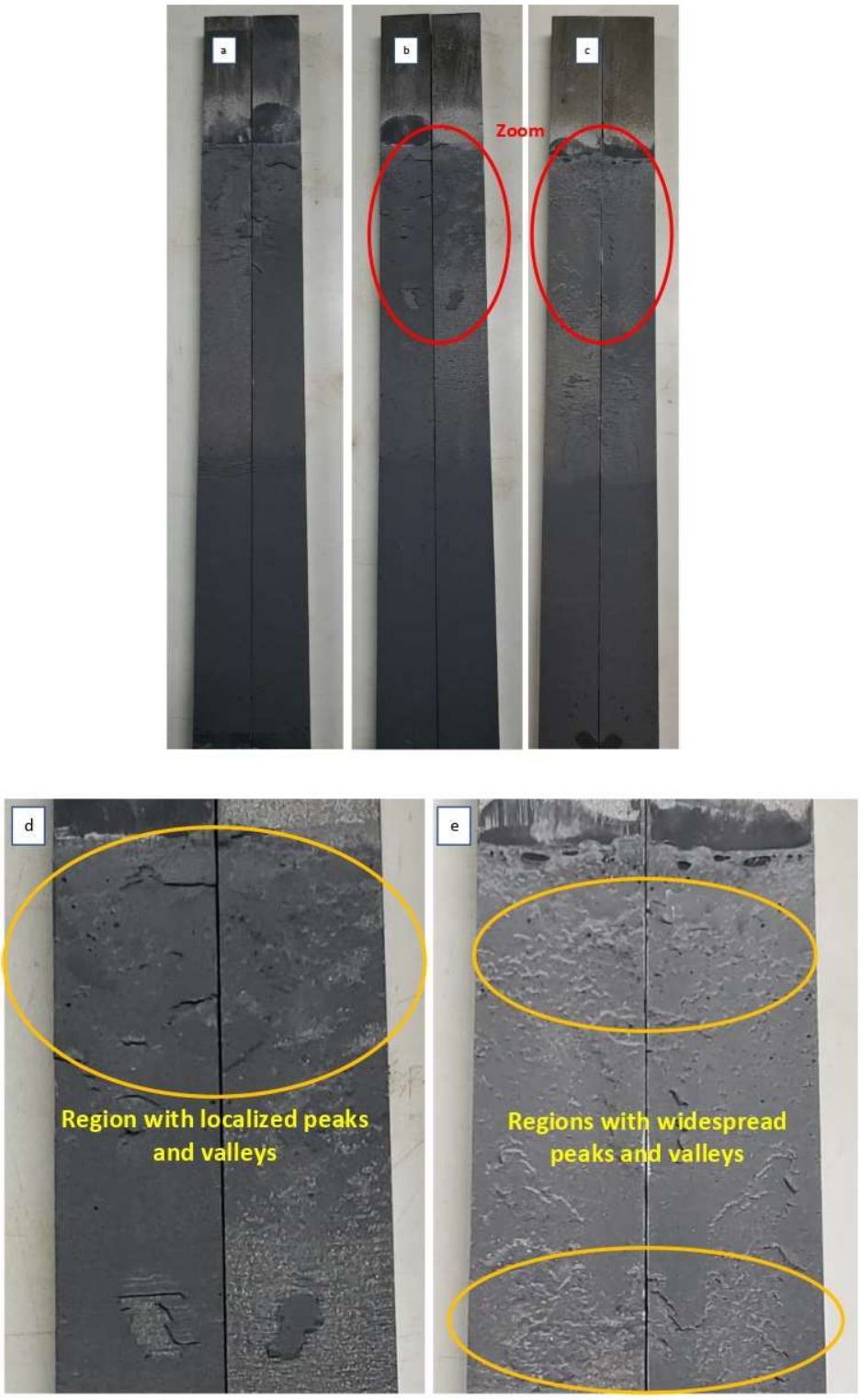

Fig. 7. Failure surfaces of ENF specimens for the sample tested at: a) 70% of P_{max} (after post creep test), b) 75% of P_{max} (after creep test), c) 80% of P_{max} (after creep test), d) detailed view of the sample tested at 75% of P_{max}, and e) 80% of P_{max}.

load of 80% of P_{max}.

The creep load as a function of the log time (creep life) is presented in Fig. 5, also demonstrating the endurance load limit for the tested conditions, which was close to 70% of P_{max}. This way, creep loads lower than 70% of P_{max} will be supported by the ENF samples without creep failure occurrence.

Fig. 6 shows the creep fracture energy as a function of creep time in log scale, for the different creep loads evaluated. In general, good repeatability was observed for all the considered creep loads. The highest standard deviation occurred for the fracture energy calculated for the samples tested at 80% of the P_{max}, was about 10%. Considering the same creep load level, the differences in time until rupture were irrelevant considering the order of magnitude (80% and 75% of P_{max} - a fraction of hour or couple hours, respectively, in comparison to 720-h for the creep load of 70% of the P_{max}). The creep fracture energy decreases for lower loads and consequently the time until rupture increases. When the creep load is close to P_{max} the failure occurs at a quite short time, but for creep loads far below P_{max}, the behavior is very different, as the displacement keep increasing even for long times without rupture (see Fig. 2c) [23]. For the tested bonded joints conditions, this transition occurred from 70% to 75%, resulting in a big difference in creep life for close creep loads, varying from around 12-h to more than 720-h for the creep loads of 75% and 70% of P_{max}, respectively. Similar result was reported by Queiroz et al. [7], although for another adhesive joint (single lap joint). The authors showed that reducing the creep load from 80% to 70% of the static strength results in a significant change in the creep life (from 8-h to 1768.5-h, respectively). The work of Zehsaz et al. [24] showed that increasing the creep load by 1% led to a considerable change in the creep life (from 24-h to 10-h), although in this work the authors used a small creep load (about 5% of the static strength). A recent work [25] also showed that a small decrease in creep load (from 25 MPa to 22.5 MPa) led to a considerable change in creep life (by a factor of about 5). These results demonstrate the complexities involved in the study of creep phenomenon in bonded joints, showing that the creep behavior and the endurance creep limit are significantly dependent on both the materials used (substrates and adhesive) and the type of the bonded joint. The G_{IIcr}-life curve was obtained considering the shear creep fracture energies obtained for the different creep loads. This exponential function can estimate G_{IICr} according to the time until failure obtained for each creep load.

4.3. Failure mode of the creep tested ENF specimens

Cohesive failures were predominant for all the tested conditions. For the creep load of 70% of P_{max}, the fracture surfaces are not relative only to creep (Fig. 7a), as the static test on ENF samples that had already experienced creep loading was performed (post creep test). This fracture surfaces presented similar quantities of adhesive in both adherends sides only at the upper part. For the lower part the failure remained cohesive, although an adhesive concentration was observed in one side. Fig. 7b and c present the fracture surfaces relative to the samples submitted to the creep loading of 75% and 80% of P_{max}, respectively. For both situations, more roughness is observed (peaks and valleys) when compared to the samples tested at 70% of P_{max}, especially for the creep load of 80% of P_{max}. In fact, the peaks and valleys are more widespread for the joints tested at the 80% of P_{max}, which can be better visualized on the detailed views of these samples shown in Fig. 7c and d. As the crack propagation in brittle adhesives occurs in only one step [26], some regions along the adhesive layer are micro / macro cracked before the quick failure [27]. When a sustained load is applied, viscous deformations take place and consequently the stress distribution may change [6]. Due to the new stress gradient, crack kinking and multisite cracking occur, which were more accentuated to higher creep loads (Fig. 7c). It allows the joint to absorb more energy, leading to higher values of creep fracture energy for higher creep loads.

5. Conclusions

This work aimed to obtain the endurance limit load of ENF samples for the time of 30 days. The creep curves were analyzed for three different creep loads. The creep strength-life diagram was constructed, which contains essential information for the designers, as it gives an idea about the time and the load that the ENF joint may fail. This way, the experimental results indicated that if a creep load of 70% of P_{max} is applied to the ENF samples for 30 days, the crack will not propagate and thus the joint will not fail due to creep.

It is important to highlight the considerable change on the creep life considering the load levels with close values. For a creep load of 70% of P_{max} the joint did not fail after 30 days, however, for 75% of P_{max} the test lasted less than 1 day. It shows the great importance of studying creep in bonded joints.

The shear creep fracture energy was obtained for the different groups evaluated. Higher creep loads had greater values of G_{IICr}. This property has important information for the designers, as well as for the simulations of bonded joints submitted to creep loading. As for the joints tested for 30 days there was no failure, these samples were unloaded and then a post creep ENF test was performed. The residual fracture energy in mode II increased 25% compared to the static values, which is in agreement with previous works [6]. The G_{IICr}-life curve was obtained, and an exponential function was used to predict G_{IICr} values for different times of failure by creep.

Finally, the fracture surfaces were also analyzed for different creep loading conditions.

Declaration of Competing Interest

The authors declare that they have no known competing financial interests or personal relationships that could have appeared to influence the work reported in this paper.

References

[1] S. Budhe, M.D. Banea, S. de Barros, L.F.M. da Silva, An updated review of adhesively bonded joints in composite materials, Int. J. Adhes. Adhes. 72 (2017) 30–42, https://doi.org/10.1016/j.ijadhadh.2016.10.010.
[2] S. Correia, V. Anes, L. Reis, Effect of surface treatment on adhesively bonded aluminium-aluminium joints regarding aeronautical structures, Eng. Fail. Anal. 84 (2018) 34–45, https://doi.org/10.1016/j.engfailanal.2017.10.010.
[3] da Silva LFM, Ochsner A, Adams RD (eds), Handbook of Adhesion Technology, Springer-Verlag Berlin Haidelberg, 2018. https://doi.org/10.1007/978-3-319-55411-2.
[4] J. Na, W. Mu, G. Qin, W. Tan, L. Pu, Effect of temperature on the mechanical properties of adhesively bonded basalt FRP-aluminum alloy joints in the automotive industry, 85, 138–148, Int. J. Adhes. Adhes. 85 (2018) 138–148, https://doi.org/10.1016/j.ijadhadh.2018.05.027.
[5] R.A. Mohammad, H. Soran, V.T. Farid, Optimum creep lifetime of Polymethyl Methacrylate (PMMA) tube using rheological creep constitutive models based on experimental data, Polym. Test. 75 (2019) 107–116, https://doi.org/10.1016/j.polymertesting.2019.01.016.
[6] R.M. Carneiro Neto, A. Akhavan-Safar, E.M. Sampaio, J.T. Assis, L.F.M. da Silva, J. Appl. Polym. Sci. (2021), e51387, https://doi.org/10.1002/app.51387.
[7] R.A. Queiroz, E.M. Sampaio, V.J. Cortines, N.RF. Rohem, Study on the creep behavior of bonded metallic joints, Appl. Adhes. Sci. 2 (1) (2014) 8, https://doi.org/10.1186/2196-4351-2-8.
[8] D.A. Dillard, Advances in Structural Adhesive Bonding, Woodhead Publishing Limited (2010), https://doi.org/10.1016/B978-1-84569-435-7.50021-3.
[9] P. Majda, J. Skrodzewicz, A modified creep model of epoxy adhesive at ambient temperature, Int. J. Adhes. Adhes. 29 (4) (2009) 396–404, https://doi.org/10.1016/j.ijadhadh.2008.07.010.
[10] B.K. Kyzy, A. Lanzutti, M. Magnan, A. Rondinella, M. Simonato, R. Furlanetto, L. Fedrizzi, Creep study of glass reinforced polypropylene: Effect of temperature and presence of notches, Eng. Fail. Anal. 128 (2021) 105624, https://doi.org/10.1016/j.engfailanal.2021.105624.
[11] H. Khoramishad, R.S. Ashofteh, Influence of multiwalled carbon nanotubes on creep behavior of adhesively bonded joints subjected to elevated temperatures, J. Adhesion 95 (11) (2019) 979–994, https://doi.org/10.1080/00218464.2018.1451333.
[12] C.D.M. Liljedahl, A.D. Crocombe, M.A. Wahab, I.A. Ashcroft, The effect of residual strains on the progressive damage modelling of environmentally degraded adhesive joints, J. Adhes. Sci. Technol. 19 (7) (2005) 525–547, https://doi.org/10.1163/1568561054352513.
[13] S. Xu, G. Shu, D.A. Dillard, Evaluation of the long-term durability of high-performance polyimide adhesives for bonding titanium, J. Adhesion 80 (12) (2004) 1153–1172, https://doi.org/10.1080/00218460490884330.
[14] R.L. Fernandes, M.F.S.F. De Moura, R.D.F. Moreira, Effect of temperature on pure mode I and II fracture behavior of composite bonded joints, Compos. B (2016), https://doi.org/10.1016/j.compositesb.2016.04.022.
[15] M. Costa, G. Viana, R. Créac'hcadec, L.F.M. da Silva, R.D.S.G. Campilho, A cohesive zone element for mode I modelling of adhesives degraded by humidity and fatigue, Int. J. Fatigue 112 (2018) 173–182, https://doi.org/10.1016/j.ijfatigue.2018.03.014.
[16] da Silva RH, Sampaio EM, Rohem NR, Carneiro Neto RM, Development of pipe repairs using bonded metal plate – Part I: Shape factor, stiffness and surface treatment, 100, 102594, 2020. DOI https://doi.org/10.1016/j.ijadhadh.2020.102594,.
[17] P.A. Zugliani, M.D. Banea, S. Budhe, R.J. Carbas, L.F.M. da Silva, N.R.F. Rohem, S. de Barros, Bonded composite repair of metallic pipeline using energy release rate method, J. Adhes. Sci. Technol. 33 (19) (2019) 2141–2156, https://doi.org/10.1080/01694243.2019.1632537.
[18] M.F.S.F. de Moura, J.J.L. Morais, N. Dourado, A new data reduction scheme for mode I wood fracture characterization using the double cantilever beam test, Eng. Fract. Mech. 75 (13) (2008) 3852–3865.
[19] P.N. Randall, Cumulative Damage in Creep-Rupture Tests of a Carbon Steel, J. Basic Eng. 84 (2) (1962) 239–242, https://doi.org/10.1115/1.3657295.
[20] Kassner ME. Fundamentals of creep in metals and alloys, third edition, 2015. ISBN: 978-0-08-099427-7.
[21] L.F.M. da Silva, A. Öchsner (Eds.), Modeling of Adhesively Bonded Joints, Springer Berlin Heidelberg, Berlin, Heidelberg, 2008.
[22] A. Akhavan-Safar, J. Monteiro, R. Carbas, E. Marques, R.K. Goyal, L. da Silva, A modified degradation technique for fatigue life assessment of adhesive materials subjected to cyclic shear loads, Proc. Inst. Mech. Eng. Part C J. Mech. Eng. Sci. 235 (3) (2021) 550–559.
[23] G. Spathis, E. Kontou, Creep failure time prediction of polymers and polymer composites, Compos. Sci. Technol. 72 (9) (2012) 959–964, https://doi.org/10.1016/j.compscitech.2012.03.018.
[24] M. Zehsaz, F. Vakili-Tahami, M.-A. Saeimi-Sadigh, Parametric study of the creep failure of double lap adhesively bonded joints, Mater. Des. 64 (2014) 520–526.
[25] X. Duan, et al., A Phenomenological Primary–Secondary–Tertiary Creep Model for Polymer-Bonded Composite Materials, Polymers 13 (2021) 2353, https://doi.org/10.3390/polym 13142353.
[26] L.F.M. da Silva, F.A.C.R.G. de Magalhães, F.J.P. Chaves, M.F.S.F. de Moura, de Magalhães FACRG, Chaves FJP, de Moura MFSF Mode II Fracture Toughness of a Brittle and a Ductile Adhesive as a Function of the Adhesive Thickness, J. Adhesion 86 (9) (2010) 891–905, https://doi.org/10.1080/00218464.2010.506155.
[27] M.F.S.F. De Oliveira, R.D.S.G. Campilho, F.J.G. Silva, R.J.B. Rocha, Comparison between the ENF and 4ENF fracture characterization tests to evaluate GIIC of bonded aluminium joints, J. Adhesion 94 (11) (2018) 910–931, https://doi.org/10.1080/00218464.2017.1387056.

ANEXO C – Modelos de dano coesivo para a avaliação da vida de fluência de cisalhamento em juntas coladas *(Cohesive zone models for the shear creep life assessment of bonded joints) – Mechanics of Time-Dependent Materials*

Mechanics of Time-Dependent Materials
https://doi.org/10.1007/s11043-022-09548-x

Cohesive zone models for the shear creep life assessment of bonded joints

R.M. Carneiro Neto[1] · F. de Medeiros Sales[1] · E.M. Sampaio[2] · A. Akhavan-Safar[3] · J.T. de Assis[2] · L.F.M. da Silva[4]

Received: 27 December 2021 / Accepted: 1 March 2022

Abstract
Epoxies are the most common structural adhesive type in bonded joints. They are viscoelastic materials that show time and temperature dependent behavior under creep. Cohesive zone models (CZM) are often used to model the adhesive bonds, but rarely to model the creep behavior of adhesive bonds. The application of creep load to end notched flexure (ENF) samples leads to a change in the shear fracture energy, which depends on both creep time and creep load. Accordingly, in order to model the creep behavior in ENF joints, fracture energies must be accessed for each time increment along the simulation. For this purpose, the proposition of functions must be addressed, which must contain two variables including creep load level and creep time. The current research presents two different functions to determine the shear fracture energies according to the different creep times and creep loads. The function parameters are obtained by linear and nonlinear regressions. The models were validated and then used in a numerical analysis as part of the adhesive constitutive behavior, using CZM. Very good agreement between the numerical and experimental creep curves was observed.

Keywords Bonded joints · Creep · Regression · Fracture energy · Cohesive zone modelling

1 Introduction

Adhesive joints are extensively used in the engineering industries. Their extensive applications in diverse sectors such as aeronautic, marine and automotive are due to their advantages, such as better stress distribution, reduced stress concentrations, reduced corrosion

✉ A. Akhavan-Safar
aAkhavan-Safar@inegi.up.pt

1 Center of Technology and Application of Composite Materials, Federal University of Rio de Janeiro, Aloísio da Silva Gomes Ave, 50, 27930-560, Macaé, RJ, Brazil

2 Laboratory of Adhesion and Adherence, Polytechnic Institute, University of State of Rio de Janeiro, Nova Friburgo, RJ, Brazil

3 Institute of Science and Innovation in Mechanical and Industrial Engineering (INEGI), Rua Dr. Roberto Frias, 4200-465 Porto, Portugal

4 Departamento de Engenharia Mecânica, Faculdade de Engenharia, Universidade do Porto, Rua Dr. Roberto Frias, 4200-465 Porto, Portugal

Published online: 16 March 2022

between dissimilar materials and better vibration absorbance, compared with conventional mechanical joining approaches (Ramalho et al. 2020; Ciardiello et al. 2020).

Epoxy adhesives are the most widely used structural adhesive type in bonded joints. They are viscoelastic materials that present time and temperature dependent behavior when subjected to constant loads, thus, the mechanical behavior of viscoelastic materials is both time and temperature dependent (Chen and Smith 2021). Thereby, when the dead load is applied in an adhesive joint for an extended time, the adhesive properties can change and special attention to this aspect should be given (Carneiro Neto et al. 2021). Creep is defined as a time-dependent deformation of materials when subjected to constant stresses at elevated temperatures. However, as epoxy adhesives present viscoelastic behavior, the creep effect is also observed even at room temperature (da Silva et al. 2018). When a dead load is applied to a material an instantaneous elastic strain occurs, then three regions are usually observed in creep curves (Dillard 2010; Madja and Skrodzewicz 2009) including i) primary creep, where a non-linear high creep strain rate is observed, ii) secondary creep, characterized by a stabilization of the creep strain rate (also called as steady state), and iii) tertiary creep, where the failure occurs due to the considerable increase in creep strain rate (Berrekheroukh et al. 2021). The creep strain can be reduced by some methods, including the addition of multi-walled carbon nanotubes (Khoramishad and Ashofteh 2019) or filleted joints (Zehsaz et al. 2014b).

The cohesive zone models (CZM) have been frequently used in recent years to simulate the behavior of bonded joints under static conditions (da Silva et al. 2018; Wolf et al. 2018). They present some important aspects of joint design, such as the crack initiation, propagation and failure, needing for this purpose the predefinition of all possible crack paths (da Silva et al. 2018). The simulation of crack propagation in CZM depends on the fracture energy, a relevant cohesive property defined by the energy needed to modify a unit area of a fracture surface from the initial unloaded state to the final state of complete separation (Jensen et al. 2011). In other words, it can be understood as the capacity of a material to support mechanical efforts until the crack has fully propagated. Fracture energies under various loading models are obtained by fracture tests relied on the concepts of so-called Linear Elastic Fracture Mechanics (LEFM). The most popular way to calculate the shear fracture energy (G_{IIC}) is to conduct a fracture test on end notched flexure (ENF) samples (Akhavan-Safar et al. 2020), which provides a load-displacement curve that is used to obtain the resistance curve (R-curve), thereby the G_{IIC} value can be obtained by the plateau region of the R-curve. A recent work (Carneiro Neto et al. 2021) has shown that the creep history of ENF samples can influence the shear fracture energy, even increasing this cohesive property according to controlled conditions. In other words, both creep load and creep time must be considered to calculate the modified value of G_{IIC}. In order to model the creep behavior of bonded joints using the CZM, the change in G_{IIC} must be accessed in numerical models through the proposition of functions with two variables (creep time and creep load). Accordingly, the creep response of ENF samples can be simulated using the CZM, which has not been considered yet. The creep behavior of bonded joints has been numerically studied by researchers, especially in the simulation of single lap joints (Zehsaz et al. 2014a; Khabazaghdam et al. 2020) and double lap joints (Zehsaz et al. 2014b; Sadigh 2016; Sadigh et al. 2019), although the authors did not consider the adhesive as a cohesive element in the creep models. Moreover, the creep effect of fracture tests in ENF samples has not been considered so far.

This work aims to present two models that calculate G_{IIC} as a function of both creep load and creep time, based on the experimental test results. To achieve this, the experimental data already obtained in the work of Carneiro Neto et al. (2021) were used. The parameters of the models were obtained by linear and non-linear regressions, using two methods: least squares

and Levenberg-Marquardt. Additional experimental results were considered to evaluate and validate the proposed models. Next, a numerical analysis using the finite element method was performed aiming to predict the creep behavior of the ENF sample. For this purpose, a subroutine user material (UMAT) was implemented to simulate the adhesive constitutive behavior, taking into account the variation of the shear fracture energy according to the proposed models.

2 Models proposed

In order to calculate the shear fracture energy, two models are presented in this section. The crack did not propagate during the creep tests performed by Carneiro Neto et al. (2021). Despite the significant effect of creep on the fracture energy of the adhesive, however, for the conditions considered in this study, the creep crack didn't propagate during the creep loading. Creep tests were stopped before any crack growth and then by performing a quasi-static test the new fracture energy of the adhesive (post-creep fracture energy) was obtained. These data were used to define the functions where the fracture energy varies depending on the pre-creep loading and the time conditions.

The models depend on both creep time and creep load and do not depend directly on crack propagation, since the main use of the models is to obtain the fracture energy values for different times and loads in accordance with the tendency observed in the experiments. This way, the models must be valid not only for the creep times (12 h, 24 h, 48 h) and creep loads (40%, 50% and 60% of the maximum load in ENF static test) used in the experiments, but also for the times and loads between the cited values and in the vicinity of the extreme values.

2.1 Mixed equation

Equation (1) is proposed for the calculation of the shear fracture energy (G_{IIC}) of the adhesive as a function of load (F) and time (t), according to the experimental data presented by Carneiro Neto et al. (2021). The exponential part of Eq. (1) was used in the work of Costa et al. (2018), aiming to consider the cohesive property degradation. The linear functions of t and F were added to the structure aiming to consider the improvement in G_{IIC}, when both creep time and load increase, as occurred in the experiments (Carneiro Neto et al. 2021). This improvement occurs until a determined time and then the G_{IIC} decreases. Hereafter, the empirical Eq. (1) will be called model 1.

$$G_{IIC}(t, F) = [\left(\frac{1}{z_1}\right)(1.93z_1 + t)\left(1 - \frac{t}{720}\right)^{z_2}[z_3F + z_4] \tag{1}$$

where z_1, z_2, z_3, and z_4 are coefficients that must be determined to fit the calculation results to the experimental data.

As these parameters have an inherently nonlinear relationship with the experiments, a nonlinear regression must be performed. The Levenberg-Marquardt (LM) method (Marquardt 1963) was used to calculate the parameters of the predefined model (mixed equation). The LM method is widely used for nonlinear regressions due to some advantages over the Gauss-Newton method, finding the solution even if it starts very far off the initial estimation (Huang and Tseng 2016).

First, the coefficients (z_1, z_2, z_3, z_4) must be estimated. Thus, the calculation of the Jacobian matrix (J_{ij}) must be done by Eq. (2).

$$J_{ij} = \frac{\partial G_{IIC}(t, F)_i}{\partial z_j} \tag{2}$$

where $i = 1, \ldots, M$, $j = 1, \ldots, N$, M is the number of experimental data (here $M = 9, 3$ data for each creep time) and N is the number of coefficients to be determined (here $N = 4$).

The residual vector (r_i) can be now obtained by Eq. (3).

$$r_i = G_{IIC}(t_i, F_i) - I_i \tag{3}$$

where I is the vector containing the experimental data.

The call of the next iteration occurs by the comparison between the initial sum of residuals squared (S_0) and the new sum (S) obtained after the first iteration. If S is less than S_0, the next iteration is called.

The calculation of the vector of unknown parameters $(\overrightarrow{Z})$ can be performed through an interactive process that aims to minimize the sum of residuals squared. Equation (4) calculates the vector of increments $(\Delta \overrightarrow{Z})$. Then Eq. (5) is used to calculate the new estimation vector.

$$[(J^n)^T J^n + \lambda^n I_D] \Delta \overrightarrow{Z}^n = -(J^n)^T \overrightarrow{F}^n \tag{4}$$

$$\overrightarrow{Z}^{n+1} = \overrightarrow{Z}^n + \Delta \overrightarrow{Z}^n \tag{5}$$

where $n = 1, \ldots, N_t$, and N_t is the maximum number of interactions. λ is the damping factor - a non-negative parameter that is adjusted at each iteration to contribute to the algorithm convergence. I_D is the identity matrix.

While the pre-established stopping criterion is not reached, the Jacobian matrix should be calculated by Eq. (2) using the vector of unknown parameters with the update values, then the same steps already described must be followed. Finally, the program must stop running when the pre-established stopping criterion is reached.

2.2 Polynomial equation

The calculation of the shear fracture energy as a function of both creep load (F) and creep time (t) must be done using Eq. (6), which contains the generating functions represented by $g_i(t, F)$.

$$G_{IIC}(t, F) = z_1 g_1(t, F) + \cdots + z_m g_m(t, F) \tag{6}$$

where $g_1(t, F), \ldots, g_m(t, F)$ are reasonable functions chosen to well describe the phenomena and $z_1, \ldots, z_m$ are the constants of the model that should be fitted to the experimental data obtained in a previous work (Carneiro Neto et al. 2021).

Both methods least squares (LSM) and Levenberg-Marquardt (LM) can be used in order to solve the parameter estimation problem.

The calculation of the parameters through the LSM is presented in this section (the LM method was detailed in Sect. 2.1). Considering the linear regression procedure using LSM, the parameters that best fit the model are those obtained by the system resolution $Ax = B$,

where x is the vector of parameters and A and B are matrices calculated using Eqs. (7) and (8), respectively.

$$A = \sum_{i=1}^{n} T_i T_i^T \tag{7}$$

$$B = \sum_{i=1}^{n} I_i T_i \tag{8}$$

where

$$T_i = \begin{bmatrix} g_1(t_1, F_1) \\ \vdots \\ g_m(t_i, F_i) \end{bmatrix} \tag{9}$$

and $(t_1, F_1), \ldots, (t_n, F_n)$ are the experimental data defined for the creep tests, and I_i represents the corresponding fracture energy in the mode II values obtained for each experimental condition of creep time and creep load. $g_i(t_i, F_i)$ represents the generating function value for (t_i, F_i).

In this step, the residual vector should be calculated (see Eq. (3)), providing the differences between the model predictions (according to Eq. (6)) and the experimental data.

The squared error function is given by Eq. (10). When the minimization of the squared error function occurs, then Eqs. (7) and (8) can be obtained.

$$E(a_1, \ldots, a_m) = \sum_{i=1}^{n} [a_1 g_1(t_i, F_i) + \cdots + a_m g_m(t_i, F_i) - I_i]^2 \tag{10}$$

Equation (11) presents a polynomial function of two variables that calculates the G_{IIC}. It will be called Model 2 hereafter.

$$G_{IIC}(t, F) = a_1 + a_2 t + a_3 F + a_4 t^2 + a_5 F^2 + a_6 t F \tag{11}$$

Thus, $m = 6$, and the generating functions are set by:

$$\begin{aligned} &g_1(t, F) = 1; g_2(t, F) = t; g_3(t, F) = F; \\ &g_4(t, F) = t^2; g_5(t, F) = F^2; g_6(t, F) = t F \end{aligned} \tag{12}$$

2.3 Validation of the proposed models

The coefficient of determination (R^2) was calculated for all regressions aiming to verify how well the experimental data are simulated by the two proposed models.

The experimental data used for the regressions analysis were tested at 40%, 50% and 60% of P_{max} for different creep times (12 h, 24 h and 48 h), all obtained in reference (Carneiro Neto et al. 2021). In the same work (Carneiro Neto et al. 2021), the results of samples tested at 60% of P_{max} for 60 h were presented, which was used in this work to validate the model as it was not used for the regressions analysis. An additional experiment presented in the current work was also used to validate the models and see their robustness.

Table 1 Adhesive and substrate properties (Carneiro Neto et al. 2021)

Description	Adhesive NVT 201E	Drawn steel A1020
Young's modulus – E	3.13 ± 0.37 GPa	200 GPa
Shear modulus – G	1.21 GPa	75 GPa
Poisson's ratio – ν	0.29 ± 0.09	0.32
Shear fracture energy	1.93 ± 0.10	–
Maximum tensile strength	28.70 ± 1.66 MPa	400 MPa

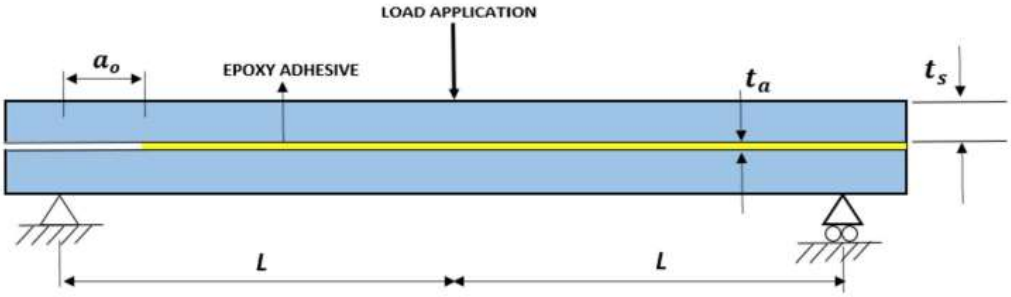

Fig. 1 Schematic representation of end notched flexure ENF specimens

The residual values and the percentage relative errors - e_i - (see Eq. (13)) were also calculated for all models and methods.

$$e_i = 100 \times abs\left(\frac{G_{IIC}(t_i, F_i) - I_i}{I_i}\right) \tag{13}$$

3 Experimental procedure

3.1 Materials

An additional experiment was performed aiming to validate the proposed models. This end notched flexure (ENF) sample was subjected to a creep load of 70% of P_{max} for 24 h. The materials used to manufacture the joint were the same as those used by Carneiro Neto et al. (2021): an epoxy adhesive (NVT 201E) and carbon steel A1020 for the substrates. The properties of both the adhesive and the substrate are presented in Table 1.

3.2 Joint geometry and manufacturing

The geometry of the ENF sample is shown in Fig. 1. The total length is $2L = 298$ mm, the thickness of the adhesive and substrates is $t_a = 0.4$ mm and $t_s = 12.7$ mm, respectively, the initial crack length is $a_o = 46$ mm. The width is 25.4 mm (not shown in Fig. 1).

The substrates were initially sand blasted and then cleaned with acetone. The bonding process must guarantee the same adhesive thickness along the joint length. For this purpose, a calibrated metal strip was placed at the right end and a double-beveled plate was positioned at the left end. This way, a pre-crack is imposed in the ENF sample, with the plate length defined according to the initial crack length (a_o). Moreover, an extra length was used to remove this part after the curing process. As recommended by the adhesive manufacturer, the curing time was 24 h at room temperature.

3.3 Test procedure

A universal testing machine (Shimadzu, Autography AG-X Plus, Japan) was used to provide load, time and displacement data during the test. The experiments were performed in two steps: i) creep tests on the ENF sample performed under a constant load for a fixed time - the creep load was 70% of P_{max} and the creep time was 24 h. ii) post creep ENF tests – where the usual ENF tests were performed on the same sample that have already experienced creep loading, aiming to calculate the modified value of shear fracture energy. This experiment was performed under displacement control conditions at a rate of 0.5 mm/min.

After the creep test, a visual inspection was performed on the sample aiming to check if the crack had propagated and if there was some plastic deformation of the substrates. Crack propagation during the test would invalidate the results, as the modified value of the fracture energy in mode II is calculated considering that the joint has not failed (Carneiro Neto et al. 2021). Plastic deformations on the substrates would also invalidate the results of the post-creep test, as this aspect is not considered in the data reduction scheme.

3.4 Data analysis

The compliance-based beam method (CBBM) has been widely used to treat the data of fracture tests, presenting the concept of equivalent crack length (a) and taking into account the effect of the fracture process zone (FPZ) ahead of the crack tip (De Moura and De Morais 2008). Equation (14) can be used to obtain the experimental compliance, which is the inverse of the stiffness (De Moura and De Morais 2008).

$$C = \frac{(3a^3 + 2L^3)}{8EBt_s^3} + \frac{3L}{10GBt_s} \tag{14}$$

where E is the Young's modulus of the substrate, a is the crack length and G is the shear modulus. The geometric parameters have already been described in Sect. 3.2.

Rearranging Eq. (14) the flexural modulus (E_f) can be obtained, as presented in Eq. (15).

$$E_f = \frac{3a_o^3 + 2L^3}{8Bt_s{}^3 C_{0corr}} \tag{15}$$

where C_{0corr} must be calculated using Eq. (16) (De Moura and De Morais 2008):

$$C_{0corr} = C_0 - \frac{3L}{10GBt_s} \tag{16}$$

The equivalent crack length (a_e) can be now obtained by substituting Eq. (15) in Eq. (14) and isolating a, as shown in Eq. (17).

$$a_e = a + \Delta a_{ZPF} = [\frac{C_{corr}}{C_{0corr}} a_o^3 + \frac{2}{3}(\frac{C_{corr}}{C_{0corr}} - 1)L^3]^{(1/3)} \tag{17}$$

Lastly, the shear fracture energy in mode II can be calculated using Eq. (18).

$$G_{IIC} = \frac{9P^2 a_e{}^2}{16B^2 t_p{}^3 E_f} \tag{18}$$

4 Numerical simulation

A CZM with a triangular shape was assumed in this work, as this shape is usually used to model brittle adhesives (Ayatollahi et al. 2019). CZM aims to simulate the fracture process through the use of both local strength and energy parameters (Delzendehrooy et al. 2021). Before the damage onset, the stress at the interface of the finite element (σ) and the vector of relative displacements between homologous points (δ_r) have a linear relationship, as presented in Eq. (19) (De Moura and De Morais 2008).

$$\sigma = K\delta_r \tag{19}$$

where K is the matrix that contains the stiffness of the cohesive elements.

As in the ENF fracture test only shear effort occurs, the stress peak is defined by the maximum shear strength (τ_o). The displacement at the damage onset is represented by δ_o. Then a linear softening process takes place at the cohesive element, where the shear fracture energy has a greater importance. The simulation of the degradation process is considered by the release of energy in a cohesive zone behind the crack tip (Sadigh et al. 2019). The damage parameter must be defined (Eq. (20)), representing the damage level at the cohesive material.

$$D = \delta_f(\delta_c - \delta_o)/\delta_c(\delta_f - \delta_o) \tag{20}$$

where δ_c is the current relative displacement and δ_f is the final displacement.

Now the softening relationship can be presented, as shown in Eq. (21).

$$\sigma = (I_d - D)K\delta_r \tag{21}$$

where I_d is the identity matrix.

The load in the static ENF test increases until it reaches a peak value, followed by a drop as a consequence of the crack propagation. This peak load is called the maximum load (P_{max}) of the ENF experiment. The work of Carneiro Neto et al. (2021) presented creep tests performed at constant load levels considering a fraction of $P_{max,}$ varying from 40% to 60%.

In order to simulate the creep behaviour of ENF samples, Models 1 and 2 must be implemented in a Fortran code linked to Abaqus (the finite element program). This allows the shear fracture energy variation due to the creep phenomenon to be included in the constitutive behavior of the adhesive material. Thus, the numerical analysis can be performed using the CZM and taking into account the change in fracture energy observed in the experiments, which is usually not done because the presented models are not available in the library of Abaqus. In short, the constitutive behavior of the adhesive is considered by the Fortran code, which takes this information to Abaqus at each time increment.

Two steps were executed in the numerical simulations, both static. The first refers to the creep load application, where the load varies from 0 to the creep load level. Here the instantaneous elastic displacement is observed. Then the constant load step takes place, where the load is kept constant.

The boundary conditions are those presented in Fig. 1. Solid elements with reduced integration (CPE4R) and cohesive elements (COH2D4 from Abaqus) with 4 nodes were used for the substrates and adhesives, respectively. The bi-dimensional model contained 11096 elements and 12979 nodes.

Finally, the numerical analysis of the joints tested at 60% of P_{max} were compared to the experimental results for two different creep times (12 h and 48 h).

Table 2 Parameters of the models proposed

Function and method	z(1)	z(2)	z(3)	z(4)	z(5)	z(6)	R^2
Function 1 – LM	−36.714	−18.869	1.3731	0.3627	–	–	0.8499
Function 2 – LSM	0.6108	0.0094	4.2830	−0.0006	−3.2250	0.0631	0.8239
Function 2 – LM	−0.5029	0.0360	6.9434	−0.0007	−4.3017	0.0192	0.8669

Table 3 Experimental and model values for the shear fracture energy and the corresponding errors

Time (h)	F (% of maximum Load)	I - Experimental Results (N/mm)	Model 1 LM - (N/mm)	Model 1 LM - Percent Error (%)	Model 2 LSM - (N/mm)	Model 2 LSM - Percent Error (%)	Model 2 LM - (N/mm)	Model 2 LM - Percent Error (%)
12	0.4	1.877	2.01	6.9%	2.130	13.5%	2.007	6.9%
24	0.4	2.283	2.21	3.3%	2.266	0.7%	2.221	2.7%
48	0.4	2.094	2.09	0.3%	1.979	5.5%	2.026	3.2%
12	0.5	2.533	2.31	8.8%	2.344	7.5%	2.337	7.7%
24	0.5	2.544	2.54	0.2%	2.556	0.5%	2.574	1.2%
48	0.5	2.259	2.40	6.3%	2.420	7.1%	2.425	7.4%
12	0.6	2.515	2.61	3.9%	2.493	0.8%	2.581	2.6%
24	0.6	2.808	2.87	2.2%	2.781	1.0%	2.841	1.2%
48	0.6	2.837	2.72	4.3%	2.796	1.5%	2.738	3.5%
60	0.6	2.522	1.81	28.1%	2.524	0.1%	2.376	5.8%
24	0.7	3.300	3.20	2.9%	2.941	10.9%	3.022	8.4%

5 Results and discussion

The Scilab program was used to perform linear and nonlinear regressions. Table 2 presents the values of the parameters of models 1 and 2, besides the methods used in each case and the coefficients of determination (R^2). The values of R^2 indicate the proximity between the values obtained by the models and the experiments. As they varied from 82% to 87%, the quality of the regression is satisfactory.

Table 3 presents the experimental values of the G_{IIC} and the values obtained by both models. In general, the percentage errors were low, occurring the maximum percentage difference for model 2 with LSM (13.5%). Considering all the other groups, the percentage difference was less than 10%, confirming the quality of the regressions.

In order to validate the proposed models, two additional experimental data (not considered in the regressions) were evaluated (the last two rows in Table 3). The G_{IIC} value of the samples tested at 60% of P_{max} for 60-h was obtained in reference (Carneiro Neto et al. 2021). The G_{IIC} value of the sample tested at 70% of P_{max} for 24 h is presented in this work and was calculated using the data reduction scheme described in Sect. 3.4. In general, the percentage errors were relatively low, except for the Model 1 with LM method, which presented a percentage error of 28.1%. This highest value must have occurred because the creep time considered (60-h) is not in the time interval considered in the regression procedure (12 h to 48 h). Even given this aspect, Model 2 returned acceptable percentage errors.

To demonstrate the differences between model and experimental values, the residual values are presented in Fig. 2. The samples tested at 50% of P_{max} for 12 h (model 1 LM) and

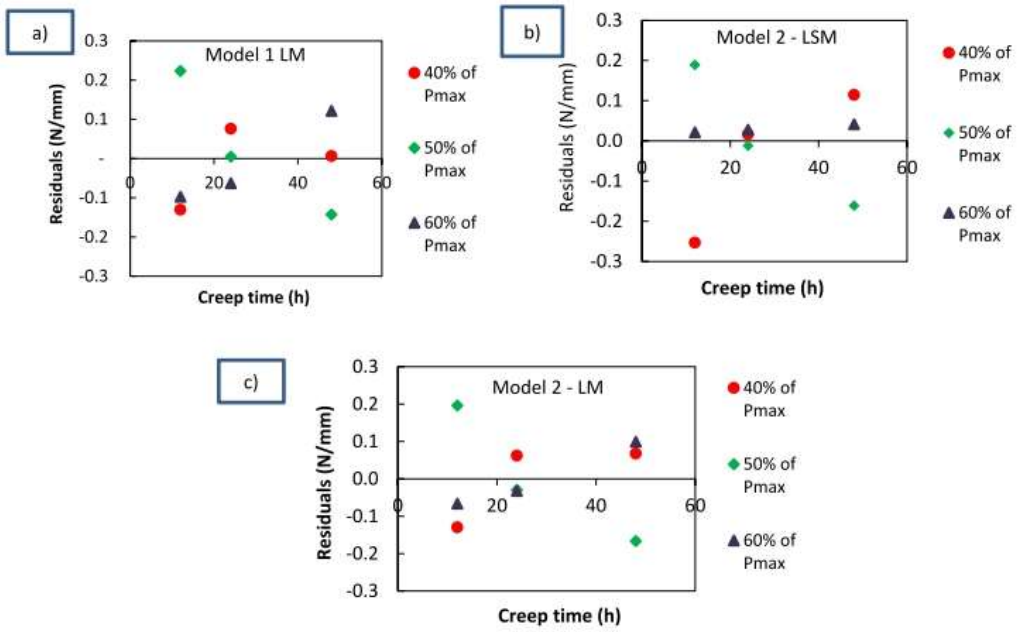

Fig. 2 Residual values for all models and methods: **a**) Model 1 using the Levenberg-Marquardt method, **b**) Model 2 using the Least Square Method and **c**) Model 2 using the Levenberg-Marquardt method

Table 4 Sum of the residuals squared for different models and methods

Model and method	$\Sigma {r_{i1}}^2$	$\Sigma {r_{i2}}^2$
Model 1 - LM	0.12134	0.63331
Model 2 - LSM	0.14225	0.27106
Model 2 - LM	0.10760	0.20605

40% of P_{max} also for 12 h (model 2 LSM) presented residual values above 0.2 N/mm, but even in these cases the values do not appear to be outliers as 0.2 is a low value in comparison to the energy values. All other groups had residual values of less than 0.2, demonstrating that the regression procedure was adequate.

In order to define the model and method that provide the greatest precision, the sum of the residuals squared was calculated for each case. These sums were performed for two different situations: i) considering only the data used for the regression - ${r_{i1}}^2$ - (blank cells in Table 3), and ii) considering all data from Table 3, including the experimental data used to validate the models - ${r_{i2}}^2$ (grey cells in Table 3). For both ${r_{i1}}^2$ and ${r_{i2}}^2$ lower value occurred for model 2 with the LM method (see Table 4).

The numerical analysis was performed in using a user material subroutine (UMAT), which aimed to simulate the creep behavior of the ENF samples, taking into account the experimental evidence that the shear fracture energy varies according to the different creep times and creep loads. Thus, the models presented in this work (Models 1 and 2) were applied to describe the constitutive behavior of the cohesive elements (adhesive). After running the analysis, some information can be accessed in Abaqus, including the von Mises stress, displacements and loads. Figure 3 presents the vertical displacement (U2) along the sample, showing little more than half of the specimen.

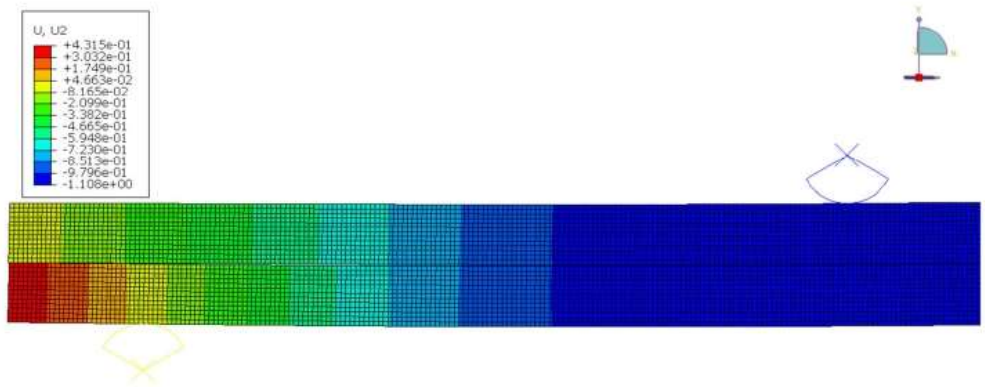

Fig. 3 Results of vertical displacement (U2) in Abaqus when the time running was 19 h. The numerical simulation was performed at 60% of P_{max} for 48 h. Only half of the span is shown (Color figure online)

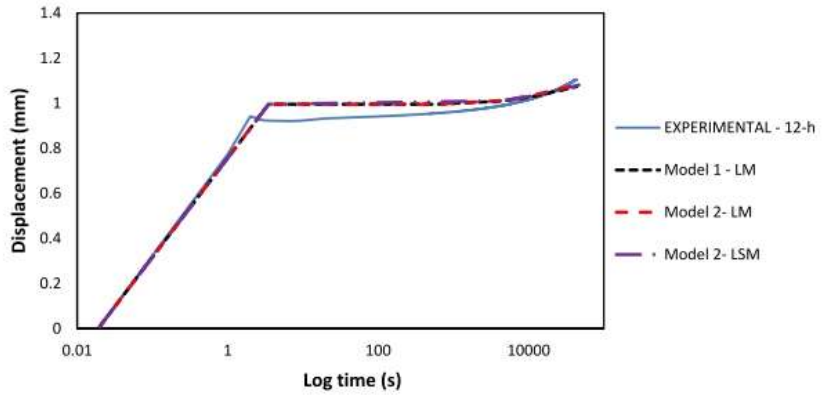

Fig. 4 Experimental and numerical creep curves for the samples tested at 60% of P_{max} for 12 h

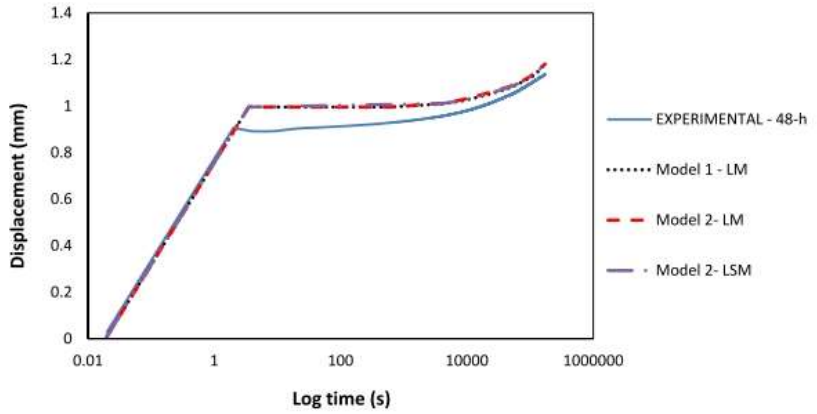

Fig. 5 Experimental and numerical creep curves for the samples tested at 60% of P_{max} for 48 h

Figures 4 and 5 show the displacement results of the numerical analysis in ENF samples, where the numerical and experimental creep curves are presented. Good agreement between

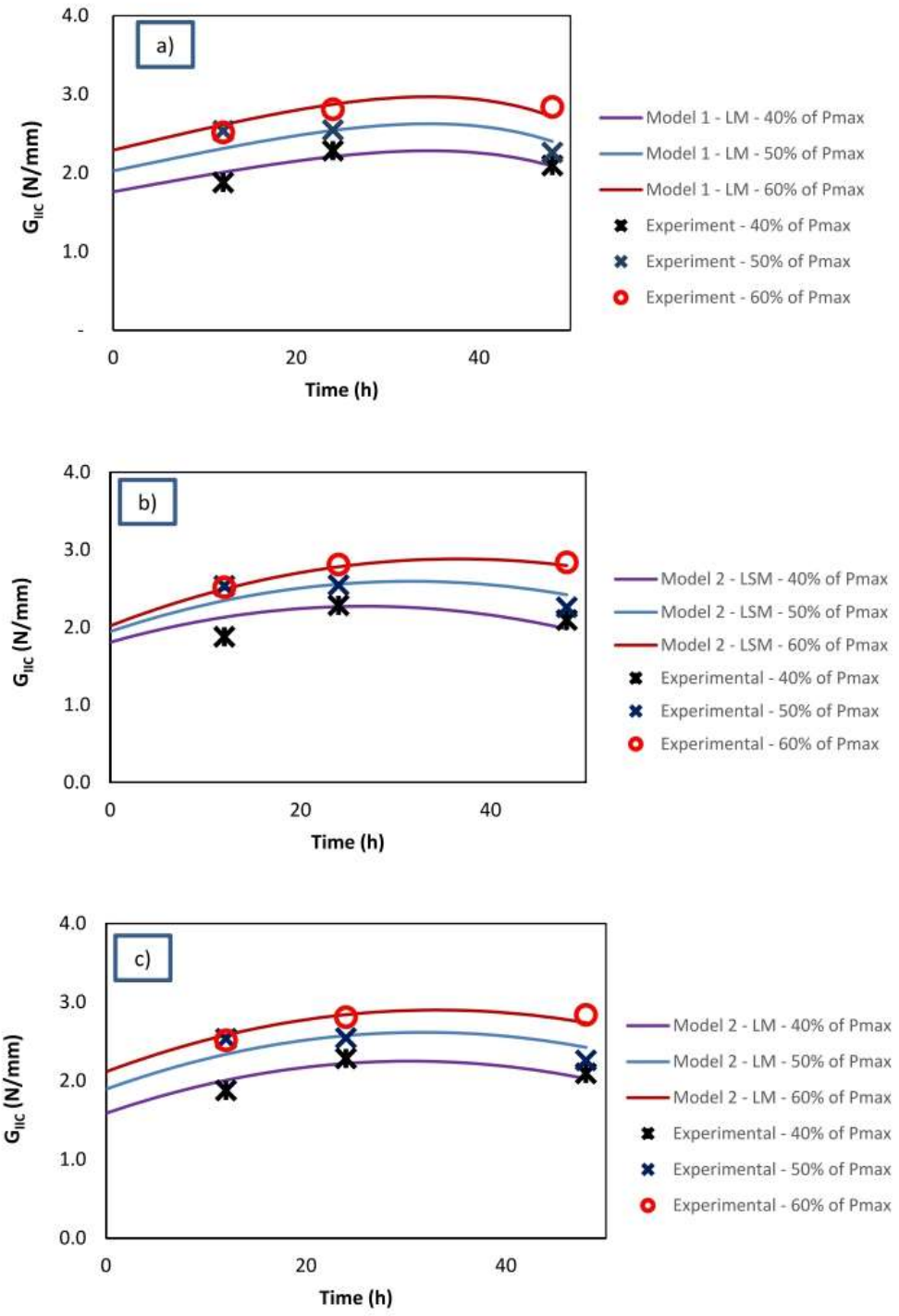

Fig. 6 Variation of shear fracture energy for different creep times and creep loads: **a**) Model 1 with the LM method, **b**) Model 2 with the LSM and **c**) Model 2 with the LM method

the numerical and experimental creep curves is observed for the joints tested at 60% of P_{max} for 12 h (Fig. 4). It can be seen that there were no considerable changes in the numerical

curves even with the different models evaluated. The numerical curve for the joint tested at 60% of P_{max} for 48 h also presented good proximity with the experimental one. The numerical values are slightly higher than the experimental ones. This is to be expected as there are no defects in the numerical model, which naturally occurs in the adhesive layer (Costa et al. 2017). The numerical creep curves obtained with the different models and methods did not present much change. It occurred due to the suitable application of the regression procedure, leading the models to return consistent values for the shear fracture energy. Thus, it shows that both models 1 and 2 are adequate to model the primary and secondary creep of ENF samples under the conditions presented in this work. As the joints were not tested until failure, the crack did not propagate and tertiary creep was not observed in both the experimental and numerical analysis.

The variation of the G_{IIC} along the creep test for different creep loads and for different creep models is presented in Fig. 6. For all methods presented, higher creep loads lead to higher values of G_{IIC}, which is in agreement with the work of Carneiro Neto et al. (2021). For the same creep load, the fracture energy increases up to a certain time and then starts to decrease, as also reported in reference (Carneiro Neto et al. 2021). This confirms the adequacy of the models and methods presented in this work.

6 Conclusions

Two models to calculate G_{IIC} as a function of creep time and creep load were presented in this work. Linear and nonlinear regressions were performed to calculate the parameters of both models using the LSM and LM methods. The regressions presented low residual values and R^2 values above 82%. The models were validated by two additional experiments that were not considered in the regression procedures.

A UMAT was developed in order to describe the particular constitutive behavior of the adhesive. In this way, the change in shear fracture energy was taken into account and the models presented in this work were implemented in a Fortran code linked to Abaqus. The numerical and experimental creep curves had good proximity. The different models did not lead to considerable changes in the numerical simulations, which demonstrates the model robustness and the regressions qualities. As model 2 with the LM method presented lower values of the sum of the residuals squared, it stands out from both model 2 with LSM and model 1 with LM method. Anyway, it is important to highlight that all models and methods returned consistent numerical results.

Further work is necessary to investigate the numerical modelling of tertiary creep (and consequently the creep life of ENF bonded joints).

Acknowledgements The authors would like to thank the Laboratory of Adhesion and Adherence for financial support.

References

Akhavan-Safar, A., et al.: Mode II fracture energy characterization of brittle adhesives using compliance calibration method. Fatigue Fract. Eng. Mater. Struct. **43**(9), 1928–1937 (2020). https://doi.org/10.1111/ffe.13244

Ayatollahi, M.R., Ajdani, A., Akhavan-Safar, A., da Silva, L.F.M.: Effect of notch length and pre-crack size on mode II fracture energy of brittle adhesives. Eng. Fract. Mech. **212**, 123–135 (2019). https://doi.org/10.1016/j.engfracmech.2019.03.024

Berrekheroukh, N., Sereir, Z., Vivet, A., et al.: Experimental and numerical models to study the creep behavior of the unidirectional Alfa fiber composite strength by the photoelasticity method. Mech. Time-Depend. Mater. (2021). https://doi.org/10.1007/s11043-021-09500-5

Carneiro Neto, R.M., et al.: Effect of creep on the mode II residual fracture energy of adhesives. J. Appl. Polym. Sci. (2021). https://doi.org/10.1002/app.51387

Chen, Y., Smith, L.V.: A nonlinear viscoelastic–viscoplastic constitutive model for adhesives under creep. Mech. Time-Depend. Mater. (2021). https://doi.org/10.1007/s11043-021-09506-z

Ciardiello, R., Greco, L., Miranda, M., Di Sciullo, F., Goglio, L.: Experimental investigation on adhesively bonded U-shaped metallic joints using the Arcan test. J. Adv. Join. Process. **1**, 100010 (2020). https://doi.org/10.1016/j.jajp.2020.100010

Costa, M., Carbas, R., Marques, E., Viana, E., da Silva, L.F.M.: An apparatus for mixed-mode fracture characterization of adhesive joints. Theor. Appl. Fract. Mech. **91**, 94–102 (2017). https://doi.org/10.1016/j.tafmec.2017.04.014

Costa, M., Viana, G., Créac'hcadec, R., da Silva, L.F.M., Campilho, R.D.S.G.: A cohesive zone element for mode I modelling of adhesives degraded by humidity and fatigue. Int. J. Fatigue (2018). https://doi.org/10.1016/j.ijfatigue.2018.03.014

da Silva, L.F.M., Ochsner, A., Adams, R.D. (eds.): Handbook of Adhesion Technology Springer, Berlin (2018). https://doi.org/10.1007/978-3-319-55411-2

De Moura, M.F.S.F., De Morais, A.B.: Equivalent crack based analyses of ENF and ELS tests. Eng. Fract. Mech. **75**, 2584–2596 (2008). https://doi.org/10.1016/j.engfracmech.2007.03.005

Delzendehrooy, F., Beygi, R., Akhavan-Safar, A., da Silva, L.F.M.: Fracture energy assessment of adhesives Part II: is GIIc an adhesive material property? (A neural network analysis). J. Adv. Join. Process. **3**, 100049 (2021). https://doi.org/10.1016/j.jajp.2021.100049

Dillard, D.A.: Advances in Structural Adhesive Bonding. Woodhead Publishing Limited, Cambridge (2010). https://doi.org/10.1016/B978-1-84569-435-7.50021-3

Huang, C.H., Tseng, W.C.: An optimal volute spiral case design for centrifugal fan: theoretical and experimental studies. Int. J. Mech. Mater. Des. **12**, 223–240 (2016). https://doi.org/10.1007/s10999-015-9303-4

Jensen, J.L., et al.: A simple unified model for withdrawal of lag screws and glued-in rods. Eur. J. Wood Prod. **69**, 537–544 (2011). https://doi.org/10.1007/s00107-010-0478-y

Khabazaghdam, A., Behjat, B., Yazdani, M., da Silva, L.F.M., Marques, E.A.S., Shang, X.: Creep behaviour of a graphene-reinforced epoxy adhesively bonded joint: experimental and numerical investigation. J. Adhes. (2020). https://doi.org/10.1080/00218464.2020.1742114

Khoramishad, H., Ashofteh, R.S.: Influence of multiwalled carbon nanotubes on creep behavior of adhesively bonded joints subjected to elevated temperatures. J. Adhes. **95**, 979–994 (2019). https://doi.org/10.1080/00218464.2018.1451333

Madja, P., Skrodzewicz, J.: A modified creep model of epoxy adhesive at ambient temperature. Int. J. Adhes. Adhes. **29**, 396–404 (2009). https://doi.org/10.1016/j.ijadhadh.2008.07.010

Marquardt, D.W.: An algorithm for least-squares estimation of nonlinear parameters. J. Soc. Ind. Appl. Math. **11**(2), 431–441 (1963). http://www.jstor.org/stable/2098941

Ramalho, L.D.C., Campilho, R.D.S.G., Belinha, J., da Silva, L.F.M.: Static strength prediction of adhesive joints: a review. Int. J. Adhes. Adhes. **96**, 102451 (2020). https://doi.org/10.1016/j.ijadhadh.2019.102451

Sadigh, M.A.S.: Creep simulation of adhesively bonded joints using modified generalized time hardening model. J. Mech. Sci. Technol. **30**, 1555–1561 (2016). https://doi.org/10.1007/s12206-016-0310-7

Sadigh, M.A.S., Paygozarb, B., da Silva, L.F.M., Tahamid, F.V.: Creep deformation simulation of adhesively bonded joints at different temperature levels using a modified power-law model. Polym. Test. **79**, 106087 (2019). https://doi.org/10.1016/j.polymertesting.2019.106087

Wolf, J., Longère, P., Cadou, J.M., et al.: Numerical modeling of strain localization in engineering ductile materials combining cohesive models and X-FEM. Int. J. Mech. Mater. Des. **14**, 177–193 (2018). https://doi.org/10.1007/s10999-017-9370-9

Zehsaz, M., Tahami, F.V., Sadigh, M.A.S.: Creep analysis of adhesively bonded single lap joint using finite element method. J. Mech. Sci. Technol. **28**, 2743–2748 (2014a). https://doi.org/10.1007/s12206-014-0508-5

Zehsaz, M., Vakili-Tahami, F., Sadigh, M.A.S.: Parametric study of the creep failure of double lap adhesively bonded joints. Mater. Des. **64**, 520–526 (2014b). https://doi.org/10.1016/j.matdes.2014.08.003

ANEXO D – Lei de tração-separação de cisalhamento customizada para modelagem de zonas coesivas de juntas ENF submetidas a fluência (*A customized shear traction separation law for cohesive zone modelling of creep loaded ENF adhesive joints) – Theoretical and Applied Fracture Mechanics*

Theoretical and Applied Fracture Mechanics 119 (2022) 103336

Contents lists available at ScienceDirect

Theoretical and Applied Fracture Mechanics

journal homepage: www.elsevier.com/locate/tafmec

A customized shear traction separation law for cohesive zone modelling of creep loaded ENF adhesive joints

R.M. Carneiro Neto [a], A. Akhavan-Safar [b,*], E.M. Sampaio [c], J.T. Assis [c], L.F.M. da Silva [d]

[a] Center of Technology and Application of Composite Materials, Federal University of Rio de Janeiro, Macaé, RJ, Brazil
[b] Institute of Science and Innovation in Mechanical and Industrial Engineering (INEGI), Rua Dr. Roberto Frias, 4200-465 Porto, Portugal
[c] Laboratory of Adhesion and Adherence, State University of Rio de Janeiro, Polytechnic Institute – Nova Friburgo, RJ, Brazil
[d] Departamento de Engenharia Mecânica, Faculdade de Engenharia, Universidade do Porto, Rua Dr. Roberto Frias, 4200-465 Porto, Portugal

ARTICLE INFO

Keywords:
Adhesive
Cohesive zone model
Creep
Mode II
ENF

ABSTRACT

Considering the creep behavior of bonded joints is of paramount importance since a constant service load can significantly change the properties of adhesives. Several models have been proposed to analyze the creep response of adhesive joints. However, none of them considers the cohesive zone modelling (CZM) as a robust damage analysis approach. The aim of the current work is to present a customized CZM based approach to predict the creep behavior of adhesives subjected to pure shear loading conditions using end notched flexure (ENF) samples. To achieve this a triangular shape cohesive law was used and the variation in cohesive properties of the adhesive was addressed through the proposition of two developed equations, one for the mode II fracture energy and the other for the shear traction. A family of numerical curves can be obtained for each creep condition, thus, the best numerical curve was achieved through a statistical analysis. The effects of the model on the cohesive parameters were also evaluated. The model was validated by an additional creep test. The numerical results were compared to the experimental data obtained in previous work and a good agreement was observed.

1. Introduction

Bonded joints are often used in diverse engineering applications due to their several advantages over other mechanical fastening methods. The benefits of adhesive bonding include a better stress distribution, less stress concentrations and better fatigue performance [1–2]. Polymeric adhesives exhibit viscoelastic or viscoplastic behavior when submitted to a creep loading [3], thus these materials can undergo creep even at low stress levels and at room temperature, which occurs due to the nature of their constituent molecular chains [4,5].

The creep effects can modify the adhesive properties due to the viscous flow that occurs at the adhesive layer leading to a viscous deformation [6]. Accordingly, to increase the durability and reliability of bonded joints submitted to dead loads, many efforts have been made aiming to accurately model the creep behavior of these joints. For this purpose, researchers usually apply rheological models or numerical methods already available in most commercial finite element programs. Zehsaz [7] used the Norton-Bailey model (a time hardening model) to analyze creep in single lap joints (SLJs). The model parameters were fitted to the experimental values obtained in tensile creep testing of bulk adhesives using a nonlinear regression. The results showed that creep strains increase considerably along the adhesive layer, especially at the corners. In order to improve the situation, the author proposed two modified methods: increasing the adhesive thickness and using filleted joints. In a recent work [4] the same model was used to investigate the creep in graphene-reinforced SLJs, but the parameters were calculated considering the true stress and strain values obtained in a tensile creep test. The creep tests revealed that, in general, the addition of graphene up to 0.5 wt% decreases the creep strain of the tested specimens. The Norton-Bailey model was adjusted considering a weight function, and accordingly the true creep strain of the composite was obtained. The numerical results showed a good agreement with the experiments up to 0.25% wt of graphene in the adhesive. A similar methodology was applied to model double lap joints (DLJs) in several works [3,8,9]. Sadigh et al. [3,8] investigated creep in DLJs using the generalized time hardening model [3] and the modified power law equation [8]. The simulations occurred at different temperatures and different stress levels, both with good accuracy. The work of Zehsaz [9] proposed a rheological model with five parameters, which were also calculated by a fitting procedure using the experimental data of tensile creep tests.

* Corresponding author.
E-mail address: aAkhavan-Safar@inegi.up.pt (A. Akhavan-Safar).

https://doi.org/10.1016/j.tafmec.2022.103336
Received 17 November 2021; Received in revised form 12 March 2022; Accepted 23 March 2022
Available online 26 March 2022

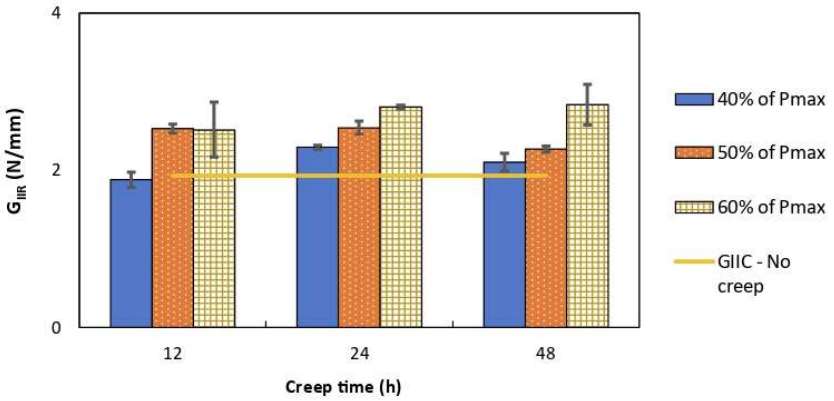

Fig. 1. Residual fracture energy in mode II for different creep times and creep loads [6].

Accordingly, an improved form of the model was proposed with only three parameters, resulting in a good prediction of experimental results.

The creep models of bonded joints available in the literature do not treat the adhesive as a cohesive material, so there are no cohesive zone models (CZMs) capable of modeling creep in bonded joints. CZMs are widely applied to model bonded joints due to their capacity to model both the damage onset and the damage propagation of adhesive joints subjected to different loading conditions including quasi-static, impact, and fatigue [10–13]. Furthermore, the strength prediction of CZM is less sensitive to the mesh size, which is an advantage over other numerical simulation methods [10]. In CZM, a traction separation law between paired nodes from the adhesive layer must be specified in order to simulate the macroscopic damage along a predefined crack path [13]. The damage onset is defined by a stress (strain) criterion and the crack propagation must be defined by a fracture criterion considering the predefined traction separation law. The damage evolution (softening) process can be represented by several laws, including triangular, exponential, or trapezoidal shapes [14]. The total area under the CZM shape in each loading mode (shear or tensile) is the fracture energy, a cohesive property that is related to the capacity of a material to withstand mechanical efforts in the presence of flaws [15]. Double cantilever beam (DCB) specimens and end notched flexure (ENF) samples are the most common joints used to calculate the fracture energies of adhesives in pure modes I and II, G_{IC} and G_{IIC}, respectively [13,16–19]. Chauffaille et al. [20] analyzed the fracture energy of single cantilever beam (SCB) samples submitted to different constant loads. The authors observed that the crack growth rate decreased for longer times up to a part of the graph. Furthermore, the static fracture energy (G_{IC}) was large than the values obtained at the creep tests, which is in agreement with a previous theoretical work [21]. A recent work [22] showed that the creep fracture energy in mode II increases for higher creep loads. Furthermore, the creep fracture energies are also different of the critical fracture energy in mode II (G_{IC}), although a larger proximity between those values was observed when compared to the previous work [20]. Another recent work [6] showed that the shear fracture energy can change considerably due to creep and this change is both time and load dependent. Accordingly, a model to be able to predict the creep behavior in bonded joints using CZM must take into account the variation in fracture energies as a function of creep load and time. This variation must occur in different ways for mode I and mode II efforts, as for mode I the creep stresses on the samples are localized ahead of the crack tip, so the energy is obtained from the regions in the specimens where creep stresses are not applied to. Now for mode II, the whole bonded layer is loaded when a creep load is applied to the joint.

Despite the extensive application of CZM for damage analysis of bonded joints, this approach has not been considered for creep fracture analysis of joints. This work aims to simulate the creep fracture behavior of bonded joints subjected to shear loading conditions using a customized CZM, taking into account the variation in creep fracture energy and also considering the shear traction degradation. To achieve this, ENF creep response was modelled in Abaqus using a user defined material (UMAT) subroutine for different tested conditions. The numerical results were calibrated with the experiments performed at the same conditions by Carneiro Neto et al. [6] and a good agreement was observed. The model was validated with an extra experiment and the cohesive properties variation was analyzed.

2. Experimental data

In this section a summary of the experimental data used to calibrate the parameters of the models is presented, as well as the experimental procedure adopted to perform the additional experiment, which aimed to validate the proposed model presented in Section 3. In all cases, the data acquisition was performed by the universal testing machine (Shimadzu, Autography AG-X Plus, Japan). The displacement, time, and load were recorded by the system machine.

2.1. Experimental data used to calibrate the parameters of the customized model

The values of both maximum load (P_{max}) and critical fracture energy in mode II (G_{IIC}) for the quasi-static test performed on ENF samples were obtained in the work of Carneiro Neto [6], whose values are P_{max} = 13.04 kN and G_{IIC} = 1.93 N/mm. Furthermore, the authors concluded that the shear fracture energy is both creep time and creep load dependent. Initially, in the first step, creep tests were performed in ENF samples at different constant loads (40%, 50%, and 60% of P_{max}) and different pre-defined creep times (12-h, 24-h, and 48-h). The data of the first step (creep curves) are not presented here as they were not used to calibrate the models. These creep curves will be presented in Section 4 (Results) in order to compare the customized model proposed with the experimental data. Then, after the conclusion of first step, the specimens

Table 1
Adherend and adhesive properties [6].

Description	Adhesive NVT 201E	Drawn steel A1020
Young's modulus - E	3.13 ± 0.37 GPa	200 GPa
Shear modulus - G	1.21 GPa	75 GPa
Poisson's ratio - ν	0.29 ± 0.09	0.32
Critical fracture energy in mode II	1.93 ± 0.10	–
Maximum tensile strength	28.70 ± 1.66 MPa	400 MPa
Maximum shear strength	12.5 MPa	–

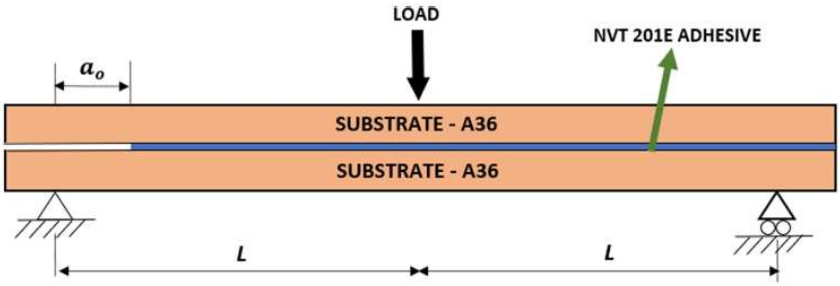

Fig. 2. Schematic representation of the boundary conditions of ENF specimens.

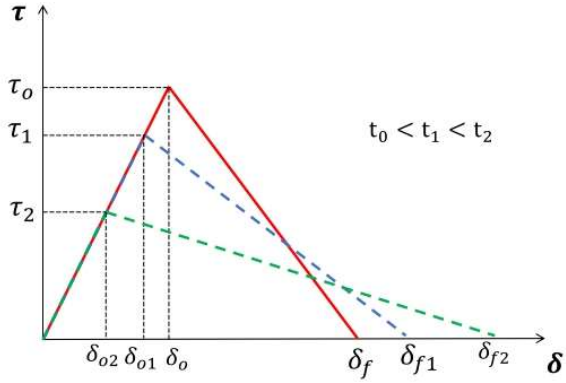

Fig. 3. Customized traction separation law for cohesive zone modelling of creep loading in ENF joints.

were immediately unloaded and soon after the post creep tests (second step) were performed under displacement control (rate of 0.5 mm/min) aiming to obtain the shear residual fracture energy (G_{IIR}), meaning a modified value of G_{IIC} due to residual stresses appearance caused by the creep load. The values of G_{IIR} (second step) are presented in this section, which were calculated using the compliance-based beam method (CBBM) [14]. The residual fracture energy has a great importance because the customized numerical model will consider the fracture energy varying with both creep time and creep load, as occurred in the experiments. Despite the numerical analysis proposed, the quasi-static results may be useful as they give an idea about the variation of fracture energy due to creep. The results of G_{IIR} for different creep times and creep loads are presented in Fig. 1.

2.2. Additional experimental procedure

In order to validate the numerical model, an additional experiment was performed. This verification test was conducted at a creep load of 45% of P_{max} (5.87 kN) for 18-h. It aimed to validate the proposed model, as this creep load was not previously considered in the calibration procedure.

The epoxy adhesive NVT 201E was used to join the carbon steel A1020 substrates, as in the work of Carneiro Neto et al. [6]. The properties of both adhesive and substrates are presented in Table 1. The thickness adopted for the substrates and adhesive were $t_s = 12.7$ mm and $t_a = 0.4$ mm, respectively. The total length was $2L = 298$ mm and the initial crack length was $a_o = 46$mm, as shown in Fig. 2. The width was $B = 25.4$ mm.

Before the bonding process, the substrates were sandblasted and then they were cleaned with acetone. Aiming to ensure the adhesive thickness along the joint length, a double-beveled plate was placed at one end and a calibrated metal strip was positioned at the other end, both with the same adhesive thickness. The double-beveled plate was used to generate a pre-crack and its length was defined in accordance with the initial crack length (a_o), besides an excess length used to remove it after the curing process (24-h at room temperature). The shape of the pre-crack tip is triangular due to the positioning of the double-beveled plate, which is also important to force a cohesive failure along the adhesive layer.

The creep test was performed under a constant load (45% of P_{max}) for 18-h. A universal testing machine (Shimadzu, Autography AG-X Plus, Japan) was used. For the load application point (see Fig. 2), the essential information for the creep curve generation (displacement and time) was recorded by the universal testing machine. This experimental curve was then compared to the numerical creep curve obtained by the customized model.

3. Numerical analysis

3.1. Customized traction separation law

In this work the classical CZM associated with finite elements is adapted aiming to predict the creep behavior of ENF samples. As the creep is being simulated, the numerical analysis is time-consuming, this way a 2D model was implemented, which gives satisfactory results with less computational effort than 3D analysis [23,24]. A UMAT subroutine was developed to define the mechanical constitutive behavior of the adhesive. Four-node two-dimensional quadrilateral solid elements with reduced integration (CPE4R) were used to simulate the behavior of the substrates (steel). Cohesive elements with 4 nodes (COH2D4 from Abaqus) were used for the adhesive layer. The direct linear equation solver available in Abaqus program uses a sparse, direct and Gauss elimination method to solve the equation systems. This approach was used in this work because it can reduce the computational time when the equations system has a sparse structure, as often occurs for structures modeled with beams [27].

The damage mechanics is the physical basis of the numerical model presented. It considers the stress-based analysis and the fracture mechanics concepts, simulating both damage onset and non-self-similar growth of damage [28]. The gradual degradation of the cohesive properties is taken into account as a consequence of the dead load

Table 2
Model parameters obtained using a linear regression.

Method	z(1)	z(2)	z(3)	z(4)	z(5)	z(6)	R^2
LSM	1.8979	0.0336	−1.3812	−0.0006	2.8011	0.0178	0.789

Table 3
Calculation of the total residual for one set of b and k values.

Time (h)	12-h			24-h			48-h		
	d_{n1}	d_{e1}	R_i2	d_{n1}	d_{e1}	R_i2	d_{n1}	d_{e1}	R_i2
0.01	d_{n1}	d_{e1}	$(d_{n1} - d_{e1})^2$	d_{n1}	d_{e1}	$(d_{n1} - d_{e1})^2$	d_{n1}	d_{e1}	$(d_{n1} - d_{e1})^2$
2	d_{n2}	d_{e2}	$(d_{n2} - d_{e2})^2$	d_{n2}	d_{e2}	$(d_{n2} - d_{e2})^2$	d_{n2}	d_{e2}	$(d_{n2} - d_{e2})^2$
4	d_{n3}	d_{e3}	$(d_{n3} - d_{e3})^2$	d_{n3}	d_{e3}	$(d_{n3} - d_{e3})^2$	d_{n3}	d_{e3}	$(d_{n3} - d_{e3})^2$
8	d_{n4}	d_{e4}	$(d_{n4} - d_{e4})^2$	d_{n4}	d_{e4}	$(d_{n4} - d_{e4})^2$	d_{n4}	d_{e4}	$(d_{n4} - d_{e4})^2$
12	d_{n5}	d_{e5}	$(d_{n5} - d_{e5})^2$	d_{n5}	d_{e5}	$(d_{n5} - d_{e5})^2$	d_{n5}	d_{e5}	$(d_{n5} - d_{e5})^2$
24				d_{n6}	d_{e6}	$(d_{n6} - d_{e6})^2$	d_{n6}	d_{e6}	$(d_{n6} - d_{e6})^2$
32							d_{n7}	d_{e7}	$(d_{n7} - d_{e7})^2$
40							d_{n8}	d_{e8}	$(d_{n8} - d_{e8})^2$
48							d_{n9}	d_{e9}	$(d_{n9} - d_{e9})^2$
	ΣR_i^2 (12-h)		R_1	ΣR_i^2 (24-h)		R_2	ΣR_i^2 (48-h)		R_3
	$R_{t1} = R_1 + R_2 + R_3$								

application on the ENF sample.

Equation (1) presents the relation between the stresses at the interface finite element (τ) and the vector of relative displacements between homologous points (δ_r) before the damage initiation [14].

$$\tau = K\delta_r \tag{1}$$

where K is the diagonal matrix containing the stiffness of the cohesive elements.

In Abaqus subroutines, K is called *DDSDDE (i,j)* matrix, where for the bidimensional cohesive model used $i = j = 2$. In fact, it is the Jacobian matrix of the constitutive model, defining the variation in the i^{th} stress component when the time increment ends caused by an infinitesimal perturbation of the j^{th} component of the strain increment array [25]. For the customized model proposed the matrix K is given by Equation (2), valid only before the damage onset.

$$K = \begin{bmatrix} E & 0 \\ 0 & G \end{bmatrix} \tag{2}$$

where E is the Young's modulus and G is the shear modulus, both from the adhesive.

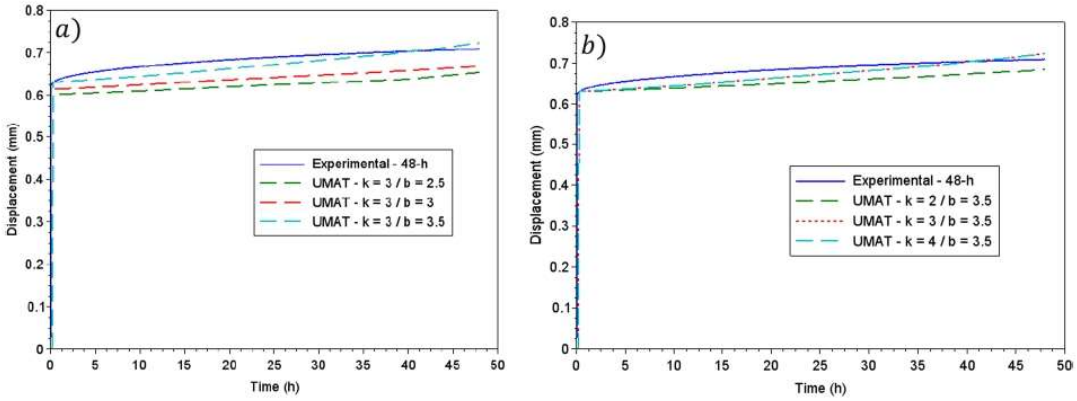

Fig. 4. – Results of numerical simulations for the creep load of 40% of P_{max}.

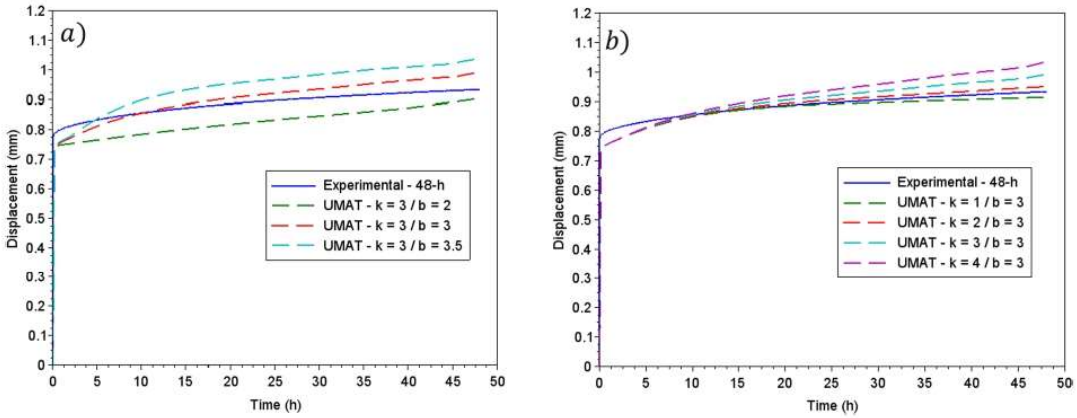

Fig. 5. Results of numerical simulations for the creep load of 50% of P_{max}.

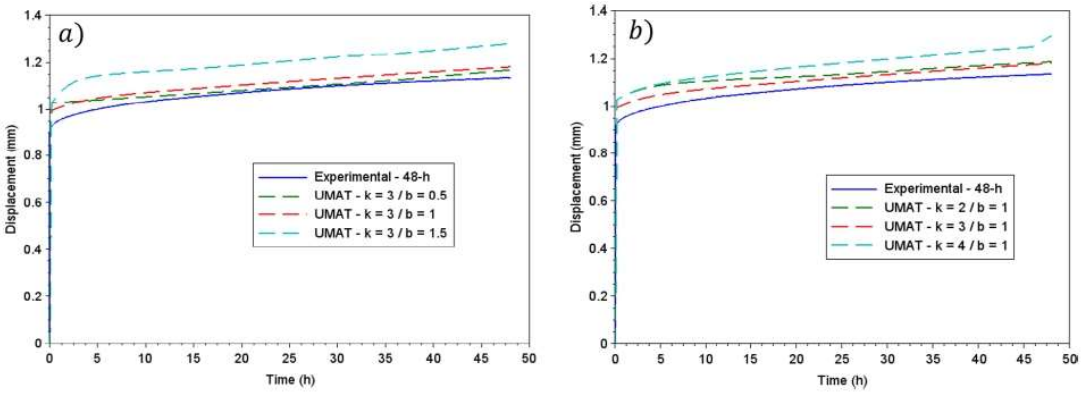

Fig. 6. Results of numerical simulations for the creep load of 60% of P_{max}.

Table 4
Total residue values for different parameters sets (b_i, k_i).

Creep Load (% of Pmax)	k	b	Rt
40%	2	3.5	0.0367
	3	3.5	0.0273
	4	3.5	0.0273
	2.5	3	0.0927
	3	3	0.0598
50%	1	3	0.0337
	2	3	0.0265
	3	3	0.0354
	4	3	0.0396
	3	2	0.1491
	3	3.5	0.0395
60%	3	1	0.0414
	2	1	0.0754
	4	1	0.1241
	3	0.5	0.0610
	3	1.5	0.2096

Equation (1) is valid only before the damage initiation. Fig. 3 presents the triangular law for shear mode (red line), which was used in this work because ENF specimens yields mode II fracture toughness. The triangular law for static conditions is represented by the red line, where τ_o, δ_o and δ_f are the maximum shear stress, the displacement at the damage onset and maximum displacement, respectively. As reported by Possart et. al. [27], even before the crack appearance an amount of mechanical energy is dissipated along the adhesive thickness, then the energy dissipation continues until failure. This aspect is not considered in this work as the CZM used treats this region with an elastic behavior. The damage starts to occur due to the rupture of the oriented network chains, which depends on the stress gradient along the adhesive layer. After the damage onset, a linear softening process occurs at the cohesive element, which is simulated by the release of energy in a cohesive zone behind the crack tip [14]. This is a very important aspect of the CZM because the fracture process zone (FPZ) is taken into account, where nonlinear effects are significantly important [28]. Thus, it is essential to implement a damage parameter aiming to represent the damage level at the cohesive material, varying from 0 (no damage) to 1 (full damage). Equation (3) represents the softening relationship [14].

$$\tau = (I_d - D)K\delta_r \tag{3}$$

where I_d is the identity matrix and D is the damage matrix (diagonal). The damage parameter for mode II (D) is given by Equation (4) [14].

$$D = \delta_f(\delta_c - \delta_o)/\delta_c(\delta_f - \delta_o) \tag{4}$$

where δ_c is the current relative displacement.The damage parameter (D) is defined in UMAT code as a solution dependent state variable, which is updated along the numerical analysis in accordance to Equation (4).

Under compression loading, Equation (1) must be used even after crack propagation. It aims to prevent the interpenetration of the surfaces [14].

As the shear fracture energy (G_{IIC}) is equal to the area under the triangular shape, the final displacement (δ_f) can be obtained by Equation (5) [14].

$$\delta_f = 2G_{IIC}/\tau_o \tag{5}$$

When creep takes place a stress redistribution mechanism along the process zone occurs [27,29] and the shear fracture energy varies [6]. As reported by Jumel et al. [29], the crack nucleation process occurs differently in creep compared to the static condition, which reinforces the need to update the values of the cohesive properties. Furthermore, a degradation in shear traction (τ_o) is assumed for the adapted CZM. As the creep load is constant, both variations are essential for the model consistency because they will allow that higher displacements be obtained for longer times in the simulations, as it occurs on the creep tests.

If a usual CZM was used, the displacement would not increase even after some hours, because it considers that a constant load leads to a constant displacement. This is the reason why taking the variation in cohesive properties into account is essential in a proper simulation of the creep behavior of adhesive joints subjected to creep loading conditions. Thus, after the application of creep load, the value of shear traction will modify from τ_o to τ_i, where i denotes the time increment (creep time), as schematically presented in Fig. 3, and consequently the displacements at the damage onset and at the total failure will change to δ_{oi} and δ_{fi}, respectively. After the damage onset the stiffness is kept constant along the analysis, in accordance to the experimental results obtained in reference [6]. The new final displacement (δ_{mf}) is obtained considering the updated values of the residual fracture energy shown G_{IIR} and the shear traction (τ_m), according to Equation (6).

$$\delta_{mf} = 2G_{IIR}/\tau_m \tag{6}$$

Thus, after the damage onset the DDSDDE(2,2) matrix is now given by $(I_d - D)K$ (see Equation (3)), varying according to the creep effects since the modified value of final displacement (δ_{mf}) will be updated along the simulation. If the current relative displacement (δ_c) is higher than δ_{mf} then the cohesive element totally failed, so there is no more stiffness (DDSDDE(1,1) = DDSDDE(2,2) = 0).

In order to obtain a relation to describe G_{IIR} as a function of the creep time (t) and the applied creep load (F), Equation (7) is proposed. This function must be able to reproduce the experimental values according to different creep loads and creep times with good precision, following the tendency observed in the experiments. This statistical approach should

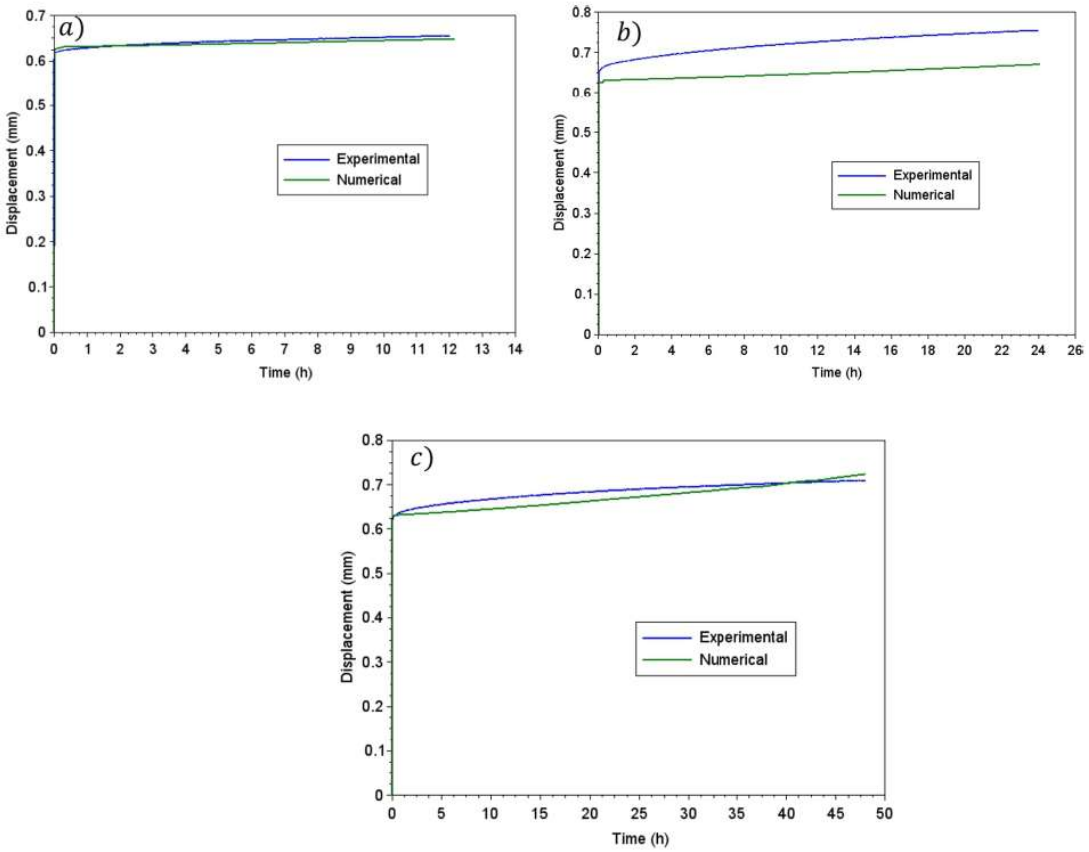

Fig. 7. Best numerical creep curve for the creep load of 40% of P_{max} versus the experimental results for different creep times: a) 12-h, b) 24-h and c) 48-h.

reflect the variation of the fracture energy as a function of time and load and also take the interactions of these two parameters into account. If another adhesive is used in an ENF sample, the application of Equation (7) should be used only after performing calibration tests aiming to confirm similar behavior. The parameters (z_1, …, z_6) were calculated using a linear regression based on the least squares method (LSM) (see Section 3.2 for more details) considering the experimental data obtained in the work of Carneiro Neto et. al. [6], as described in Section 2. The parameters values are presented in Table 2.

$$G_{IIR}(t,F) = z_1 + z_2 t + z_3 F + z_4 t^2 + z_5 F^2 + z_6 tF \tag{7}$$

In Equation (7), F is just the percentual value of the maximum load obtained in ENF tests. For example, for the creep load of 40% of the maximum load, F is equal to 0.4.

In this work, the decrease in shear maximum strength is considered time dependent, being smaller for longer times as shown in reference [30]. Accordingly, Equation (8) is proposed in order to represent this degradation.

$$\tau_m = (\tau_o - b)\left(1 - \frac{t}{t_t}\right)^k \tag{8}$$

where t is the current time increment representing the creep time, t_t is the total time until crack propagation, b and k are fitting parameters. As will be shown ahead, b influences the primary creep and k influences the secondary creep.

In short, over time both τ and G_{IIR} vary. The variation of τ (shear maximum strength) influences the peak of Fig. 3. Now the change in G_{IIR} influences the final displacement, according to Equation (6). Both cohesive properties are essential parameters in any CZM. Applying the proposed traction separation law varying the triangular shape dimensions according to Equations (7) and (8) has as main consequence to take into account the properties degradation and also the particular crack nucleation process along the adhesive layer.

The simulations were performed in two steps, both static. The creep load was applied in the first step, where the load varied linearly from 0 to the respective creep load. The static properties of the adhesive were maintained in step 1 to their initial conditions (see Table 1). Then, in the second step, the cohesive properties were changed as a function of time increment (creep time), as already described. The boundary conditions are presented in Fig. 2. The total time was assumed as 1 month (720-h).

The customized traction separation law presented was developed specifically to modelling the ENF sample although it can be useful to simulate other types of bonded joint.

3.2. Statistical analysis

3.2.1. Least squares method

The least squares method (LSM) considers the minimization of the squared error function (E), given by the quadratic differences between the numerical and experimental values of G_{IIR}, as presented by Equation (9).

$$E(z_1,\cdots,z_6) = \sum_{i=1}^{n} \left[z_1 g_1(t_i,F_i) + \cdots + z_6 g_6(t_i,F_i) - I_i\right]^2 \tag{9}$$

where n is the number of experimental data, $(g_1,\cdots,g_6)$ are the generating functions (see Equation (7)), and I is the vector with experimental

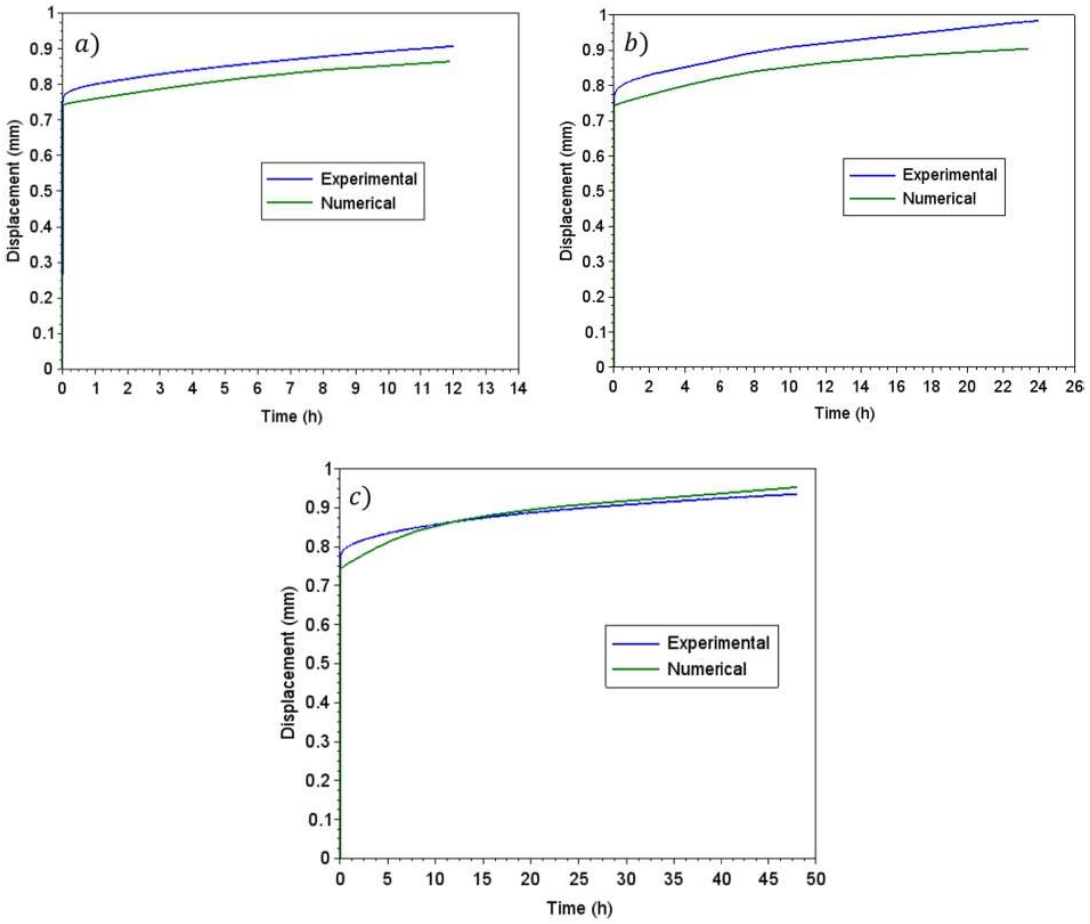

Fig. 8. Best numerical creep curve for the creep load of 50% of P_{max} versus the experimental results for different creep times: a) 12-h, b) 24-h and c) 48-h.

data. The pair (t_i, F_i) represents the creep time and creep load for the i^{th} experimental data.

3.2.2. Obtaining the best numerical curves

The creep curves obtained by the numerical simulations are dependent on the shear traction degradation rate (see Equation (8)) through b and k parameters. This way, in order to obtain the numerical curve that best approximates the experimental data, a statistical analysis is performed.

A residual vector (r) is defined by Equation (10), that shows the differences between the experimental and numerical results for a determined number of data points.

$$r_i = d_{ni} - d_{ei} \tag{10}$$

where d_{ni} and d_{ei} are the numerical and experimental displacements at the loading point in the ENF specimen for the same time, and i is the number of points analyzed along the creep curve. For the creep times of 12-h, 24-h and 48-h the number of points analyzed were 5, 6 and 9, respectively.

Next, the sum of the residuals squared was calculated for each creep time, as presented in Table 3. Then, for this set of b and k parameters, the total square residue (R_{t1}) was calculated taking into account all the sums of the residual squared obtained for different creep times (R_1, R_2, R_3), as shown in Table 3.

Finally, the procedure described was repeated for the different sets of parameters, so that the other values of total square residue were obtained (R_{t1}, R_{t2},…, R_{tn}), where n is the number of parameters sets (b_i, k_i) evaluated. The best numerical curve is then obtained considering the lower value of the total squares residues.

Additionally, the percentage relative errors (e) were calculated using Equation (11) aiming to analyze the proximity between the numerical and experimental curves.

$$e_i = 100 \times abs\left(\frac{d_{ni} - d_{ei}}{d_{ei}}\right) \tag{11}$$

4. Results and discussion

4.1. Defining parameters b and k

The simulations were performed in Abaqus software using a developed subroutine UMAT to take into account the variation of the cohesive properties as a function of creep time. The fitting procedure included several simulations aiming to identify the range of values of parameters b and k that returned consistent results. In general, the ranges of b and k values were similar even for the different creep loads, since k varied from 1 to 4, and b varied from 2 to 3.5, except for the creep load of 60% of P_{max}, where b varied between 0.5 and 1.5. Fig. 4 shows the numerical simulation results for the samples submitted to the creep load of 40% of P_{max}, showing the effect of both parameters (b and k) variation in Equation (8). The experimental results for the samples tested at the same

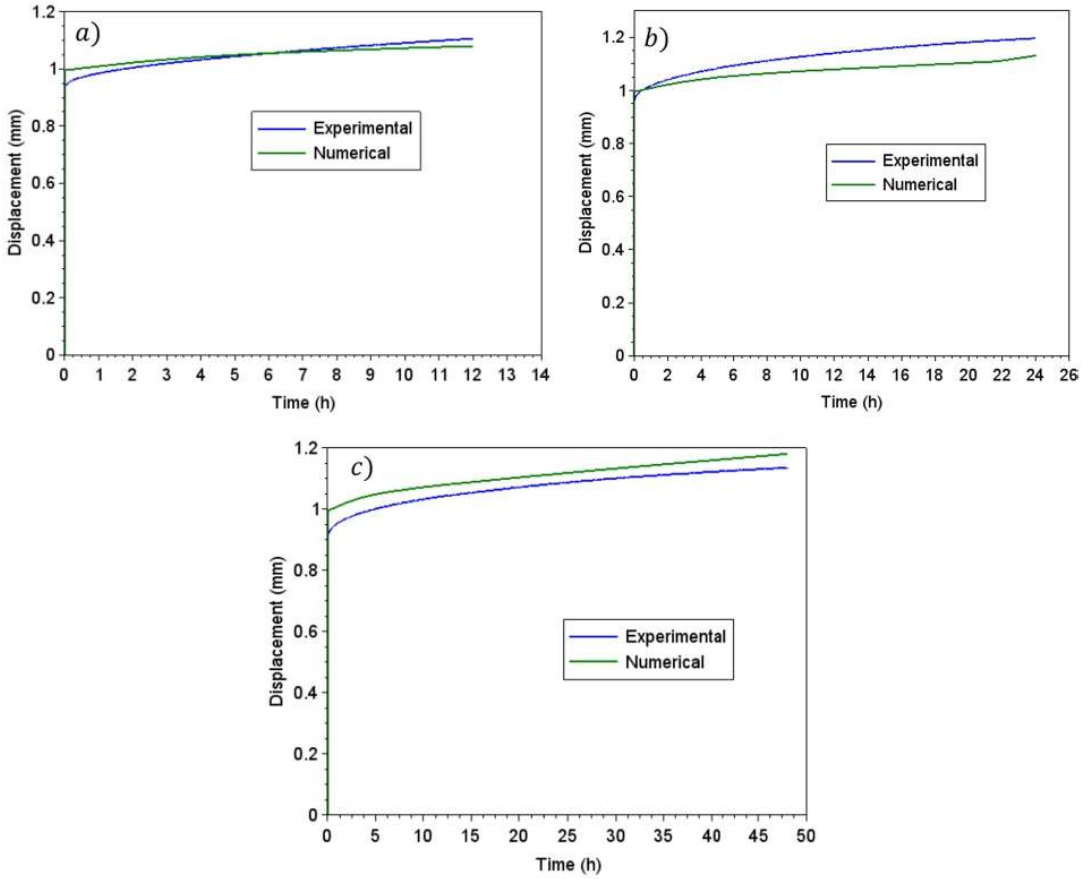

Fig. 9. Best numerical creep curve for the creep load of 60% of P_{max} versus the experimental results for different creep times: a) 12-h, b) 24-h and c) 48-h.

conditions for 48-h [6] were also plotted in the same graph for comparison. The parameter b mainly influences the primary creep (Fig. 4a), as for higher values of b higher displacement rates are obtained on the primary creep. When b is set to 3.5, there is no considerable difference by varying the k parameter between 3 and 4. The secondary creep is most affected by the parameter k (Fig. 4b), thus, the higher the parameter k the greater the obtained creep displacement, since the line that represents the secondary creep is steeper. There is a good agreement between the numerical and experimental data, especially for the higher values of b.

The numerical and experimental results for the creep load of 50% of P_{max} are presented in Fig. 5. In Fig. 5a the effect of parameter b is even clearer, which is related to the primary creep. It has low influence on the secondary creep as can be seen compared to the slope of the curves with different b values. Higher values of k parameter lead to higher values of creep displacements (Fig. 5b). Furthermore, when different values of k parameter are evaluated considering the same value of b ($b = 3$ in Fig. 5b), the curves presented are coincident until approximately 10-h, which confirms that the b parameter influences predominantly the primary creep. A good agreement between numerical and experimental data was observed, although it is not clear which numerical curve gives the best approximation. For this purpose, a comparison analysis using a statistical procedure becomes necessary, which will be done in Section 4.2.

The numerical curves for the creep load of 60% of P_{max} are presented in Fig. 6. The numerical instantaneous elastic displacements are about 10% higher than the experimental one, although this difference is acceptable. This value depends on the static properties and it is modelled in step 1, as described in Section 3.1. The same trends for the parameters b and k are also observed and a good proximity between the numerical and experimental curves is achieved.

Generally, the presented numerical curves show the expected behavior of the ENF samples subjected to creep load where the curves start with an instantaneous elastic displacement (step 1), followed by a creep part (step 2). In the second step a slow displacement rate is observed. When the constant load is applied to the joint, even before the crack growth, the properties of the adhesive layer may change due to the crack nucleation process that occurs because of the residual stresses, as a consequence of the creep effect. Also based on the results [6,22], it was shown that creep as a time dependent phenomenon, makes permanent damages within the adhesive layer. The way to consider this effect adopted in this work was to make the cohesive properties dependent of both creep time and creep load, which lead to new stress gradients along the time, as predicted by the authors [2729].

4.2. Statistical analysis to obtain the best numerical curve

This section addresses how to perform a statistical analysis in order to get the best numerical curve for each creep condition. Table 4 shows the values of the total square residue (R_t) for different sets of parameters and different creep loads. The lower R_t values are highlighted for each creep load, as well as the set of parameters that produce the best agreement between numerical and experimental data, considering all the conditions tested.

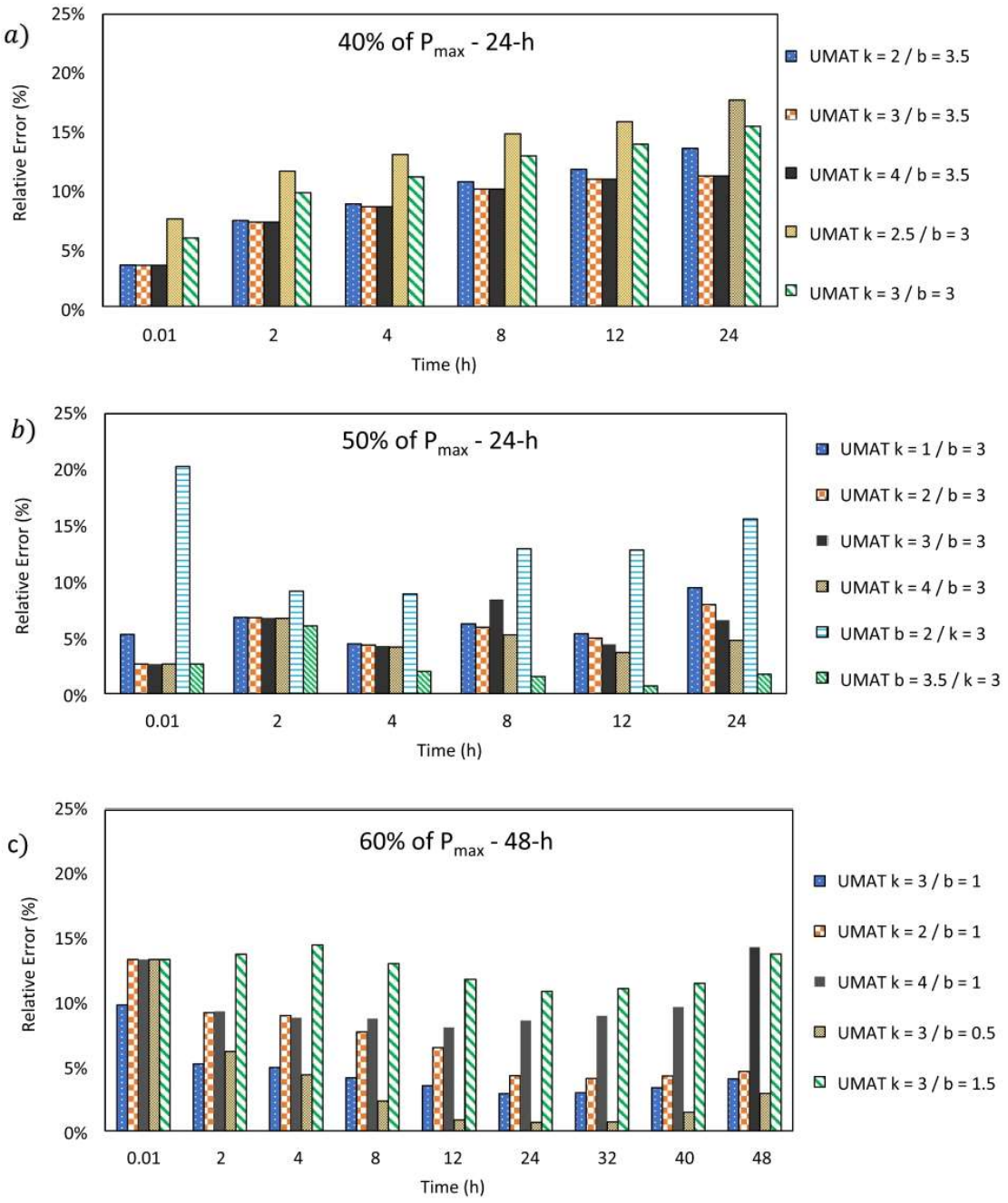

Fig. 10. Highest relative errors found considering all numerical analysis for each creep load: a) 40% of P_{max}, b) 50% of P_{max} and c) 60% of P_{max}.

The selected parameters were then used in the numerical simulation and the respective numerical curves for each creep load are presented in Figs. 7-9, as well as the experimental data. In general, a good agreement between numerical and experimental data is observed for all the groups. Furthermore, the numerical curves show the retarded and decelerating displacement of the samples, as expected for a viscoelastic material [29]. For the creep load of 40% of P_{max}, the creep time of 24-h (Fig. 7b) presented the biggest difference between numerical and experimental data considering all the six instants of times evaluated (see Table 3), although the maximum relative errors for this case was only 11%. Considering the creep load of 50% of P_{max} (Fig. 8) all the relative errors were less than 8%, demonstrating the model suitability. In the same way, the numerical creep curves for the loads of 60% of P_{max} (Fig. 9) presented good agreement with the experimental data and the highest value of the relative error was 7%.

It is important to note that the numerical values obtained using all the sets of parameters (b and k) are acceptable since the maximum obtained relative error was only 20% (for the creep load of 50% of P_{max}, creep time of 24-h, and where $b = 2$ and $k = 3$, see Table 3). It means that since the range of values of b and k parameters are known, in general the numerical prediction is less sensitive to the small changes in parameters b and k which makes the proposed method more applicable for the

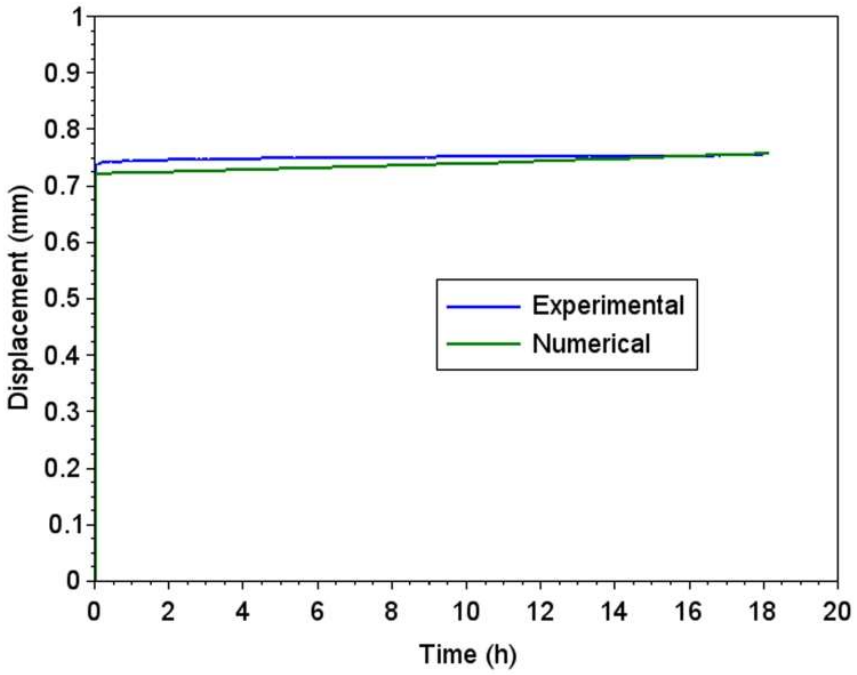

Fig. 11. Numerical and experimental creep curves for the ENF sample tested at 45% of P_{max} for 18-h.

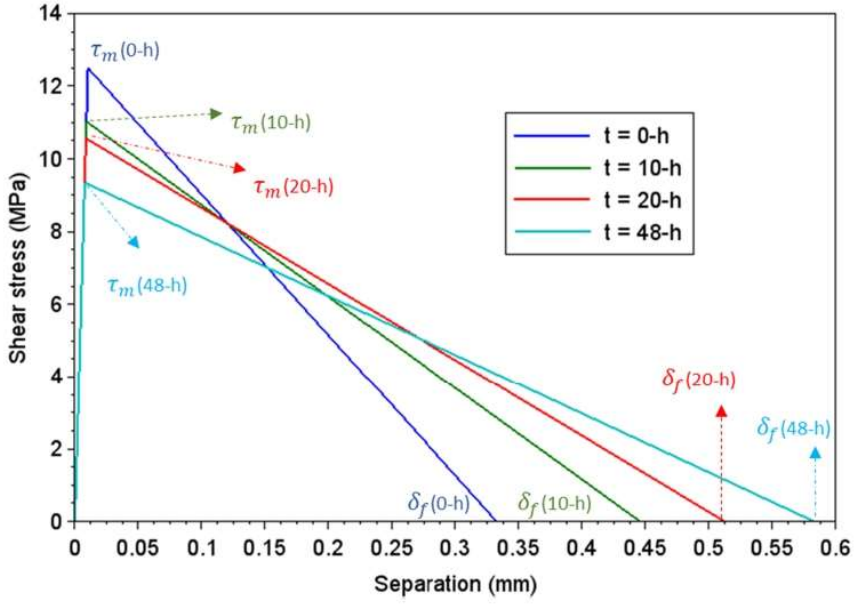

Fig. 12. Traction separation law for different times along the simulation (creep load of 50% of P_{max}).

prediction of the creep response of joints. For parameter k, the range was similar for all the creep loads, but for parameter b the range changed from (0.5 – 1.5) to (2–3.5) for the creep load of 60% and the other creep loads (40% and 50% of P_{max}), respectively. All the other values of relative errors were less than 18% which is an acceptable error. Fig. 10 presents the relative errors obtained when the worst set of parameters (those that led to greater errors) were used for each creep load. However, most errors are less than 10% and only in five cases it is more than 15%, which demonstrates that the model has great potential to be applied for the creep of ENF samples.

4.3. Model validation

The proposed model should be able to predict the creep behavior of ENF samples not only for the creep loads of 40%, 50%, and 60% of P_{max}, but also for other creep loading conditions. Accordingly, for further

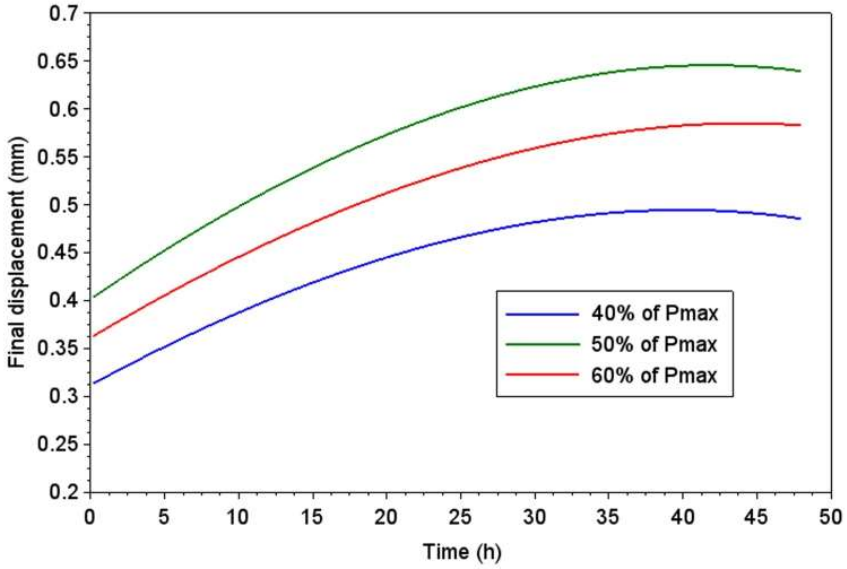

Fig. 13. Final displacements along time for different creep loads.

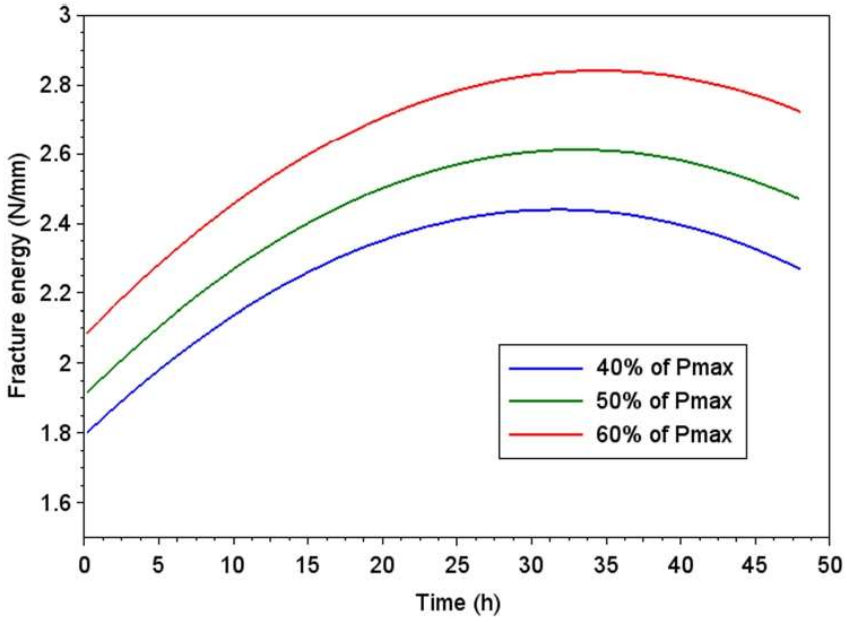

Fig. 14. Residual fracture energy along time for different creep loads.

validation of the proposed approach, one ENF sample was creep tested at the creep load of 45% of P_{max} for 18-h. The same conditions were simulated numerically and the creep response was predicted using the developed method. The experimental and numerical results are presented in Fig. 11, where the values of parameters b and k were both set to 3, which are similar to the values obtained for the best curves for the creep tests of 50% and 60% of P_{max}. A very good agreement between the numerical and experimental curves is observed, validating the customized CZM proposed and demonstrating the model robustness.

Although the proposed model depends on previous creep tests, as well as the post creep tests aiming to evaluate the change in shear fracture energy, it presents the advantage of simulating a range of creep loads between 40% and 60% of P_{max}, while the Bailey Norton model [8,9] or the generalized time hardening model [10] are usually applied for only one creep load in adhesively bonded joints. Furthermore, the parameters of rheological models are stress dependent [11], which also restricts its application to the creep loads previously tested.

4.4. CZM shapes as a function of creep time

The traction separation law with triangular shape as a function of creep time and for the creep load of 50% of P_{max} is presented in Fig. 12.

As shown in Fig. 12 the shear strength decreases for longer creep times, as predicted by Equation (8). This degradation occurs due to the creep phenomenon and it is suitable to predict the behavior of ENF joints submitted to constant loads.

The final displacement (δ_f) is related to both the residual fracture energy (G_{IIR}) and shear traction (τ_m), as presented in Equation (6). The change of δ_f and G_{IIR} for different creep loads are presented in Figs. 13 and 14. As presented in Fig. 14, the higher the creep load the higher the residual fracture energy. Higher creep loads do not necessarily lead to higher values of δ_f, because it depends not only on the fracture energy G_{IIR} (which increases for higher creep loads), but also on the shear strength, which decreases with creep time, in accordance to the b and k values (see Equation (8)).

5. Conclusions

This work presented a customized traction separation law for cohesive zone modelling of creep loaded ENF adhesive joints. Two relations were proposed in order to take into account the variations in shear strength and residual fracture energy due to creep effects.

The numerical results presented a very good agreement with the experimental data. The degradation on the shear traction depends on parameters b and k choice, which influences primary and secondary creep, respectively. The best numerical curves were obtained for all the creep loads by a statistical analysis. For these best curves, the maximum relative error was only 11%, demonstrating the adequacy of the proposed model. Furthermore, even for the other set of parameters, a good proximity between the numerical and the experimental data was obtained.

The customized proposed CZM was further validated through a creep experiment, where an ENF sample was tested at a different creep load level (45% of P_{max}). Again, a good agreement between numerical and experimental results confirmed that the model is suitable to predict creep behavior in bonded joints. Finally, the cohesive properties were analyzed through the variation of the triangular law, final displacement and residual fracture energy.

For mixed mode loading conditions not only the same study should be conducted for pure mode I loading conditions, the interaction of the creep loadings in mode I and mode II should be also analyzed. Another parameter that should be taken into account in the developed equations, is the mode ratio that plays a key role in defining the cohesive parameters. Accordingly, the models developed in this study would be more complex for mixed mode creep loading conditions. Further studies are needed to analyze the creep response of bonded joints subjected to mixed mode loading using CZM.

Declaration of Competing Interest

The authors declare that they have no known competing financial interests or personal relationships that could have appeared to influence the work reported in this paper.

References

[1] S. Bayramoglu, K. Demir, S. Akpinar, Investigation of internal step and metal part reinforcement on joint strength in the adhesively bonded joint: experimental and numerical analysis, Theor. Appl. Fract. Mech. 108 (2020) 102613.

[2] M. Lißner, E. Alabort, H. Cui, R. Rito, B.R.K. Blackman, N. Petrinic, Experimental characterisation and numerical modelling of the influence of bondline thickness, loading rate, and deformation mode on the response of ductile adhesive interfaces, J. Mech. Phys. Solids 130 (2019) 349–369.

[3] M.A.S. Sadigh, Creep simulation of adhesively bonded joints using modified generalized time hardening model, J. Mech. Sci. Technol. 30 (2016) 1555–1561, https://doi.org/10.1007/s12206-016-0310-7.

[4] A. Khabazaghdam, B. Behjat, M. Yazdani, L.F.M. Da Silva, E.A.S. Marques, X. Shang, Creep behaviour of a graphene-reinforced epoxy adhesively bonded joint: experimental and numerical investigation, The Journal of Adhesion 97 (13) (2021) 1189–1210.

[5] Budhe S, Banea MD, de Barros S, da Silva LFM, An updated review of adhesively bonded joints in composite materials, International Journal of Adhesion and Adhesives, 72, 30–42, 2017.10.1016/j.ijadhadh.2016.10.010.

[6] R.M. Carneiro Neto, A. Akhavan-Safar, E.M. Sampaio, J.T. Assis, L.F.M. da Silva, J. Appl. Polym. Sci. (2021), e51387, https://doi.org/10.1002/app.51387.

[7] M. Zehsaz, F.V. Tahami, M.A.S. Sadigh, Creep analysis of adhesively bonded single lap joint using finite element method, J. Mech. Sci. Technol. 28 (2014) 2743–2748, https://doi.org/10.1007/s12206-014-0508-5.

[8] M.A. Saeimi Sadigh, B. Paygozar, L.F.M. da Silva, F. Vakili Tahamid, Creep deformation simulation of adhesively bonded joints at different temperature levels using a modified power-law model, Polym. Test. 79 (2019), https://doi.org/10.1016/j.polymertesting.2019.106087.

[9] M. Zehsaz, F. Vakili-Tahami, M.-A. Saeimi-Sadigh, Parametric study of the creep failure of double lap adhesively bonded joints, Mater. Des. 64 (2014) 520–526.

[10] L.D.C. Ramalho, R.D.S.G. Campilho, J. Belinha, L.F.M. da Silva, Static strength prediction of adhesive joints: a review, Int. J. Adhes. Adhes. 96 (2020) 102451.

[11] S. Akpinar, R. Sahin, The fracture load analysis of different material thickness in adhesively bonded joints subjected to fully reversed bending fatigue load, Theor. Appl. Fract. Mech. 114 (2021) 102984.

[12] A. Akhavan-Safar, J. Monteiro, R. Carbas, E. Marques, R.K. Goyal, L. da Silva, A modified degradation technique for fatigue life assessment of adhesive materials subjected to cyclic shear loads, Proc. Inst. Mech. Eng. C: J. Mech. Eng. Sci. 235 (3) (2021) 550–559.

[13] C.D.M. Liljedahl, A.D. Crocombe, M.A. Wahab, I.A. Ashcroft, Damage modelling of adhesively bonded joints, Int J Fract 141 (2006) 147–161, https://doi.org/10.1007/s10704-006-0072-9.

[14] M.F.S.F. De Moura, Numerical simulation of the ENF test for the mode-II fracture characterization of bonded joints, J. Adhes. Sci. Technol. 20 (1) (2006) 37–52, https://doi.org/10.1163/156856106775212422.

[15] J. Manterola, et al., Effect of the width-to-thickness ratio on the mode I fracture toughness of flexible bonded joints, Eng. Fract. Mech., 218, 106584, 2019. 10.1016/j.engfracmech.2019.106584.

[16] J. Monteiro, A. Akhavan-Safar, R. Carbas, E. Marques, R. Goyalc, M. El-zeind, L.F. M. da Silva, Mode II modeling of adhesive materials degraded by fatigue loading using cohesive zone elements, Theor. Appl. Fract. Mech. 103 (2019), 102253, https://doi.org/10.1016/j.tafmec.2019.102253.

[17] M.F.S.F. De Moura, J.J.L. Morais, N. Dourado, new data reduction scheme for mode I wood fracture characterization using the double cantilever beam test, Eng. Fract. Mech. 75 (2008) 3852–3865, https://doi.org/10.1016/j.engfracmech.2008.02.006.

[18] K. Senthil, A. Arockiarajan, R. Palaninathan, Experimental determination of fracture toughness for adhesively bonded composite joints, Eng. Fract. Mech. 154 (2016) 24–42, https://doi.org/10.1016/j.engfracmech.2015.11.015.

[19] J.M. Gorman, M.D. Thouless, The use of digital-image correlation to investigate the cohesive zone in a double-cantilever beam, with comparisons to numerical and analytical models, J. Mech. Phys. Solids 123 (2019) 315–331, https://doi.org/10.1016/j.jmps.2018.08.013.

[20] S. Chauffaille, J. Jumel, M.E.R. Shanahan, Pre-cracking behaviour in the single cantilever beam adhesion test, Int J Fract 169 (2011) 133–144, https://doi.org/10.1007/s10704-011-9586-x.

[21] A.J. Paris, P.C. Paris, Instantaneous evaluation of J and C, Int. J. Fract. 38 (1) (1988) R19–R21.

[22] R.M. Carneiro Neto, A. Akhavan-Safar, E.M. Sampaio, J.T. Assis, L.F.M. da Silva, Assessment of the creep life of adhesively bonded joints using the end notched flexure samples, Eng. Fail. Anal. 133 (2022) 105969.

[23] R.D. Adams, J. Comyn, W.C. Wake, Structural adhesive joints in engineering. Chapman and Hall, 1997.

[24] D.A. Dillard, A.V. Pocius, The mechanics of adhesion, Elsevier, Amsterdam, 2002.

[25] ABAQUS HTML documentation, Dassault Syst. (2017).

[27] W. Possart, J. Jumel, M. Budzik, J. Guitard, M.E.R. Shanahan, Experimental study of cohesive strain prior to crack initiation in constant force single cantilever beam test, J. Adhes. Sci. Technol. 29 (9) (2015) 896–909.

[28] T. Yang, X. Yang, R. Huang, K.M. Liechti, Rate-dependent traction-separation relations for a silicon/epoxy interface informed by experiments and bond rupture kinetics, J. Mech. Phys. Solids 131 (2019) 1–19, https://doi.org/10.1016/j.jmps.2019.06.013.

[29] J. Jumel, S. Chauffaille, M.K. Budzik, M.E.R. Shanahan, J. Guitard, Viscoelastic foundation analysis of single cantilevered beam (SCB) test under stationary loading, Eur. J. Mech. A/Solids 39 (2013) 170–179.

[30] M. Costa, G. Viana, R. Créac'hcadec, L.F.M. da Silva, R.D.S.G. Campilho, A cohesive zone element for mode I modelling of adhesives degraded by humidity and fatigue, Int. J. Fatigue 112 (2018) 173–182.

APÊNDICE A - Declaração de não Violação de Direitos Autorais de Terceiros

Declaração de não Violação de Direitos Autorais de Terceiros

Eu, RANULFO MARTINS CARNEIRO NETO, CPF: 024.771.215-96, aluno de Doutorado do Programa de Pós Graduação em Modelagem Computacional do Instituto Politécnico do Rio de Janeiro da Universidade do Estado do Rio de Janeiro, declaro para os devidos fins:

a) que a *Tese* com título:

"*Desenvolvimento de modelos de dano coesivo modificados para juntas coladas submetidas a fluência em modo II*", assim como os 4 (quatro) artigos científicos que compõem a mesma (Anexos I, II, III e IV), de minha autoria, não violam os direitos autorais de terceiros, sejam eles pessoas físicas ou jurídicas;

b) que a *Tese* não se constitui em reprodução de obra alheia, ainda com direitos autorais protegidos ou já em domínio público;

c) que em havendo textos, tabelas e figuras transcritos de obras de terceiros com direitos autorais protegidos ou de domínio público tal como idéias e conceitos de terceiros, mesmo que sejam encontrados na *Internet*, **os mesmos estão com os devidos créditos aos autores** originais e estão incluídas apenas com o intuito de deixar o trabalho autocontido;

d) que os originais das autorizações para inclusão dos materiais do item c) emitidas pelos proprietários dos direitos autorais, se for o caso, estão em meu poder;

e) que tenho ciência dos Artigos 297 e 298 do Código Penal Brasileiro.

Nova Friburgo, 06 / 04 / 2022

Assinatura: Ranulfo M Carneiro Neto

Ciente, 06 / 04 / 2022

Orientador: JOAQUIM TEIXEIRA DE ASSIS

(Assinatura)